# Reactive Power Compensation of Fixed Speed Wind Turbines Using a Hybrid Wind Turbine Technology


**Oluwagbenga Apata**

**Thesis Presented for the Degree of**

**DOCTOR OF PHILOSOPHY**

**In the Department of Electrical Engineering**

**Faculty of Engineering and Built Environment**

**University of Cape Town**

**January 2022**

# DECLARATION

I, Oluwagbenga Apata declare that the thesis titled "Reactive power compensation of fixed speed wind turbines using a hybrid wind turbine technology" is my original work. All materials generated and published by other researchers and have been used in this thesis are explicitly referenced as appropriate. Some parts of this thesis have been published in full peer-reviewed conferences and journals. This work is submitted to the Department of Electrical Engineering, University of Cape Town, South Africa towards the award of the Doctor of Philosophy degree in Electrical Engineering. This research work has not been submitted to any other university or institution for any other degree or examination.

Signed by candidate

.....

Oluwagbenga Apata

**January 31, 2022**

……..

Date

# Declaration on Inclusion of Publication

**Note:** PhD students who have been granted approval by the DDB to include publications in their thesis, must add the following separate signed statement, listing the publications that they were given permission to include (this statement must be included in your thesis, after the declaration that it is your own work):

**"I confirm that I have been granted permission by the University of Cape Town's Doctoral Degrees Board to include the following publication(s) in my PhD thesis, and where co-authorships are involved, my co-authors have agreed that I may include the publication(s)"**

a. **O. Apata** and D. T. O. Oyedokun, "Improving The Dynamic Performance Of Grid Connected Fixed Speed Wind Farm Using Variable Speed Wind Turbines," 2020 IEEE PES/IAS PowerAfrica, Nairobi, Kenya, 2020, pp. 1-5, DOI: 10.1109/PowerAfrica49420.2020.9219955.

b. **O. Apata** and D. T. O. Oyedokun, "A Mathematical Approach To Hybrid Wind Farm Modelling," 2020 IEEE PES/IAS PowerAfrica, Nairobi, Kenya, 2020, pp. 1-5, DOI: 10.1109/PowerAfrica49420.2020.9219918.

c. **O. Apata** and D. T. O. Oyedokun, "Impact Of StatCom On Voltage Stability Of Fixed Speed Wind Farms," 2020 IEEE PES/IAS PowerAfrica, Nairobi, Kenya, 2020, pp. 1-5, DOI: 10.1109/PowerAfrica49420.2020.9219989.

d. **O. Apata** and D. T. O. Oyedokun, "Novel Reactive Power Compensation Technique for Fixed Speed Wind Turbine Generators," 2018 IEEE PES/IAS PowerAfrica, Cape Town, 2018, pp. 628-633, DOI: 10.1109PowerAfrica.2018.8521131.

e. **O. Apata** and D. T. O. Oyedokun, "Wind turbine generators: Conventional and emerging technologies," 2017 IEEE PES PowerAfrica, Accra, 2017, pp. 606-611, DOI: 10.1109/PowerAfrica.2017.7991295.

f. **Apata, O**., and D. T. O. Oyedokun. "An Overview of Control Techniques for Wind Turbine Systems." DOI 10.1016/j.sciaf.2020.e00566, Elsevier Scientific African Journal.

SIGNATURE: Signed by candidate DATE: **31 January 2022**

**Oluwagbenga Apata** **APTOLU002**

STUDENT NAME: _____ STUDENT NUMBER: _____

## Acknowledgments

Firstly, my gratitude goes to God who has helped me in achieving this. To my supervisor Dr. D.T.O. Oyedokun, I want to say a big thank you for your guidance. To my parents, Engineer Tunde Apata and Mrs. Folasade Apata, I say thank you for all your support and prayers throughout this journey.

To my beautiful wife and our beautiful daughter, Mrs. Marilyn Apata and Joanna Apata: thank you for your understanding, encouragement, support, and prayers.

I would like to use this medium to appreciate all those who have contributed to the success of this research in one way or the other, especially family, colleagues, and friends.

# ABSTRACT

**Reactive Power Compensation of Fixed Speed Wind Turbines Using a Hybrid Wind Turbine Technology**

**By**

**Oluwagbenga Apata**

There has been significant growth in the use of wind energy as an alternative form of energy by many countries globally. This is in direct response to calls to reduce environmental pollution from the usage of fossil fuels in energy generation. Due to the intermittency of wind energy, the integration of wind energy into an existing power system grid can lead to increased exposure to instability. This has prompted power systems operators to revise the connection requirements for grid codes that require wind turbine generators to contribute to power control and stay online during a network disturbance. These revisions have resulted in technical migrations from the fixed speed wind turbine (FSWT) to the variable speed wind turbines (VSWTs). The fixed speed induction generator (FSIG) powers the FSWT while the VSWT is based on the permanent magnet synchronous generator (PMSG) or the doubly-fed induction generator (DFIG).

Irrespective of this technical migration in wind power systems, the FSWTs still represent a considerable percentage of globally installed wind turbines (WTs). Furthermore, some wind turbine (WT) manufacturers have introduced life expansion programs for these FSWTs to increase their operating life to as much as thirty years.

The FSWT is common in wind power systems due to its robustness, mechanical simplicity, and low production cost. Its major setback is the inability to compensate for its reactive power need and improve voltage stability during a fault condition. In steady-state conditions, these WTs

experience large fluctuations in the generator terminal voltage because of the uncontrolled consumption of reactive power. During grid fault conditions, the FSWT consumes large quantities of reactive power to stay grid-connected and prevent the rotor from over-speeding, thereby losing synchronization. It is therefore imperative to provide voltage and reactive power support for the FSWT-power system. This is important to enable the wind power system to fulfil the grid codes as prescribed by the system operator and successfully go through a fault condition.

Flexible AC transmission system (FACTS) devices are often used in enhancing the voltage stability and reactive power control in the FSWT- power system. It has been shown however from the available literature that the installation of these devices alongside the WT inflates the total cost of the wind power system thereby making the overall wind system more expensive.

The PMSG-WT is becoming more attractive for wind energy systems. This class of WTs has fully-rated converters that control the active and reactive power of the WT, enabling the WT system to ride through a grid fault condition successfully. This improves the low voltage ride through (LVRT) ability during a grid disturbance. This characteristic makes it a very suitable choice for grid-connected operations. A unique feature of this category of a wind system is the possibility of controlling its fully rated converters to support a nearby induction generator WT system, making it a suitable choice for the development of a hybrid wind farm.

This research proposes exploring this characteristic of the PMSG-WT in developing a hybrid wind system of the PMSG-WT and FSIG-WT. The proposed hybrid wind system utilizes the ability of the PMSG in supporting a nearby wind farm. Therefore, systematic control of the PMSG and FSIG wind system is proposed using the fully rated converters of the PMSG-WT system in providing the required voltage support and reactive power needed by the FSIG-wind system during a grid disturbance. The proposed strategy, therefore, eliminates the need for FACTS devices.

To develop the proposed coordinated control strategy of the PMSG and FSIG-hybrid wind power system, a current allocation strategy is first developed for the grid side converter (GSC) of the PMSG. This is based on the converter capacity and current capability of the GSC in providing reactive power needed by the FSWT-based wind system in the event of a grid fault condition. With this approach, the GSC capacity of the PMSG is utilized efficiently to improve the LVRT capability of the FSWT-based wind farm and voltage support of the hybrid wind farm. In a steady state, the control priority ensures that both wind systems operate efficiently and reliably.

The proposed solution offers both technical and economic advantages compared to the traditional voltage support methods available to the FSIG-wind system under grid fault conditions. This method can be applied to existing wind power systems operating with the FSIG and can be further applicable to any new wind farm, which would be established with this hybrid configuration. Results from the proposed strategy show an improvement in the grid voltage of the hybrid wind farm, there is a reduction in grid voltage sags while the FSIG-based wind farm experiences an improvement in its output power and reactive power profile while it rides through a fault condition.

# Table of Contents

# Chapter 6 Simulation Protocol, Results, and Discussions



# Chapter 7 Conclusions

# List of Figures

# List of Tables

# Chapter 1

# Introduction

This chapter presents an insight into the growth of the wind energy industry in the last few years. Different countries are beginning to embrace renewable energy, wind energy in particular as a preference to fossil fuels, as a part of their energy mix. Background to the thesis is provided followed by the purpose and main contribution of this research. The research questions and methodology is presented and finally, the chapter concludes with the thesis outline and research outputs from this thesis.

## 1.1. Renewable energy and wind power

Renewable energy sources have been accepted globally as viable alternatives to fossil-powered power systems. This is in direct response to the increased demand for energy and the desire to reduce the effect of carbon pollution from conventional power systems. Wind, solar, geothermal heat, hydropower, and sea waves have been identified as the major sources of renewable energy while the most commonly used nowadays are solar and wind energy. Globally, countries are seeking solutions to mitigate high-energy prices by embracing renewable energy as a preference to conventional energy generation sources.

The total installed global wind capacity culminated at 743 GW in 2020 representing a 14% increase compared to the installed global wind capacity in 2019 [1], shown in Figure 1.1. In its 2019 report, the Global Wind Energy Council (GWEC) indicated 51.3 GW of installed wind energy was added globally while the offshore wind market experienced a 0.5% growth of 4.49 GW of new WT installations culminating in a total of 23 GW installed wind capacity, and the global wind installed capacity increased to about 651 GW [2]. In 2018, China, the USA, and Germany emerged as the

top three onshore markets. Mature regions in Europe and the USA will continue to generate stable volumes of renewable energy and significant growth driven by developing markets in the South Eastern parts of Asia, Africa, and the global offshore markets.

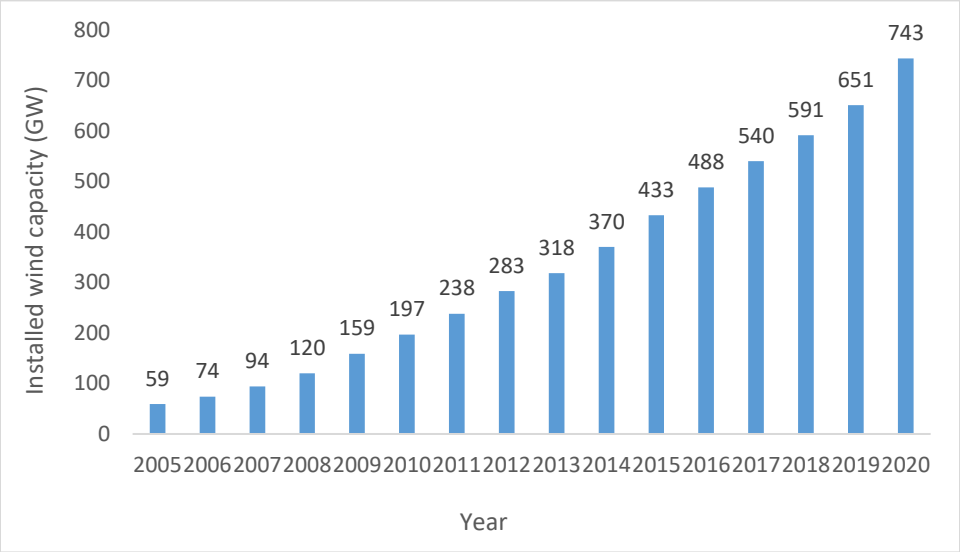


Figure 1.1. Installed global wind capacity

Wind energy is now an important component of the energy plan in several nations underscoring the importance of this renewable energy source. Denmark in its 2012 Energy Act set out a plan that aimed to have 50% of its energy from wind by 2020 [3]. The African continent is not left behind in this shift towards renewables and wind energy in particular. The government of South Africa has incorporated renewables as part of its energy plan. The Renewable Energy Independent Power Producer Procurement Programme (REIPPPP) policy document has been developed and published with wind energy set to play a significant role. As seen in Figure 1.2, South Africa's installed wind capacity grew from 3.16 MW in 2005 to an all-time high of 569 MW in 2014 [4], and peaking at 2500 MW in 2020. Through the Department of Energy (DoE), the government of South Africa in 2019, introduced a revised and updated energy plan (2010-2030) aimed at increasing the

installed capacity of renewable energy sources and decommissioning about 12 GW of coal plants by 2030 [5].

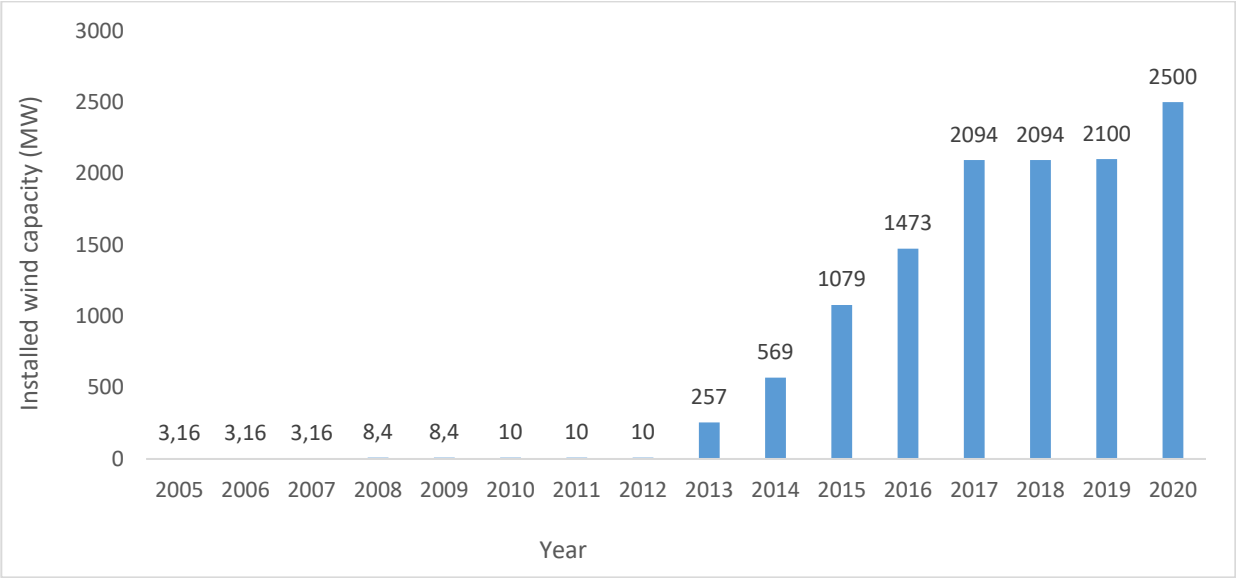


Figure 1.2. South Africa's installed wind capacity

The Department of Energy in South Africa has projected that by 2030, there will be over 23.6 GW of renewable energy installations in South Africa with wind energy contributing 9.2 GW to the renewable energy installations. The revised twenty-year REIPPPP proposed increasing installed wind capacity to 11.4 GW at the end of 2030, as shown in Figure 1.3, accounting for 15% of total installed renewable energy capacity in South Africa [5]. These statistics indicate that wind energy is fast becoming a viable alternative to conventional power generation across the globe and South Africa is no exception. Figure 1.4 [6] represents the wind atlas of South Africa, showing the different regions in the country with high and low wind speeds. The wind atlas is applied to assist in the development of large grid-connected wind farms, providing more accurate and reliable wind data to identify potential off-grid electrification opportunities.

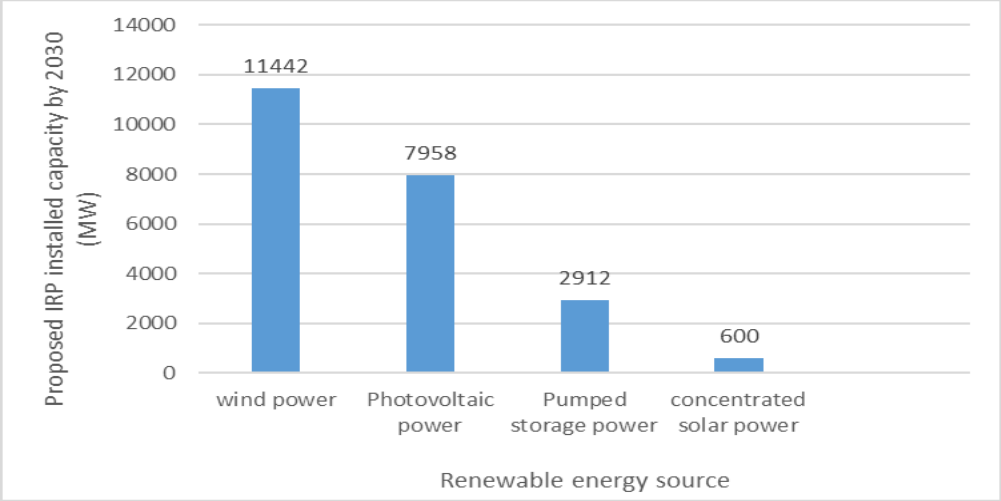


Figure 1.3. South Africa's 2030 renewable energy goal

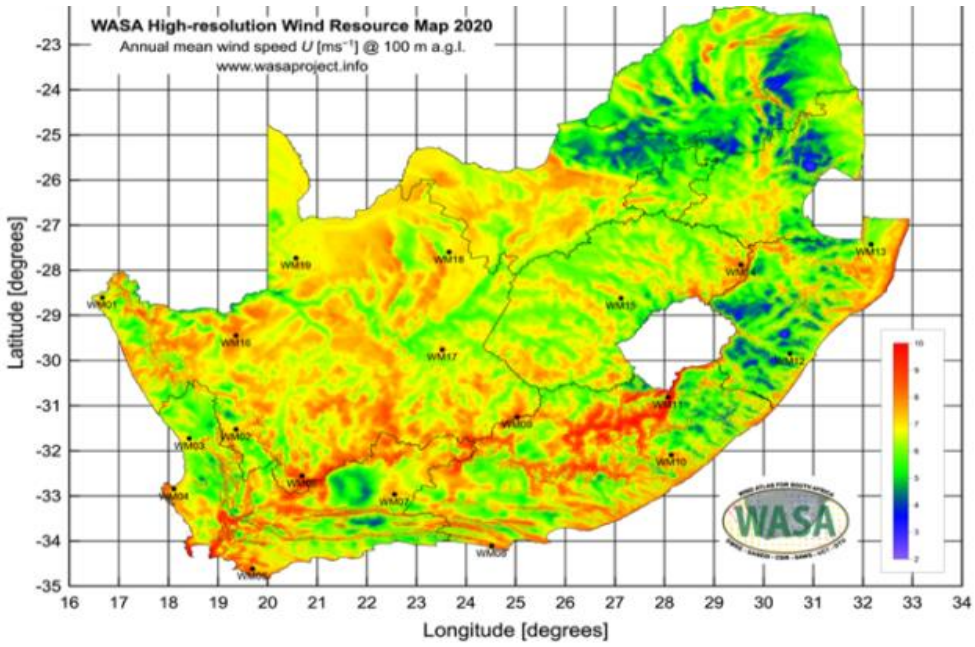


Figure 1.4. Wind Atlas of South Africa [6]

## 1.2. Background to Thesis

The increased effort to tackle climate change has prompted different countries to develop energy plans that deviate more from reliance on fossil-based conventional power plants to embracing renewable energy. It is, therefore, necessary to ensure that these renewable energy power systems, including wind power systems, are grid compliant. For wind power systems, this is necessary to ward off the likelihood of instability in the wind power system. Unlike conventional power plants, wind power plants operate using wind generators that are either induction generators or synchronous generators [7]. The DFIG and FSIG are the most commonly used induction generators in a wind power system while the PMSG is the most popular synchronous generator associated with wind energy applications. Each of these generator topologies creates different opportunities and challenges for the grid.

The FSIG system is popular in wind power systems especially in standalone power systems due to its simple construction, cost, and ruggedness [8]. However, the drawback of this wind generator is its inability to effectively control reactive power and poor fault-ride through capability under grid fault conditions [9]. When a grid fault occurs, its rotor deviates from synchronous speed, resulting in the consumption of large amounts of reactive power at the stator terminal of the wind generator. This leads to a grid voltage degradation during post-fault recovery and can result in cascaded tripping causing the entire wind farm to disconnect from the grid [10]. To solve this problem, the generator terminals of the WT are connected to capacitor banks to provide the needed reactive power [11], [12]. Since wind speed is intermittent, this approach cannot keep the terminal voltage of the WT generator constant.

Power systems operators have revised grid code regulations to accommodate the need for reactive power support in the FSWTs. These regulations require that wind generators contribute to power

control and stay grid connected during a network disturbance, which may occur due to fault conditions. The result of these revisions is the technical improvements in wind technologies that have resulted in a migration from the FSWT to the VSWT. Irrespective of this technical migration in wind power systems, the FSWT still represents a considerable percentage of globally installed WTs. The FSWT market share is still projected to grow at a compound annual growth rate (CAGR) of 3.3% between 2021 and 2026 [13]. This implies that despite this technical migration to the VSWT wind systems, a considerable percentage of globally installed WTs are FSWTs [8]. Furthermore, some WT manufacturers have introduced life expansion programs for these FSWTs to increase their operating life to as much as thirty years [14]. There is therefore a need to improve the operating conditions of these WTs.

The DFIG based WTs are currently dominating the WT markets due to their varied-speed operation, as well as the flexible control of reactive power. The DFIG-based WT system has been touted as a viable solution for stability in wind farms [14], [15]. Though the DFIG-WTs enjoy the dominance in the wind market, the PMSG-based WT system is becoming more attractive for wind turbine systems [16]. The fully rated power electronic converters permit flexible control of active and reactive power and have a strong FRT ability during grid fault conditions. Its fully rated power converter ensures that disturbances on the grid do not have a direct effect on the WT generator by totally decoupling the generator from the grid during a range of grid disturbances. In comparison to the DFIG, the PMSG has higher efficiency, and its power converters can be used to enhance the voltage stability, and provide the required reactive power needed by a nearby FSWT wind farm during a grid fault occurrence [17], [18]. This is realized by coordinated control of the power converters, automatically changing the control priority of the GSC to voltage control rather than voltage control of the dc-link [19]. With this approach, the GSC capacity of the PMSG can improve

the voltage stability of both WTs when a grid fault occurs. In steady-state, the control method ensures the PMSG-WT operates efficiently and reliably. This invariably improves the overall efficiency of the wind power system and reduces the investment cost.

## 1.3. Purpose and contribution of Thesis

This research work firstly provides a detailed review of existing FACTS devices used in the compensation of reactive power in FSWT-based wind power systems. The STATCOM has emerged as the favourite FACTS device for the compensation of reactive power in fixed-speed wind systems [21]. However, a major setback of the STATCOM is the arbitrary allocation of reactive current in compensating for reactive power, which invariably leads to overcompensation of the wind power system and increases the cost of reactive power compensation.

To solve this problem, this thesis, therefore, explores the characteristic of the PMSG, which allows it to support a nearby wind farm operating with a FSIG. The GSC of the PMSG is controlled to act as a STATCOM. A novel reactive current allocation method for the GSC of the PMSG is proposed to support and provide the required reactive power needed for the FSIG wind system. The proposed current allocation strategy is developed bearing in mind the current capability and converter capacity of the GSC of the PMSG wind system, this is important to avoid overcompensation. The proposed strategy solves the problem of over-compensation that occurs in the STATCOM during the process of reactive power compensation and voltage support in the FSIG based wind system when a grid fault condition occurs.

Based on the characteristic of the PMSG wind power system, a hybrid wind system is designed and developed. The designed hybrid wind farm consists of the PMSG and FSIG-based wind system, and the proposed current allocation method is implemented in a coordinated control strategy that

supports the provision of the required reactive power demand of the FSWT wind system during the occurrence of the fault condition. In this thesis, the GSC of the PMSG is modified and controlled for voltage unbalance compensation.

This strategy not only eliminates the need for an additional external support device like the STATCOM in a FSIG- wind system, it also improves the grid voltage condition of the hybrid-wind power system. The proposed coordinated control strategy can be applied to existing wind farms operating with FSWTs whose operational lives are to be extended and can be further applied to new wind farm installations with the FSWTs.

## 1.4. Research Hypothesis and Questions

This research seeks to test the following hypothesis:

**The hybrid operation of the PMSG and FSIG- based wind power system can compensate for the reactive power challenges associated with the FSIG-based wind power system, improving its power output and the grid voltage of the hybrid wind power system.**

The validity of the above hypothesis is tested by investigating the following research questions

1. What are the advantages or limitations of the different wind turbine systems?
2. Why is reactive power compensation and voltage support in the FSIG based WT systems needed and what devices are used for providing voltage and reactive power support in the FSIG? Are there any limitations to these devices?
3. Can wind farms be hybridized for improved dynamic performance?
4. What are the possible hybrid wind farm configurations?
5. How can the answers to Q3 and Q4 be used in mitigating the limitations of the FSIG based WT?

6. What capacity of the PMSG can stabilize the FSIG based WT?
7. Is the proposed PMSG scheme able to stabilize the hybrid wind farm under different transient conditions?

## 1.5. Research methodology

To be able to carry out this research, the following approaches will be adopted:

1. A detailed literature review of all concepts relating to wind turbine technology and wind energy integration will be conducted.
2. The aggregate modelling approach is used during this research. This modelling approach is preferred over the detailed modelling approach because unlike the detailed modelling approach, it significantly reduces time spent on simulations without compromising the validity of results obtained.
3. The entire wind turbine systems will be mathematically modelled using the voltage equations of the individual wind generators and the proposed hybrid topology will be designed and simulated using the Simulink power system environment of MATLAB.
4. A reactive current allocation method is developed for the compensation of the required reactive power in the FSIG based wind farm during a grid fault condition.
5. The reactive current allocation strategy is applied in designing a control strategy for the hybrid wind farm to support the FSIG-wind power system.

## 1.6. Thesis Outline

The rest of this thesis is organized as follows:

**Chapter 2** gives an overview of WT systems. The principles of extracting power from the wind are presented, followed by the mathematical modelling of the various components of the WT system. This Chapter also gives a detailed review of both the FSIG and PMSG wind power systems.

**Chapter 3** discusses voltage stability and reactive power support in the FSWT power system, the different devices available for reactive power and voltage support are discussed.

**Chapter 4** introduces the concept of hybrid wind systems for improved voltage stability. The individual wind farms making up the hybrid wind farm are then mathematically modelled.

**Chapter 5** presents the development of the proposed hybrid solution in the FSIG-based wind system.

**Chapter 6** discusses the simulation protocol, simulation results, and discussion of the simulation results.

**Chapter 7** concludes this thesis by presenting a summary of the research. The contribution of this research to academic knowledge is also highlighted.

## 1.7. Research Outputs

**The refereed peer-reviewed conferences from this thesis are:**

**C1. O. Apata** and D. T. O. Oyedokun, "Improving The Dynamic Performance Of Grid Connected Fixed Speed Wind Farm Using Variable Speed Wind Turbines," 2020 IEEE PES/IAS Power Africa, Nairobi, Kenya, 2020, pp. 1-5, DOI: 10.1109/PowerAfrica49420.2020.9219955.

**C2. O. Apata** and D. T. O. Oyedokun, "A Mathematical Approach To Hybrid Wind Farm Modelling," 2020 IEEE PES/IAS PowerAfrica, Nairobi, Kenya, 2020, pp. 1-5, DOI: 10.1109/PowerAfrica49420.2020.9219918.

**C3. O. Apata** and D. T. O. Oyedokun, "Impact Of StatCom On Voltage Stability Of Fixed Speed Wind Farms," 2020 IEEE PES/IAS PowerAfrica, Nairobi, Kenya, 2020, pp. 1-5, DOI: 10.1109/PowerAfrica49420.2020.9219989.

**C4. O. Apata** and D. T. O. Oyedokun, "Novel Reactive Power Compensation Technique for Fixed Speed Wind Turbine Generators," 2018 IEEE PES/IAS PowerAfrica, Cape Town, 2018, pp. 628633, DOI: /10.1109PowerAfrica.2018.8521131.

**C5. O. Apata** and D. T. O. Oyedokun, "Wind turbine generators: Conventional and emerging technologies," 2017 IEEE PES PowerAfrica, Accra, 2017, pp. 606-611, DOI: 10.1109/PowerAfrica.2017.7991295.

**The refereed peer-reviewed journals from this thesis are:**

**J1. Apata, O**., and D. T. O. Oyedokun. "An Overview of Control Techniques for Wind Turbine Systems." DOI 10.1016/j.sciaf.2020.e00566, Elsevier Scientific African Journal.

# Chapter 2

# Wind Power System

A review of WT systems is presented in this Chapter. The horizontal and vertical-axis WT systems are discussed while the basic principles of extracting wind power are presented. The control of WT systems is also examined. The different WT topologies available for wind power systems are explored, and the chapter concludes with an introduction to WT power converter topologies.

## 2.1. Wind Turbine Systems

There are various criteria for classifying WT systems. One of such classifications is according to the rotational axis of the turbine blades. Based on the axis of rotation, WTs are designed with a vertical or horizontal axis rotation. However, in today's wind energy market, most grid-connected WT systems have a horizontal axis rotation [22]. Figure 2.1 gives a pictorial representation of both the vertical and horizontal axis WT system.

The main advantage of a WT with vertical axis rotation is the prospect of easily servicing the turbine machinery in the nacelle since they can be located on the ground. With vertical axis rotation, the yaw control of the WT is not required to keep the WT facing into the wind. Since this WT type does not have to face the right wind direction, it can be used in generating wind power in both gusty winds and steady wind conditions. The vertical axis WT however has its disadvantages. It cannot harness the higher wind speeds associated with higher levels since the vertical WTs are usually closer to the ground level. The airflow at ground level can increase the vibration on the turbine blade as a result of increased turbulence, resulting in increased maintenance costs.

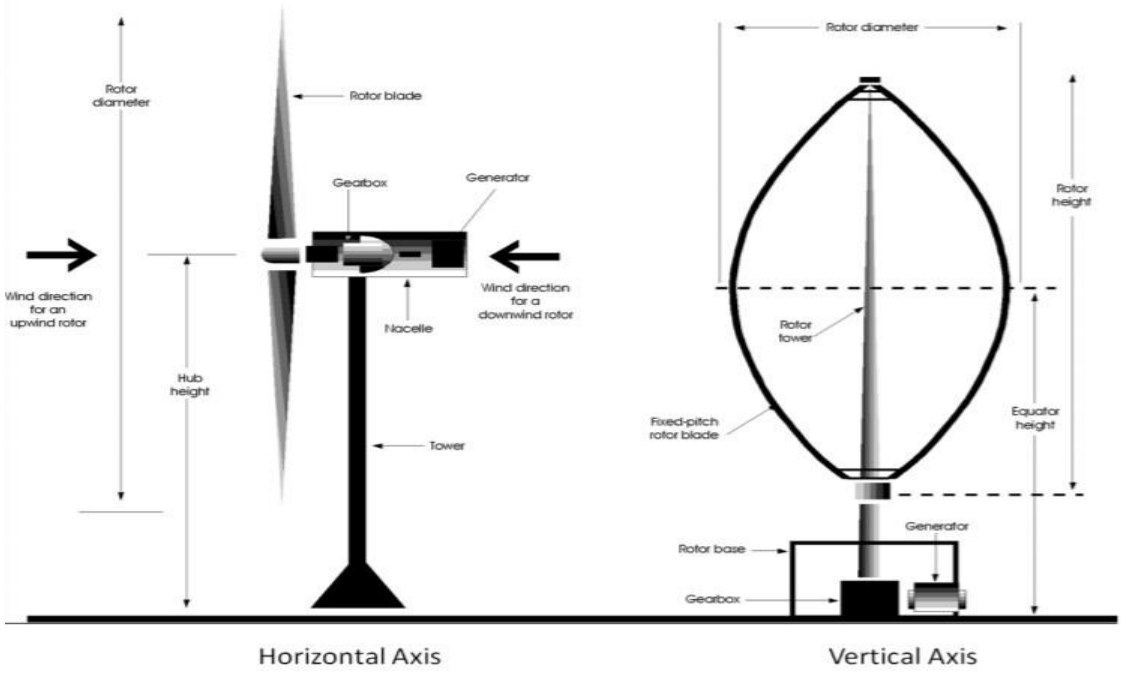


Figure 2.1. Horizontal and vertical axis wind turbine [23]

The horizontal axis WT is further classified as upwind or downwind. The upwind horizontal WT operates more smoothly and delivers more power than the downwind WT. However, the major drawback of the upwind-horizontal axis WT is the complexity of the yaw control system required to keep the turbine blades facing the wind. Most horizontal WTs are upwind. The downwind horizontal WT has the advantage of naturally orienting itself correctly to the wind direction. The disadvantage of the downwind horizontal WT is the increased possibility of blade noise and a reduction in power output due to flexing of the WT blades.

Various sub-units make up a WT system as shown in Figure 2.2. Most WTs have either two or three blades that rotate with corresponding wind speed. An anemometer measures the wind speed while the data obtained from the wind speed is transmitted to a controller. The wind vane measures

the direction of the wind, communicating with the yaw drive. The brakes can stop the rotor of the WT in emergencies mechanically, hydraulically, or electrically.

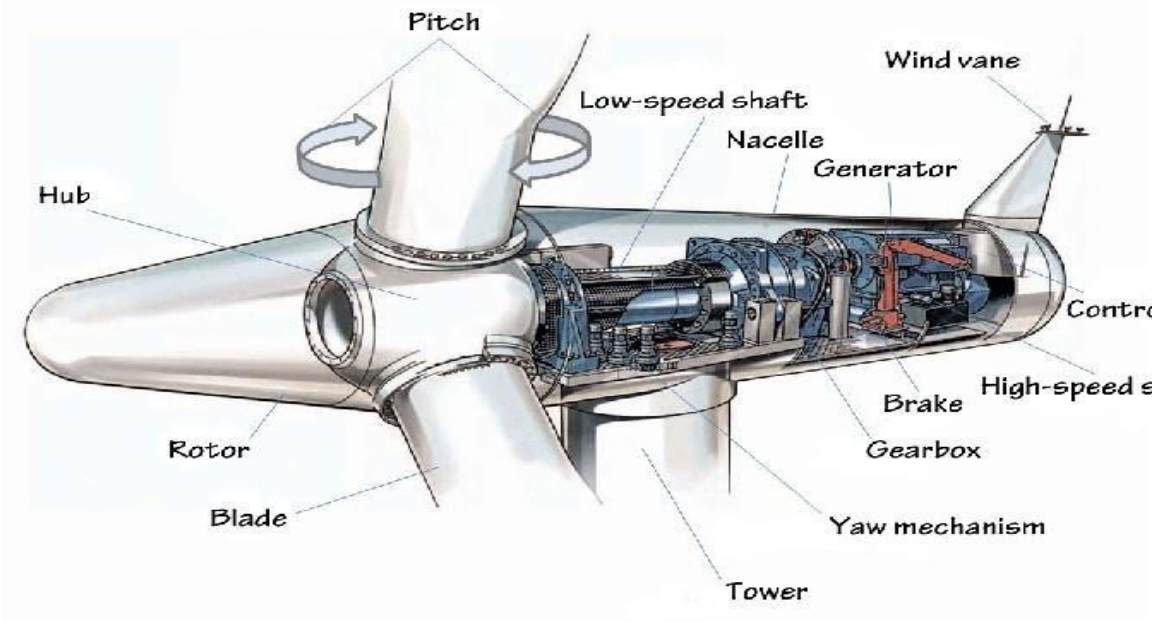


Figure 2.2. Wind turbine system [24]

## 2.2. Wind Power

The speed of the wind is a very important factor to consider in determining the amount of wind power available in a wind power system. Since wind speed is dependent on environmental factors, varies considerably, and behaves in a stochastic manner, it is modelled as a stochastic process. However, in analyzing the operation of the WT in a wind power system, wind speed variation is modelled as a summation of harmonics in the 0.1Hz to 10Hz range. As the rotor blades of the WT begin to rotate with a corresponding increase in wind speed, a drag force, and an aerodynamic lift is created on the blades of the rotor by the force of the wind, producing a torque on the WT rotor.

To understand the fundamentals of wind power technology, it is important to have a basic understanding of the theory behind the extraction of wind energy.

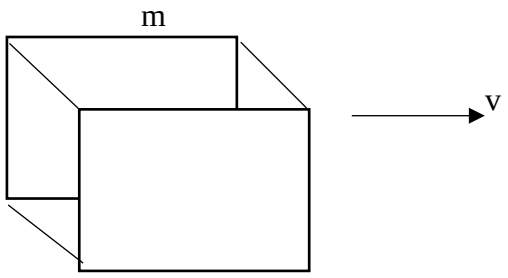


Figure 2.3. Packet of air

It is assumed that Figure 2.3 is a "box" of air whose mass $m$ is travelling at a speed $v$. Its kinetic energy $E_k$ is represented as

$$0.5\ m\ v^2 \tag{2.1}$$

Since power can be expressed in per unit time of energy, the power flow in the mass of air travelling with velocity $v$ over an area A, represented in Figure 2.4, will be

$$\text{Energy / Time} = 0.5\left(\frac{mass}{time}\right)v^2 \tag{2.2}$$

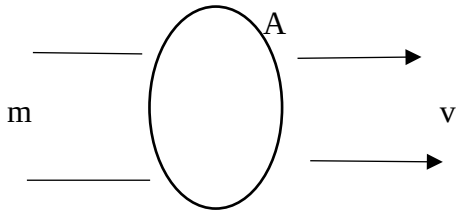


Figure 2.4. Mass of air

The rate of mass flow m through A is expressed as the product of air density ρ, speed v, and cross-sectional area $A$ as shown in (2.3)

$$m = \rho A v \tag{2.3}$$

combining (2.2) and (2.3), the power in wind $P_w$ is derived as represented in (2.4)

$$P_w = 0.5\,\rho A v^3 \tag{2.4}$$

It is seen from (2.4), that there is a direct relationship between the power in the wind and the area swept by the WT rotor.

The output power of a WT can be studied by observing the WT stream tube shown in Figure 2.5 [22]. The wind velocity through the rotor blades plane is given as $v_b$, the undisturbed wind upwind velocity is v, and $v_d$ represents the downwind velocity, m is the rate of the mass flow of air in the tube and remains the same everywhere within the stream tube.

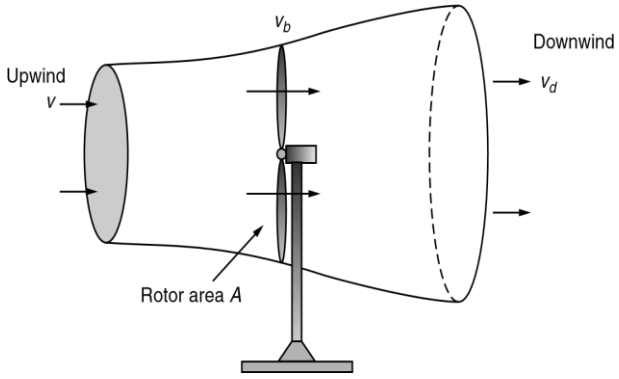


Figure 2.5. Wind turbine wind stream [22]

The differential in kinetic energy between upwind and downwind airflows is equal to the power extracted by the WT blades $P_{wt}$ represented by (2.5) and given as

$$P_{wt} = 0.5m\,(v^2 - v_d^2) \tag{2.5}$$

Assuming the average of both upwind and downwind airflows is the wind velocity through the plane of the rotor, equation (2.5) is re-written as

$$P_{wt} = 0.5\ \rho\ A\left(\frac{v+ v_d}{2}\right)(v^2 - v_d^2) \tag{2.6}$$

For simplicity, the downstream-upstream wind speed ratio is defined as λ:

$$\lambda = ({}^{V_d}/_{V}) \tag{2.7}$$

(2.7) is substituted into (2.6) to give

$$P_{wt} = 0.5\ \rho\ A\left(\frac{v + \lambda v}{2}\right)\left(v^2 - v_d^2\right)$$

$$0.5\ \rho\ Av^3.\ [0.5\ (1+\lambda)(1-\lambda^2)] \tag{2.8}$$

$0.5\ \rho\ Av^3$and $[0.5(1+\lambda)(1-\lambda^2)]$represents wind power and the fraction of wind power extracted respectively. The fraction of wind power extracted is a function of the WT rotor efficiency, represented as $C_p$.

$$\text{Rotor efficiency} = C_p = C_p = 0.5\ (1+\lambda)(1-\lambda^2) \tag{2.9}$$

If (2.9) is substituted into (2.8), the power delivered by the WT rotor is expressed as

$$0.5\ \rho\ Av^3.C_p \tag{2.10}$$

The value of $C_p$ can extend to 0.593 or 59.3 %. This coefficient is referred to as the *Betz coefficient* [25]. Due to the frictional losses caused by WT blade surface roughness and the continuous change in wind speed, an ideal WT would extract less than that fraction of wind power. Under optimal wind conditions, a good fraction will be between 35% - 40 % [25]. For a given wind speed, the rate at which the rotor turns is an indication of the level of the rotor efficiency. A very slow movement of the rotor might be an indication of a drop in efficiency because the blades would be allowing a lot of wind to pass by unaffected. If the rotor turns very quickly, the blades will

experience turbulence that will also affect the rotor efficiency. The rotor efficiency of the WT is usually expressed as a derivative of its tip-speed ratio (TSR) λ. The pitch angle β and tip speed ratio λ of the WT determine the $C_p$ values based on the WT characteristics. The relationship between λ, β and $C_p$ is therefore given as

$$C_p(\lambda, \beta) = c_1 \left( {}^{c_2}/_{\lambda_1} - c_3\beta - c_4 \right) e^{\frac{-c_5}{\lambda_1}} + c_6\lambda \tag{2.11}$$

$$\lambda = \frac{\omega_r R}{U_w} \tag{2.12}$$

$$\frac{1}{\lambda} = \frac{1}{\lambda - 0.8\beta} - \frac{0.035}{\beta^3 + 1} \tag{2.13}$$

$c_1$ to $c_6$ represent the characteristic coefficients of the WT, the WT rotational speed is represented by $\omega_r$, expressed in rad/sec. It should be noted that the values of $c_1$ to $c_6$ are dependent on the various wind turbine design. For this thesis, the values of $c_1$ to $c_6$ are expressed by the following figures as given in [26]: $c_1$ to $c_6$, are expressed by the following figures:

$c_1$= 0.5176, $c_2$ = 116, $c_3$ = 0.4, $c_4$ = 5, $c_5$ = 21 and $c_6$= 0.068

Since the coefficient of power $C_p$ represents a fraction of the power extracted from the wind by the WT, the actual output mechanical power of the WT is expressed as:

$$P_{wt} = 0.5\, \rho\, \pi R^2\, C_p(\lambda, \beta)\, v_w^3 \tag{2.14}$$

ρ defines air intensity and the radius of the rotor is given by R.

## 2.3. Wind Turbine Drive Train

The components of the WT drive train include the wind generator, a rotor shaft, a blade pitching system, a gearbox with brakes, and a hub with blades. Modelling of the WT drive train is done using either the one-lumped model or the model of the two-mass shaft [26], [27]. The modelling approach adopted for the drive train of any WT system is dependent on the complexity of the drive train itself. The one-lumped mass model is implemented when the WT drive train is focused on the interplay within the wind farm and AC grid [28], [29] while the two-lumped mass model is implemented for problems like torsional fatigue where the dynamics of all parts of the WT system is to be considered. Though the one-mass lumped model can be considered for modelling simplicity, taking into consideration all the rotating parts of the wind turbine train, this thesis adopts the two-mass model for a proper analysis of severe disturbances in the power system. Based on the equations of rotational motion, the two-mass model drive train is described by equations (2.15 – 2.18) [30] and further highlighted in [31]

$$\frac{d\omega_m}{dt} = \frac{T_m - T_e}{J_m} \tag{2.15}$$

$$\frac{d\omega_{turb}}{dt} = \frac{T_{turb} - K_s\gamma}{J_{turb}} \tag{2.16}$$

$$\frac{d\gamma}{dt} = (\omega_{turb} - \omega_m) \tag{2.17}$$

$$T_m = K_s\gamma - D_{turb}\,(\omega_{turb} - \omega_m \tag{2.18}$$

Where $T$ is torque, $\gamma$ represents angular displacement between the two ends of the shaft, the inertia is given as $J$ and $K_s$ represents the stiffness of the shaft while the subscripts $r$, $m$, and $e$ represent

the wind turbine rotor, the generator mechanical and generator electrical, respectively. Fig 2.6 shows the two-mass wind turbine drive train model implementation in the Simulink environment.

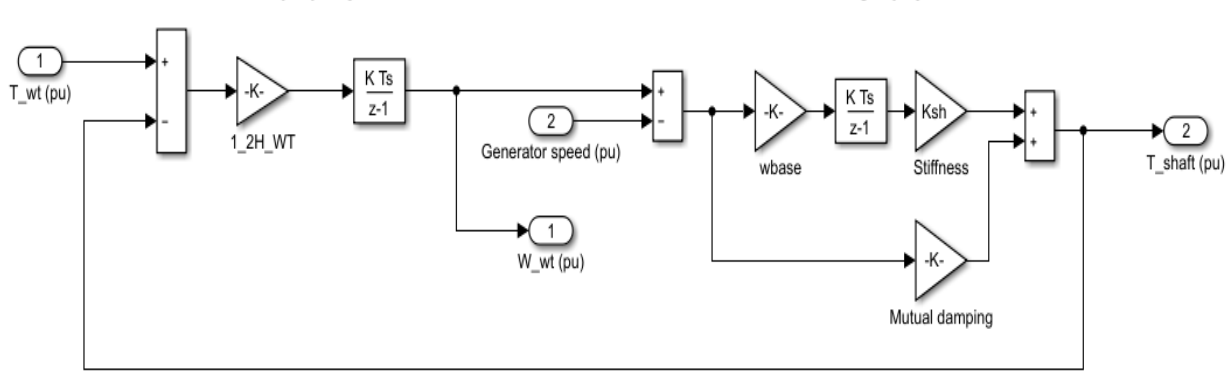


Figure 2.6. Two-mass wind turbine drive train modelled in Simulink environment

## 2.4. Wind Speed Model

To model the wind speed, a flexible modelling approach is used to generate low and high wind speed sequences, creating the possibility of simulating wind speed sequences alongside their desired characteristics. In modelling the wind speed, an assumption has been made that wind speed has four parts [32] namely:

- the average value, $v_{wa}$
- the gust component which represents wind gust, $v_{wg}(t)$
- the turbulence component, $v_{wt}(t)$
- the ramp, representing a steady increase in the speed of wind, $v_{wr}(t)$

Based on [32], the speed of wind at any given time $(t)$ is therefore represented as

$$v_w(t) = v_{wr}(t) + v_{wt}(t) + v_{wa} + v_{wg}(t) \quad (2.19)$$

The ramp component is $v_{wr}(t)$, the turbulence component is $v_{wt}(t)$, the average wind speed is given as $v_{wa}$ and $v_{wg}(t)$ is a gust component of the wind speed. The various components of the wind speed model are all measured in $m/s$. Equations (2.20 – 2.23) The ramp component consists of three parts: the starting time $T_{sr}(s)$, end-time $T_{er}(s)$ and amplitude $A_r(m/s)$. (2.20) describes the ramp component of wind speed.

$$t < T_{sr}, \text{ for } V_{wr} = 0;$$

$$T_{sr} \leq t \leq T_{er}, \text{ for } V_{wr} = A_r \frac{(t - T_{sr})}{(T_{er} - T_{sr})}; \tag{2.20}$$

$$T_{eg} < t, \text{ for } V_{wg} = A_r$$

The gust component comprises of the starting time $T_{sg}$, end time $T_{eg}$ and the wind speed gust amplitude, $A_g$ measured in m/s. The gust component is described in (2.21)

$$t < T_{sg}, \text{ for } V_{wg} = 0;$$

$$T_{sg} \leq t \leq T_{eg}, \text{ for } v_{wg} = A_g \{1 - \cos(2\pi \left(\frac{t - T_{sg}}{T_{eg} - T_{sg}}\right))\}; \tag{2.21}$$

$$T_{eg} < t, \text{ for } V_{wg} = 0$$

$$v_w(t) = v_{mw}(1 + \sum_k A_k \sin(\omega_k t)) + v_{wg}(t) \tag{2.22}$$

$v_{mw}$ is the mean value of the wind speed, amplitude of the $k_{th}$ harmonic is represented as $A_k$, $\omega_k$ is the frequency of $A_k$ and the wind gust is represented by $v_{wg}(t)$ modelled by the function:

$$v_{wg}(t) = {2v_{wgmax}}\Big/{1 + e^{-4(\sin(f_{wg}t) - 1}} \tag{2.23}$$

## 2.5. Wind Turbine Control

With the evolution of WT systems from simple designs to complex generation units, there is a need to design WT control systems that ensure the efficient operation of such WT systems [33]. The primary goals of WT control are grid integration stability, wind power maximization, and mitigation of both dynamic and static loads in the WT system [34]. Optimal control of the generator torque and pitch angle of the WT blade is a priority to achieve the above-mentioned control objectives. Improvements in power electronics systems have also played a significant role in WT control systems [35]. This thesis, therefore, utilizes the control of the WT power electronics interface.

The control technique used in a WT system depends on the design of the WT. This thesis has identified three control techniques available for WT systems. These are classified as:

- Passive-stall
- Active-stall
- Pitch-control

### 2.5.1. Passive Stall Control

Passive stall of WTs is a simple and low-cost control technique devoid of the intricacies of controlling WT systems and the rotating parts of the WT rotor [33]. With passive stall of WTs, the WT blades are usually connected to the hub at a fixed angle. This control method is usually executed in the FSWT system to prevent the WT from exceeding its rated power in high wind speed conditions. The setback of this control technique is poor power regulation of the WT due to the constrained operation. This control method is also very limited since it depends on the WT blades stalling naturally, this exposes the turbine blades to power fluctuations and torque spikes. Implementation of the passive stall in a WT system causes the output power of the WT to peak

slightly higher than its rated limit and then decreases to cut out speed. With this approach, the WT generator avoids overloading when the wind speed goes over the nominal values.

## 2.5.2. Active Stall Control

This control technique is designed to complement the setbacks associated with the passive stall control of the FSWT systems and is designed for larger WT systems with a rating of 1 MW and above [33]. FSWT systems operating in high-speed wind conditions can also be controlled by the active stall. Under low wind speed conditions, the WT blades are step-pitched to produce large torque. To avoid overloading the WT generator at rated power, the WT is controlled to increase the angle of attack of the rotor blades such that the blades go into a deeper stall to reduce the rotational speed and lift of the WT blades [32]. In comparison to passive stall, this control technique allows for flexible control of the output power of the WT, preventing it from overshooting its rated power at the beginning of a wind gust [36]. Also, with the active stall of WT systems, there is the possibility of operating the WT almost at rated power at all high wind speeds. This is a sharp contrast to the passive stall technique, where the WT experiences a drop in its electrical power output during higher wind speeds as the rotor blades go into a deeper stall.

## 2.5.3. Pitch Control of Wind Turbine

The output power of a pitch-controlled WT is sensed several times per second with the aid of electronic controllers that adjusts the WT rotor blades proportionately every time there is a change in wind speed. This ensures that the angle is kept at optimum and output power maximized. The turbine blades are pitched away from the wind by an electronic signal generated by the controllers when the power level of the WT exceeds the prescribed safe level. This process is reversed when the power level gets back to the prescribed safe level, at an optimal angle of attack, the turbine blades are turned back into the wind when the power level gets lower, to catch the wind. Figure

2.7 illustrates the power curve of a pitch-controlled WT system, represented as a function of wind speed.

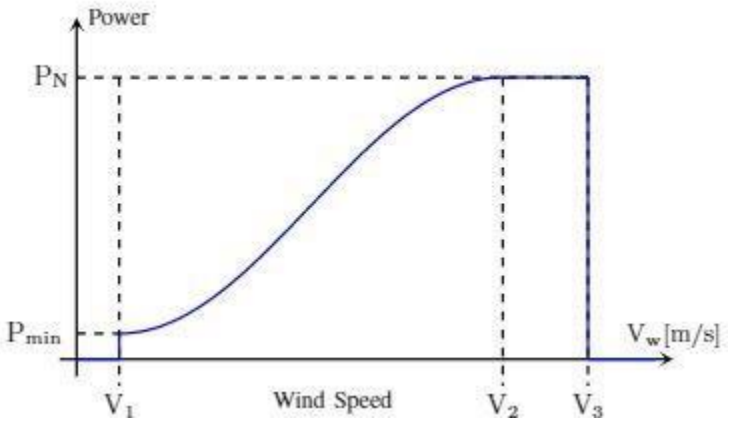


Figure 2.7. Pitch control of a WT

Electric power is produced at the cut-in wind speed $V_1$ and continues to increase with wind speed until it reaches the nominal wind speed $V_2$. Pitch control enables the WT to continue producing nominal power at wind speeds greater than $V_2$ also reducing the possibility of mechanical stress on the unity of the WT. The WT is turned off at wind speeds greater than the cut off speed $V_3$ to protect it from damages.

The pitch control of WTs can be achieved collectively, known as collective pitch control (CPC), or on an individual basis, known as individual pitch control (IPC) [37], [38]. The implementation of both control techniques is achieved using either an electric controller or a hydraulic controller [39].

The implementation of collective pitch control in a WT is achieved by applying the same control strategy collectively for the turbine blades of the wind power system [40]. Pitching of the turbine blades is executed the same way for all the turbine blades irrespective of the independent servomechanisms. CPC of WTs is dependent on traditional proportional-integral (PI) control laws

targeted at rotor speed regulation. Though the traditional implementation strategy for CPC is PI control with gain scheduling, the consistent need to reduce loads in the WT system has led to approaches that are more modern in CPC of WT systems. The setback of the CPC is the thinking that all the WT blades have the same physical characteristics therefore subject to the same aerodynamic load. This erroneous belief can expose the rotor disk of the WT to risks during an unbalanced load, inducing stress and an eventual failure of the WT.

IPC reduces the effect of mechanical loads on the WT by controlling the pitch angles of the WT individually. Though there has been a lot of research on IPC in the last decade, this control technique is yet to be implemented on a commercial scale in WTs. The belief is that this research area of WT control will produce validated results that will be implemented on a commercial scale with the next generation of WTs with larger and more flexible blades [41], [42]. IPC reduces fatigue damage in WTs, gives room for measuring variables like tower displacement, and is capable of reducing the load on the WT system [43], [44], [45]. The control target of IPC is the reduction of blade root moment or damping of structural modes by adjusting the WT pitch angle. As the name implies, each of these WT blades is individually controlled by using additional sensors. Since this control strategy requires the installation of extra sensors and individual pitch commands for each of the WT blades, the control system of the WT implementing IPC becomes a basic multiple-input-multiple-output (MIMO) system. A setback of the IPC control strategy is the reliability of the additionally installed sensors.

Most of the research on IPC is focused on reducing the load on the rotor blade of the WT using the Coleman transform [38] which expresses the rotor blade bending moment as a function concerning the fixed direct-quadrature (d-q) axes as shown in (2.24).

$$\begin{pmatrix} M_d \\ M_q \end{pmatrix} = {}^{2}/_{3} \begin{pmatrix} \cos(\psi) & \cos\left(\psi+\frac{2\pi}{3}\right) & \cos\left(\psi+\frac{4\pi}{3}\right) \\ \sin(\psi) & \sin\left(\psi+\frac{2\pi}{3}\right) & \sin\left(\psi+\frac{4\pi}{3}\right) \end{pmatrix} \begin{pmatrix} M_1 \\ M_2 \\ M_3 \end{pmatrix} \tag{2.24}$$

The rotor blade load represented by $M_1$,$M_2$, and $M_3$ is determined by estimation or detection. The rotor blade load is transformed into the orthogonal d-q axes signal namely $M_d$ and $M_q$. The Coleman transformation is inverted in (2.25) by transforming the d-q pitch angle $\beta_d$ and $\beta_q$ respectively into pitch angle increments $\Delta\beta_1$ , $\Delta\beta_2$ and $\Delta\beta_3$ for the three blades of the WT.

$$\begin{pmatrix} \Delta\beta_1 \\ \Delta\beta_2 \\ \Delta\beta_3 \end{pmatrix} = {}^{2}/_{3} \begin{pmatrix} \cos(\psi) & \sin(\psi) \\ \cos\left(\psi+\frac{2\pi}{3}\right) & \sin\left(\psi+\frac{2\pi}{3}\right) \\ \cos\left(\psi+\frac{4\pi}{3}\right) & \sin\left(\psi+\frac{4\pi}{3}\right) \end{pmatrix} \begin{pmatrix} \beta_d \\ \beta_q \end{pmatrix} \tag{2.25}$$

A block diagram of the individual pitch control of the WT system is shown in Figure 2.8; a summary of the three main control methods available to WT systems is presented in Table 2.1.

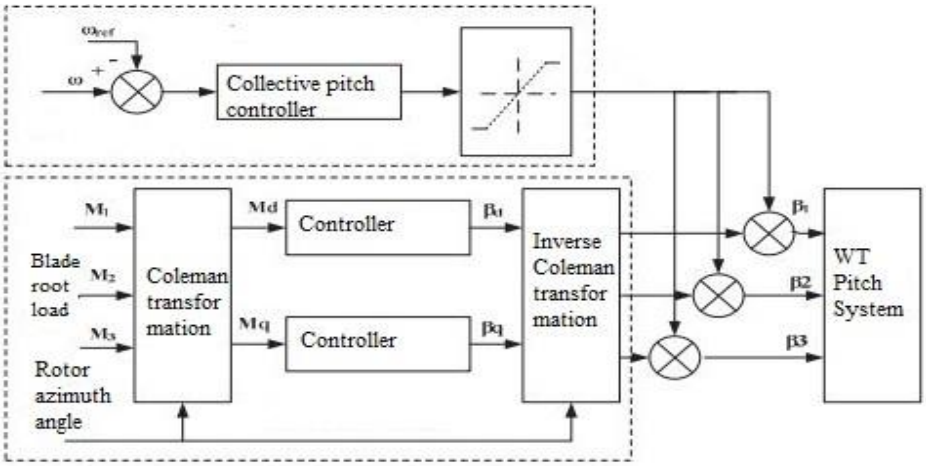


Figure 2.8. Block diagram of individual pitch control of WTs

Table 2.1. Wind Turbine control Techniques

| **Control method** | **Advantage** | **Disadvantage** |
|---|---|---|
| Passive stall | Simple and low complexity.<br>Low cost and cheaper than other control systems.<br>It is robust compared to the active stall and pitch control.<br>It has a faster response to wind gusts compared with other control systems. | Not suitable for large WTs.<br>It is less efficient at low wind speeds.<br>It causes variations in the maximum steady-state power as a result of variations in grid frequencies and air density. |
| Active stall | Higher power production compared to the passive control method as a result of the blade angle of the WT being optimized according to the wind speed.<br>Better and more accurate control of power output.<br>The ability to counteract power peaks very efficiently without a change in rotational speed.<br>Lower load and power peaks compared to pitch control. | Forced reduction of the generator speed to stall the rotor blades during an increase in wind speed. |
| Pitch control | Efficient power control.<br>Assisted start-up.<br>Emergency stop | High power fluctuations in high wind speed conditions. Extra complexities and increased costs. |

## 2.6. Wind Turbine and Generators

Electric power is produced in a wind power system when the WT blades convert the available energy in the wind into a rotating shaft power that spins the wind generator. The rotor is an important part of the wind generator, spinning inside a stationary housing referred to as the stator. The type of WT generator used is dependent on the type of the WT system. This thesis has broadly classified wind generator types into two categories namely the induction generators and the synchronous generators as illustrated in Figure 2.9. The induction generators can be either a FSIG, which is usually applicable in FSWT systems or the DFIG applicable to VSWT systems. The synchronous generator can either be a PMSG or the electrically excited synchronous generator (EESG) both applicable to VSWT systems.

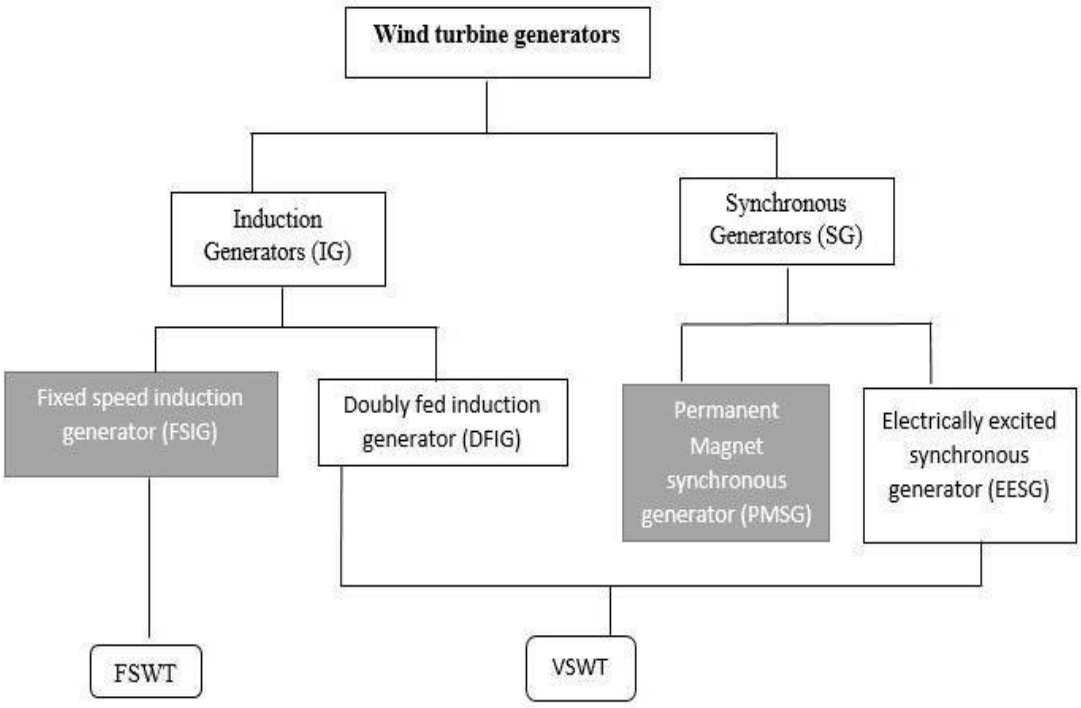


Figure 2.9. Classification of wind generators

The WT system can also be grouped into two categories based on rotational speed [32]. The design of the FSWT enables it to achieve maximal efficiency at a fixed speed while the VSWT adapts its rotational speed to the available wind speed for increased power production and achieving maximal efficiency within a wide radius of wind speed.

### 2.6.1 Fixed Speed Wind Turbine

The fixed-speed wind turbine has the advantage of being simple, robust and reliable. Though the DFIG and PMSG are the most commonly used in modern-day WT systems, the FSWT still accounts for a non-negligible amount of WT systems [10]. Figure 2.10 presents a schematic of a grid-connected FSWT while Figure 2.11 presents a generalized model of the FSWT. This WT system consists of subsystems such as the rotor, the wind generator, the drive train, and the wind speed model.

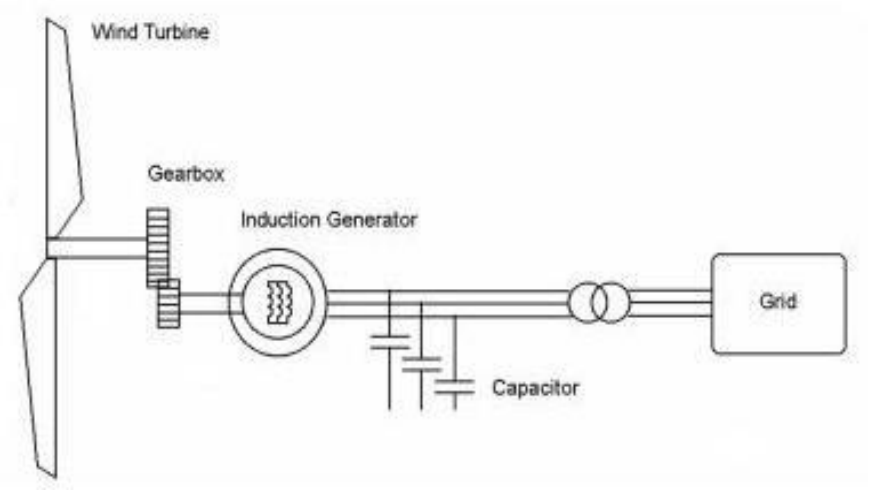


Figure 2.10. Schematic of a FSWT system

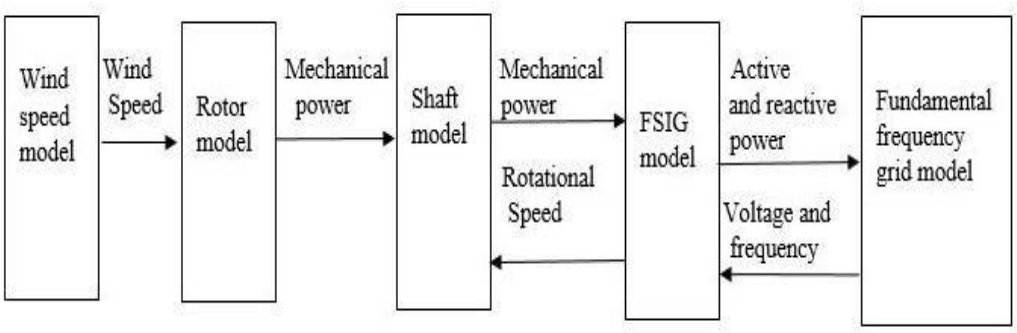


Figure 2.11. A generalized model of a FSWT- based wind system

The FSWT can deliver power directly to the grid by transforming the kinetic energy of the wind into mechanical energy, and further converting this into electric power. In comparison to the WT speed, the rotational speed of the FSWT is relatively high; therefore, the generator speed must be stepped down with the aid of a multiple-stage gearbox.

There is a unique relationship between the active power, reactive power, terminal voltage, and rotor speed of the FSWT. The implication of this is that when the WT produces more active power, the wind generator draws a large quantity of reactive power from the grid. Usually, the absorbed reactive power is not controllable because of its variability with the condition of wind.

In the absence of reactive power support for the FSWT-based wind system, the required reactive power is drawn from the grid. This can result in grid instability. To forestall this possibility of grid instability, capacitor banks are placed at the generator terminal of the WT. The installation of auxiliary hardware devices is also useful for compensating the reactive power needs of the FSWT. The major advantages of the FSWTs are the low investment and maintenance costs, simple design, and reliability. The disadvantages include its high mechanical stress during high wind speed conditions, low aerodynamic efficiency, difficulty in riding through a grid fault condition, and the requirements of reactive power support.

## 2.6.2 Variable Speed Wind Turbine (VSWT)

These classes of WTs are built for a wide range of rotor speeds. Based on their design specifications, the rotor speed varies with wind speed. In comparison to the FSWTs, the VSWT system can extract more energy from wind. The independent control of both active and reactive power by the VSWT wind system is a unique advantage over the FSWT-wind system. The DFIG and PMSG based WTs are the most popular VSWTs. This thesis however focuses on the PMSG-WT.

### 2.6.2.1 PMSG Wind Turbine

This WT type is shown in Figure 2.12. It uses a synchronous wind generator whose stator windings are grid-connected by a fully rated power converter and a permanent magnet excited rotor. The generator can function at very low speeds because of the presence of a large number of rotor mounted poles. Since the generator is directly coupled to the WT rotor, there is no need for a gearbox. Flexible control of active and reactive power is possible since it has fully rated power electronic converters; this enables the WT system to readily go through a grid fault condition without the need for external compensation devices by totally decoupling the generator from the grid during a range of grid disturbance.

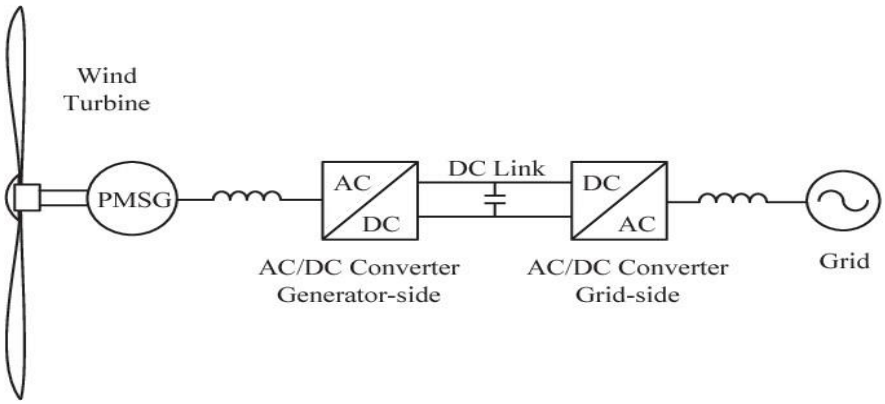


Figure 2.12. Grid-connected PMSG wind turbine system

The modelling of the various sub-systems of the PMSG-based WT has been described in [31] while [46] describes its electrical model. A generalized model of the PMSG wind system is represented in Figure 2.13. The flexible geometry of the PMSG is an added advantage that makes it possible to be operated in different topologies. These topologies are grouped based on the direction of flux penetration. These are transversal flux, axial flux, and radial flux [47]-[49].

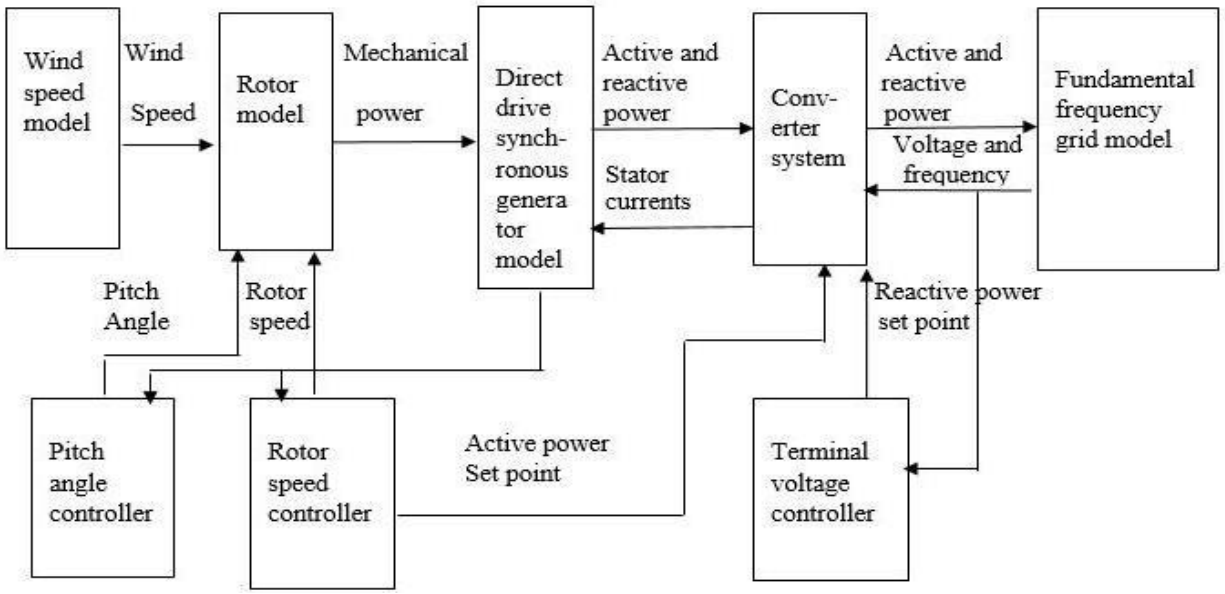


Figure 2.13. A generalized model of a PMSG wind system

## 2.6.2.2. DFIG Wind Turbine

The DFIG-WT system consists of partially rated power electronic converters and a multi-stage gearbox, the rotor is grid-connected by the power converters while the stator connects directly to the grid without any interface. The machine side converter of the WT system is connected to a crowbar for the protection of the converters as seen in Figure 2.14. A unique characteristic of this WT system is its ability to deliver wind energy at super-synchronous and sub-synchronous speeds.

The ideal variable speed range of the DFIG wind system is about 30% of synchronous speed, and its nominal converter power is only 30% of the rated WT power [50]. Pitch control is applied to keep output power to the rated power for wind speeds above rated power while the generator speed of the WT is regulated for optimal power extraction from the wind.

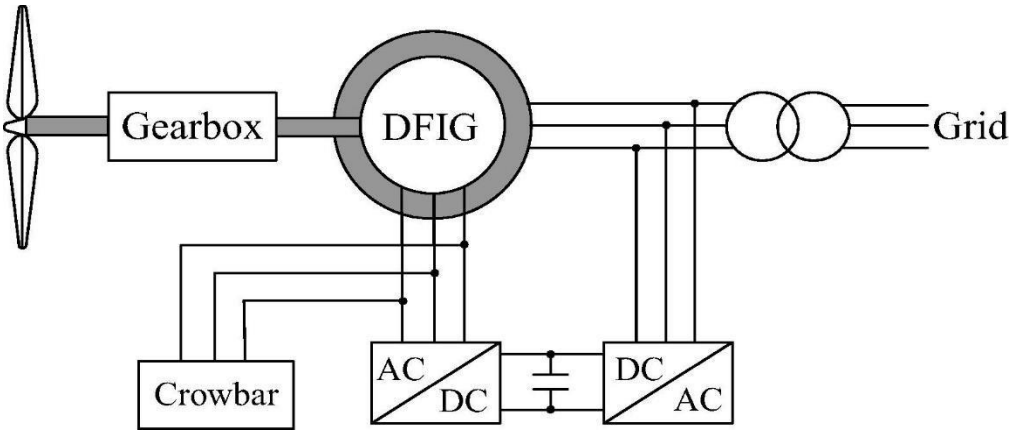


Figure 2.14. DFIG wind turbine system

The disadvantages associated with the DFIG-WT system include the need for frequent maintenance of the generator slip rings and brushes, increasing the risk of both electrical losses and machine losses. Another inherent setback of this wind system is the relatively weak fault ride-through capability, because of connecting the stator directly to the grid.

The Brushless-DFIG (B-DFIG) has been proposed as a better alternative to the DFIG wind system. Though it operates with the same characteristics like the conventional DFIG, the B-DFIG is more robust and reliable due to the absence of brush gears and slip rings [10]. The brushless nature of the B-DFIG is what gives it the added advantage over the conventional DFIG making it more suitable for offshore wind application.

## 2.6.2.3. Wind Turbine Power Converters

The power converters in a wind system make provision for an AC-DC-AC connection in the WT system. The advantages of this connection are but are not limited to frequency and voltage control of the local grid, better grid integration of wind energy, and improvement of power quality [51]. The commonly used types of power converters for the PMSG wind system in wind energy applications are the two-level and three-level converters [52], [53], [54], both consisting of a common DC link circuit and a two-three phase pulse width modulation (PWM) converters.

The two-level converter comprises a power circuit with three-phase back-to-back voltage source converters connected by a DC capacitor as illustrated in Figure 2.15. The three-phase input voltages from the stator side converter are converted into a DC voltage $V_{dc}$ that provides the input voltage to the grid side converter. The output voltages of the grid side converter are represented as $V_{ga}$, $V_{gb}$ and $V_{gc}$ in Figure 2.15. Table 2.2 illustrates the switching state and input voltages of the two-level converter.

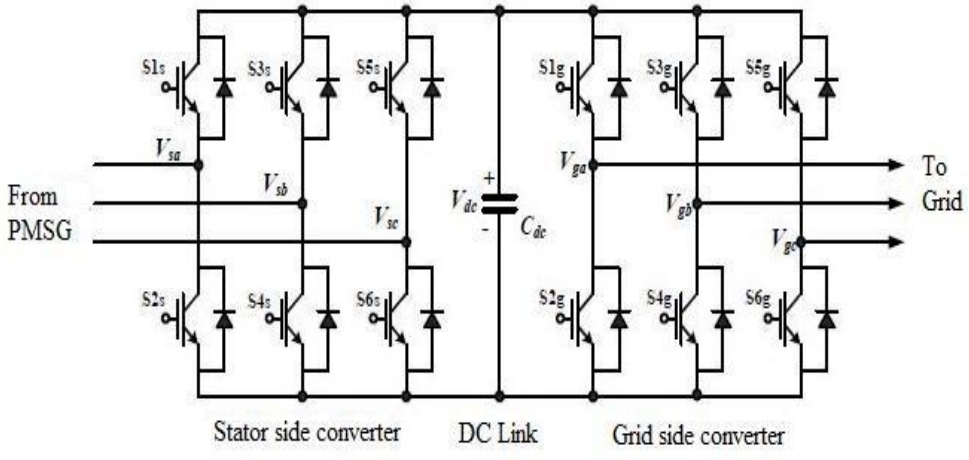


Figure 2.15. The two-level converter circuit configuration

Table 2.2. Two-level converter-switching states

| **Input Voltage** | **Switching states (S)** | | | | | |
|---|---|---|---|---|---|---|
| | 1 | 2 | 3 | 4 | 5 | 6 |
| $+V_{dc}/_2$ | 1 | 0 | 0 | 1 | 0 | 0 |
| $+V_{dc}/_2$ | 1 | 0 | 0 | 0 | 0 | 1 |
| 0 | 0 | 0 | 1 | 0 | 0 | 1 |
| $-V_{dc}/_2$ | 0 | 1 | 1 | 0 | 0 | 0 |
| $-V_{dc}/_2$ | 0 | 1 | 0 | 0 | 1 | 0 |
| 0 | 0 | 0 | 0 | 1 | 1 | 0 |

Figure 2.16 shows the three-level power converter made up of two converters, neutral point clamped and linked by DC capacitors. Each of the converters uses six diodes and twelve switches. The switching pulses are generated for the converters by measuring the carrier waves at the fundamental frequency. The switching states of the three-level converter are described in Table 2.3.

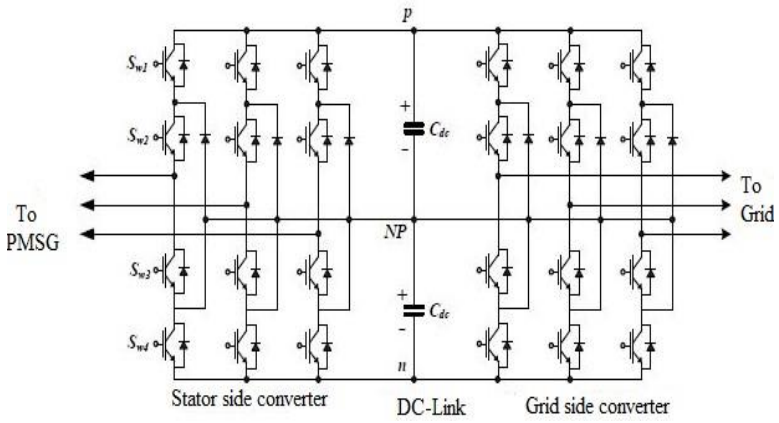


Figure 2.16. A three-level back-to-back converter circuit configuration

Table 2.3. Three-level converter-switching states

| **Input Voltage** | **Switching state (S)** | | | |
|---|---|---|---|---|
| | 1 | 2 | 3 | 4 |
| $V_{dc}/2$ | 1 | 1 | 0 | 0 |
| 0 | 0 | 1 | 1 | 0 |
| $-V_{dc}/2$ | 0 | 0 | 1 | 1 |

# 2.7. Chapter Summary

This chapter has presented an introduction to WT systems, classifying them into two groups namely, horizontal- and vertical- axis WTs depending on the rotation axis of the turbine blades. Thereafter the theory of energy extraction from wind is presented. This chapter also presents a review of wind generators for WT systems and the focus of this thesis is the FSWT and PMSGWT. The advantages and disadvantages of each of these WT generator types are well researched in [55][56] while the performance comparison of the various WT systems has been reviewed in [10]. Though the FSWT is regarded as an old WT technology, it still features prominently in several WT systems installed globally, with a projected compound annual growth rate (CAGR) of 3.3% between 2021 and 2026. Table 2.4 presents a technical summary of the various WT types.

There is no hard rule to deciding the appropriate control technique for a WT system, however, turbine technology and cost are critical deciding factors. Passive stall control has been implemented in first-generation FSWT wind systems, however, due to the inherent setbacks associated with this control technique, the active stall control technique was designed to cater to

the setbacks of passive stall control of WTs. From the available literature, pitch control of WT systems is proposed for higher efficiency and better performance.

Table 2.4. Technical summary of wind turbine systems

| **Wind Turbine Type** | **FSIG-WT** | **Variable speed DFIG-WT** | **Variable speed PMSG-WT** |
|---|---|---|---|
| **Wind Generator** | Fixed speed induction generator (FSIG) | Doubly fed induction generator (DFIG) | Permanent magnet induction generator (PMSG) |
| **Grid connection** | Direct grid connection by capacitor banks and a soft start | Partial scale converters | Full-scale converter |
| **Drive Train** | Gear | Gear | Gearless |
| **Blade Angle control** | Stall/Active stall control | Pitch angle control | Pitch angle control |

This chapter has established that the FSWT though still very much in use in WT systems, has a limitation of reactive power control and voltage support in grid fault conditions. This requires a need for external devices to provide the reactive power required by the FSWT during a grid disturbance.

Chapter 3 discusses the various devices available for providing the required voltage support and reactive power compensation in the FSWT wind system.

The major contribution of this chapter is the review of various WT- systems and the associated control techniques. These have also been published in the peer-review conference and journal paper listed below:

**Apata, Oluwagbenga, and D. T. O. Oyedokun. "Wind turbine generators: Conventional and emerging technologies." 2017 IEEE PES PowerAfrica. IEEE, 2017.**

**Apata, O., and D. T. O. Oyedokun. "An Overview of Control Techniques for Wind Turbine Systems." Elsevier Scientific African (2020): e00566**.

# Chapter 3

# Voltage Stability of Fixed Speed Wind Farms

The grid integration of FSWTs has created a few challenges for utilities concerning power quality, energy efficiency, and voltage stabilization. As seen in Chapter 2, the FSWT is grid-connected without a power electronic interface, and the wind generator consumes a lot of reactive power during and after a grid fault condition to remain connected to the grid. This can result in a disconnection of the wind power system from the grid if there is no external supporting device to provide the required reactive power. Various auxiliary devices have been proposed in different literature to tackle this problem. These devices are generally referred to as FACTS and are used as stabilizers to improve the power quality, support reactive power needs and improve voltage stability of grid integrated FSWT systems**.** This chapter, therefore, discusses the various FACTS devices available for reactive power support and improving the voltage stability of a grid-connected fixed speed wind turbine.

## 3.1. Need for Reactive Power Support

During a grid fault condition, the FSWT power system experiences a drop in grid voltage, this causes an unbalance between its output electromagnetic and input mechanical torque. This unbalance can result in the over-speeding of the wind generator rotor beyond its safety limits thereby losing stability and causing the wind farm to be disconnected from the grid. An increase in the rotor speed of the FSWT during a grid fault condition will mean the WT requires a large

amount of reactive power from the grid to stay connected. This can lead to voltage collapse in the power system. Because of the large consumption of reactive power from the grid, the wind power system will be unable to inject reactive power during the fault condition as required by the grid code. This deteriorates the voltage sag and worsens the voltage level across the network, making the restoration of the terminal voltage within an acceptable level difficult [57], [58].

A grid-connected WT system, without reactive power support, will disconnect from the grid when the terminal voltage falls below the specified voltage for LVRT. This can lead to severe voltage stability issues in the power system [58]. Voltage swells can also occur because of the disconnection of large amounts of load from the grid within a short period or during intermittent active power production. This voltage swell can also be a result of inefficient capacitor bank switching or reactive power sources.

To prevent disconnection of the WT system from the power system during a voltage sag or swell, grid operators have introduced stringent conditions known as grid codes for managing and control of reactive power. These codes provide detailed reactive power requirements the FSWT must fulfil. However, the requirements vary for the point of common coupling (PCC) and the voltage level at the PCC. Therefore, to fulfil the requirements of the grid code and ensure grid power stability, the wind generator must have proper reactive power support.

## 3.2. Reactive Power Support Devices

Reactive power support in FSWTs can be viewed from the aspect of load compensation and voltage support. Voltage support is required for reduction in voltage variations on the transmission line, while balancing the real power drawn from the ac supply requires load compensation, eliminating current harmonics, and increasing the system power factor. Several technologies have been

proposed for reactive power control and voltage stabilization in FSWTs [59], [60]. However, it is shown that the installation of these devices alongside the WT increases the overall cost of the wind power systems making it more expensive [60].

These devices are based on the concept of:

- Supplying localized capacitive or reactive current for the control of reactive power
- Injecting AC components in parallel or series with the nodes of the power network to create superimposed voltages or current flows.
- Modulation of impedance and apparent admittance (Y) at PCC.
- Switching or modulation of the equivalent driving point impedance (Z) by controlled switching at the interface bus.

The control strategies employed for these devices are based on power angle, voltage or reactive power flow control using the conventional proportional-integral-derivative (PID) controllers, heuristic soft computing control, multi-objective control performance index, and optimal control.

This thesis has classified the various FACTS devices into shunt compensation and series compensation techniques based on their connection configurations while other works of literature have included a third category of FACTS devices that are a combination of shunt and series connections. Examples of shunt compensation devices include the static synchronous compensator (STATCOM), static var compensator (SVC), and superconducting dynamic synchronous condenser (SDSC) while examples of series compensation devices include the dynamic voltage restorer (DVR), thyristor controlled series compensator (TCSC), fault current limiter (FCL), magnetic energy recovery switch (MERS) and the series dynamic braking resistor ( SDBR). These devices will be further described in detail in the next sections. The series and shunt compensation strategies are used in modifying the natural electrical characteristics of an ac power system. While

series compensation is used in modifying the distribution or transmission parameters, shunt compensation modifies the equivalent impedance of the load. Irrespective of the technique used, the control strategies of FACTS devices are all based on the control of reactive power, voltage, and power using the conventional proportional –integral- derivative (PID) controllers, heuristic control strategies, and/or a multiobjective control performance index. Figure 3.1 illustrates the conventional devices available for voltage support in FSWTs.

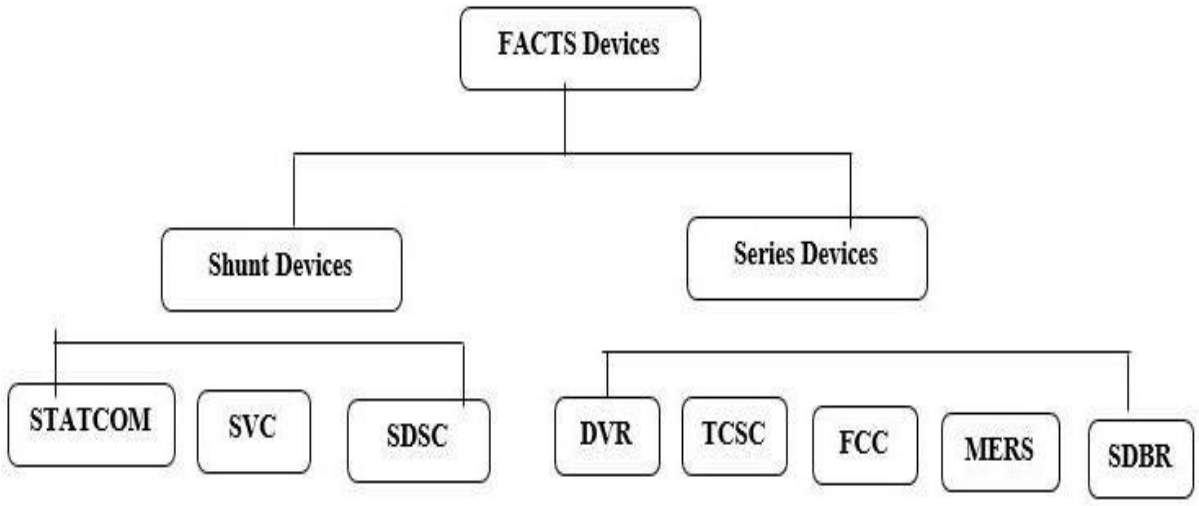


Figure 3.1. Reactive power support devices

## 3.3. Shunt Compensation Devices

Fast steady-state and transient voltage control can be provided for the FSWT wind power system using shunt compensated devices. Shunt compensation devices inject a current at the point of connection and control reactive power depending on the phase angle between line voltage and injected current. Shunt-connected devices have been proven to be the most effective solution for the FSWT system in fulfilling the grid codes. This is because the output current of these devices can be adjusted to control the reactive power injected at the voltage terminal [59].

In Figure 3.2, an electric power system requiring reactive power support is shown. It is assumed that the load is inductive and requires reactive power support for the power system to function properly. This is provided by the source that increases current from the generator through the power line. By minimizing the line current, power loss is reduced while voltage regulation improves with reactive power provided near the load. The supply of reactive power is achieved by using a capacitor, a current source, or a voltage source.

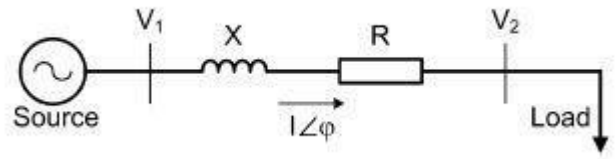


Figure 3.2. Radial ac system without reactive power compensation.

The load current reactive component ($I_Q$) is compensated for in Figure 3.3 using a shunt-connected current source. This reduces or almost eliminates the reactive current component from the source and improves voltage regulation in the system. The use of a voltage or current source var generator rather than capacitors or inductors provides an advantage of the generated reactive power being independent of the voltage at the point of connection.

Some of the commonly used shunt-connected solutions for reactive power and voltage support in the FSWT are discussed in the following subsections.

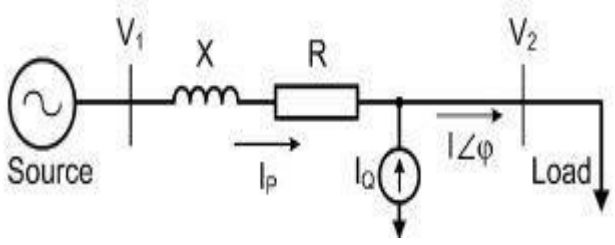


Figure 3.3. Shunt compensation using a current source

## 3.3.1. Static Synchronous Compensator (STATCOM)

The control system of the STATCOM is usually defined in the synchronous d-q axis to give effective and independent control of the DC voltage and reactive power of the STATCOM respectively. Figure 3.4 shows the STATCOM connected to the terminal of the FSWT wind system by a three-phase transformer. The control system is responsible for the operation of the STATCOM controller to improve the LVRT capability of the FSWT. The STATCOM provides grid voltage stability by responding to voltage reduction independently while continuously providing controllable reactive current $I_Q$.

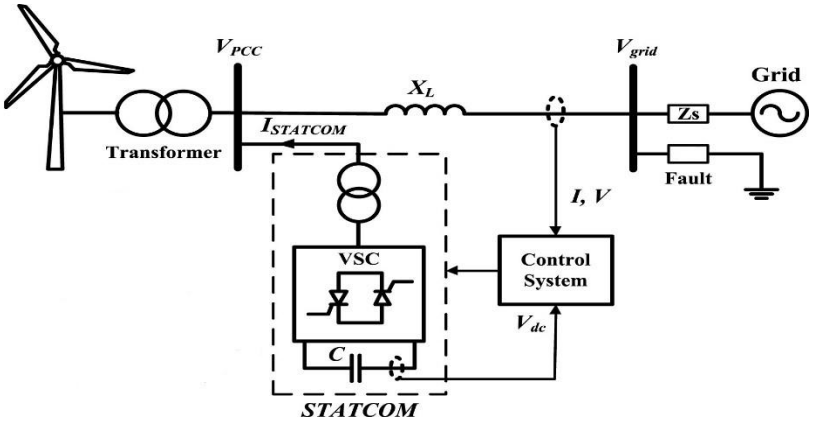


Figure 3.4. STATCOM connected to the terminal of an FSWT wind system

The STATCOM is based on a solid-state voltage source implemented with an inverter connected in parallel to the power system [61]. This device however has no overload ability and no inertia. The modular voltage source converter (VSC) of the STATCOM, fitted with pulse width modulated insulated gate bipolar transistors (IGBT) can be referred to as its most critical component. Various research has been carried out in literature to show the effectiveness of the STATCOM in improving the low voltage ride-through of the FSWT [62] – [69].

If the output of the STATCOM is greater than the line voltage, the VSC will inject lagging reactive power into the power system and in a situation where the line voltage is greater than the STATCOM output voltage, then the STATCOM absorbs the lagging reactive power from the system [61]. The voltage-current characteristics of the STATCOM is shown in Figure 3.5. Voltage regulation occurs at the point $V_{REF}$ provided the reactive current is within the range of the minimum and maximal current values imposed by the VSC rating. The voltage-current characteristic of the STATCOM is expressed as

$$V = V_{REF} + X_s I \tag{3.1}$$

Where V represents the positive sequence voltage (p.u), the reactive current measured in $(p.u/P_{nom})$ is represented as I, while the droop reactance or slope also measured in $(p.u/P_{nom})$ is represented by $X_s$.

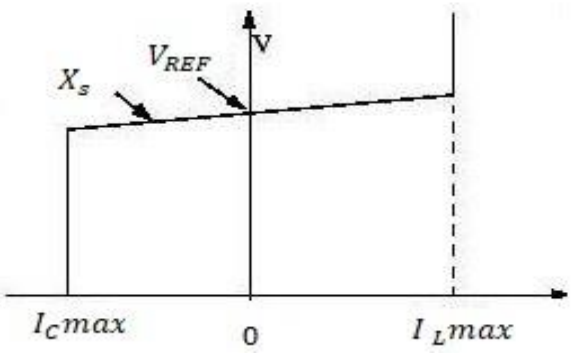


Figure 3.5. STATCOM V-I characteristics

## 3.3.2. Static Var Compensator (SVC)

The SVCs comprise capacitors and reactors that are controlled to provide variable and rapid reactive power, voltage support of critical loads, and improvement of transient stability in FSWT systems [70]. They are usually either a combination of at least two of a thyristor switched capacitor

(TSC), thyristor-controlled reactor (TCR), harmonic filter (HF), or a mechanically switched capacitor (MSC) that is connected to the WT terminal for fast voltage support. The combination of a TSC and TCR is the most common configuration of the SVC. Figure 3.6 shows a single line diagram of the SVC and its control block. A proportional-integral controller controls the firing angle of the thyristors of both the TSC and TCR to keep the voltage at PCC at 1 p.u during and immediately after a grid fault condition. Extensive research and discussions on the SVC as an auxiliary device for voltage support and improved FRT have been presented in [71] – [74].

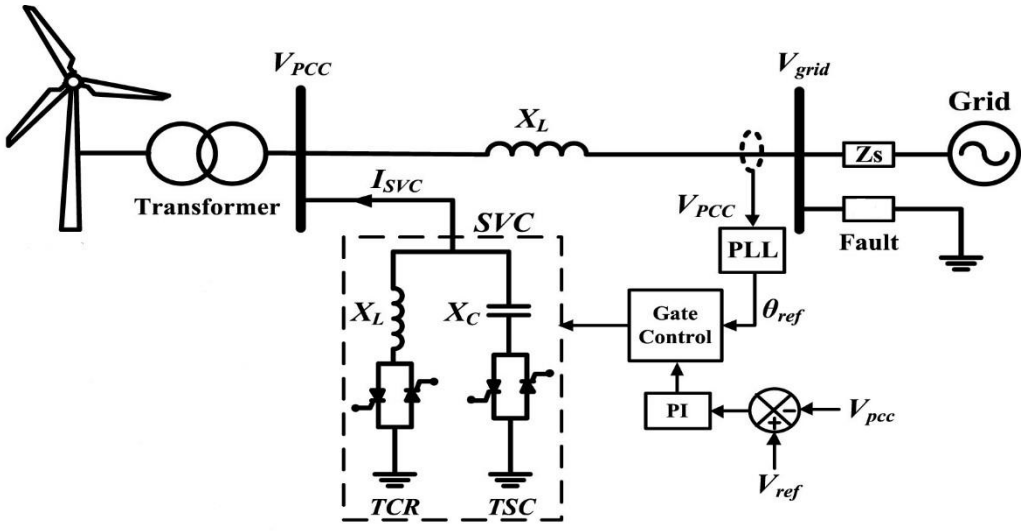


Figure 3.6. SVC configuration with a basic control system

Depending on the demand of the wind power system, the SVC can either absorb or inject reactive power into the power system based on the power system demand. During a grid fault condition, reactive power is generated (capacitive) and absorption of reactive power occurs in high voltage conditions (inductive). Like the STATCOM, the SVC operates in two modes namely VAR control and voltage regulation mode respectively. In voltage regulation mode, the SVC exhibits the voltage-current characteristic shown in Figure 3.7. At $V_{ref}$ voltage is regulated provided the SVC

susceptance (B) is within the maximal and minimal limits of the total reactive power of the capacitor banks and reactor banks respectively. The V-I characteristics of the SVC can be represented by the set of equations in (3.2) to (3.4).

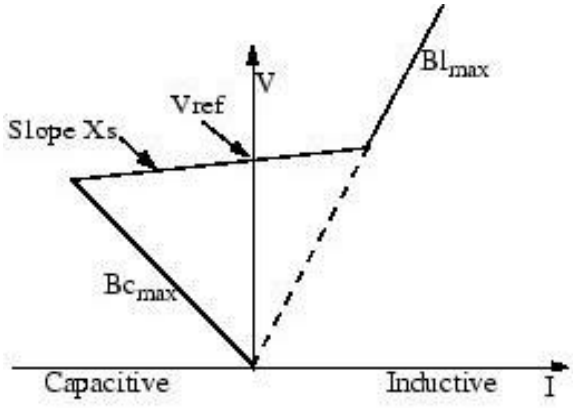


Figure 3.7. SVC V-I characteristics

$$V = V_{REF} + X_s I \tag{3.2}$$

$$V = -\,{}^{I}/_{B_{c\,max}} \tag{3.3}$$

$$V = {}^{I}/_{B_{l\,max}} \tag{3.4}$$

Where V represents the positive sequence voltage (p. u), the reactive current measured in (p. $u/P_{nom}$) is given as I. If I > 0, it indicates an inductive current. The droop reactance or slope measured in (p. $u/P_{nom}$) is represented by $X_s$, $B_{c\,max}$ is the maximum capacitive susceptance measured in ($pu/P_{nom}$) and $B_{l\,max}$ is the maximum inductive susceptance also measured in (p. $u/P_{nom}$). The SVC in equation (3.2) is operating in regulation range where $-B_{c\,max} < B < B_{l\,max}$. (3.3) and (3.4) is possible only if the SVC is fully capacitive and fully inductive respectively with ($B = B_{c\,max}$) and ($B = B_{l\,max}$) respectively for (3.3) and (3.4). A major drawback of the SVC is the unstable voltage oscillations, which occur because of its fast response to a fault condition.

When used with a weak grid, the fast response of the closed-loop voltage control of the SVC results to severe voltage oscillations. Another problem with the SVC is the injection of uncontrollable reactive current dependent on grid voltage [59]. This causes the injected current to reduce linearly with voltage sags and a quadratic diminishing of the injected reactive power.

### 3.3.3. Superconducting Dynamic Synchronous Condenser

Compared to the conventional synchronous condenser, the superconducting dynamic synchronous condenser (SDSC) is more durable and can boost voltage better in severe fault conditions by providing more reactive power support in the course of transient system faults [75]. The SDSC is a rotating synchronous condenser that runs synchronized with the grid. The fields are controlled with a voltage regulator to either generate or absorb reactive power as needed by the wind power system. By absorbing or injecting reactive power, the SDSC is able to respond quickly to transient changes in voltage levels. This makes it ideal for helping wind farms meet their interconnection agreement with the utility by improving the stability of the power system and at the same time providing voltage regulation. This is possible because the SDSC is able to perform with a high field current over a long period. However, in low voltage drop conditions the SDSC is less effective. Other setbacks of the synchronous condenser technology includes a higher level of losses and mechanical wear [76]. Figure 3.8 shows a pictorial view of the SDSC.

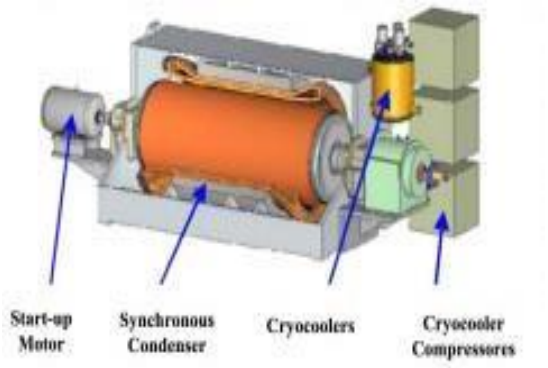


Figure 3.8. Structure of the superconducting dynamic synchronous condenser [59]

# 3.4. Series Compensation Devices

The target of series compensation is to reduce the equivalent reactance of the power line at rated grid frequency to boost transmission capacity and improving the transient stability of the transmission grid. These techniques are also implemented with voltage or current source devices as shown in Figure 3.9. The compensation device is usually connected in series with the power system. In this case, a change in the angle of $V_2'$ is achieved by adding a voltage $V_{COMP}$ between the load and line to represent voltage at the load side. With a proper adjustment in the magnitude of the voltage $V_{COMP}$, a unity power factor is obtained at $V_2$. Discussed below are some of the series-connected solutions popular with FSWT based wind farms.

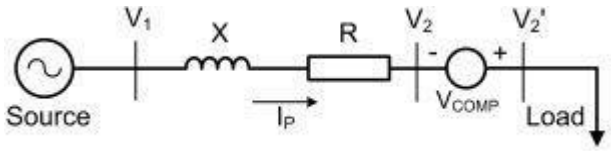


Figure 3.9. Principle of series compensation with a voltage source

## 3.4.1. Dynamic Voltage Restorer (DVR)

The DVR has been effectively used in the compensation of voltage fluctuations during a fault occurrence, usually series connected with the wind power system and used in keeping the load voltage constant irrespective of the source of voltage fluctuations [8]. The DVR responds to voltage sags by injecting three ac voltages in series with the incoming three-phase network voltages. It can also act as energy storage for generating the missing voltages at the WT terminal during voltage sag. To mitigate voltage sag, this device requires a fast control response. A major drawback of the DVR for reactive power support during a fault condition is the requirement for it to absorb part of the extra active power that is generated by the wind generator to keep the dc-link voltage at the desired level [77]. Therefore, the DVR is required to have an energy dissipation capability. Other technical limitations of the DVR have been discussed in [78]. The principle of operation of a DVR during a voltage sag is shown in Figure 3.10.

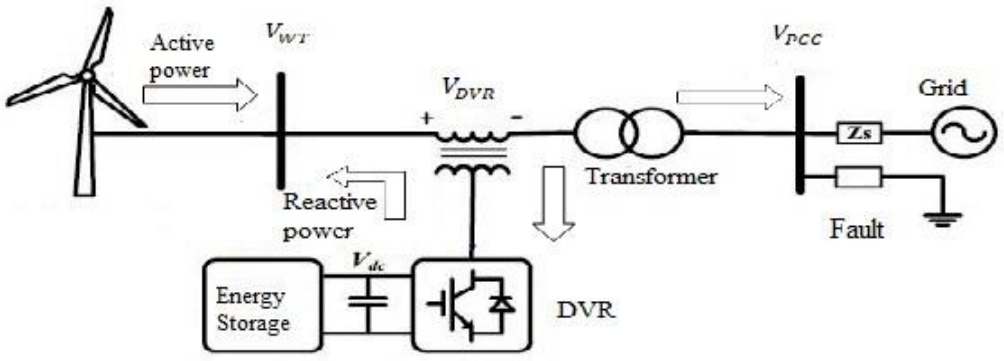


Figure 3.10. Operation of a DVR during voltage sag compensation.

## 3.4.2. Thyristor Controlled Series Compensator (TCSC)

The TCSC has proven to be very useful for limiting fault currents and controlling voltage unbalance in FSWT systems. The idea is control of power flow on the grid lines and effectively limiting power oscillations. A typical model of the TCSC consists of a bypass inductor, forward-biased thyristor, and capacitor banks. The control scheme of the TCSC has been described in detail in [79]. Reactive power compensation is achieved by generating a variable capacitive reactance that is obtained by firing the thyristor to inject extra current into the capacitor with the help of the bypass inductor thereby increasing the capacitive reactance value above the original reactance [80]. This technology is suitable for wind farms located further away from the PCC. The control is carried out by a simple PI controller which is used in generating the necessary gate drive signals for the thyristors during the fault condition. The firing angle of the thyristor can be varied to vary the value of the inductor. This way, the line impedance is also varied depending on load conditions.

The TCSC can operate in three modes namely the capacitive boost mode, the blocking mode, and the bypass mode:

- Capacitive boost mode: In this mode, the current is allowed to pass through the inductive branch to add to the capacitive current. This is achieved by slightly triggering the thyristor valve before the capacitor voltage crosses zero thereby allowing current to flow through the inductive branch and effectively increasing the observed capacitance of the TCSC eliminating the need for a larger capacitor within the TCSC.
- Blocking mode: In the blocking mode, the thyristor valve is always turned off thereby causing the TCSC to operate as a fixed series compensator

- Bypass mode: Thyristor valve is always on in the bypass mode thereby causing the TCSC to operate as a capacitor and inductor in parallel, reducing current through the TCSC.

The mode of operation of the TCSC is dependent on the requirement of the wind power system. A major advantage of this device is its ability to limit current during a grid fault condition, damping sub-synchronous resonance that may arise because of torsional and inter-area oscillations. A basic TCSC module installed with a basic control scheme is shown below in Figure 3.11.

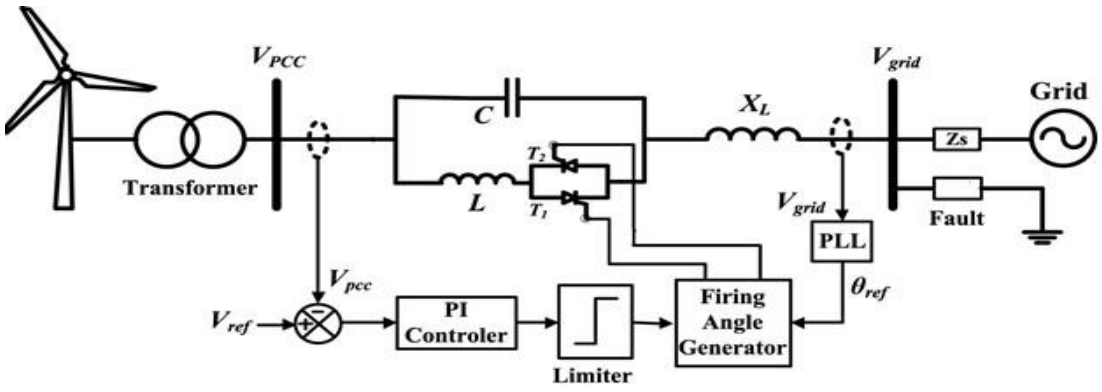


Figure 3.11. Thyristor controlled series compensator

## 3.4.3. The Fault Current Limiter (FCL)

The increased rise in the fault current levels because of large-scale WT penetration into the power grid has increased the need for FCLs. The mode of operation of the FCL is similar to the operation of surge protectors in an electrical system that limits damaging currents to household devices. The use of the FCL under fault conditions greatly improves the stability of the FSIG based wind farm by limiting the stator current of the FSIG and decreasing the voltage reduction level of the generator terminal. This ensures that the peak value of the short circuit currents on the wind farm is limited within the switchgear and allows the deployment of light circuit breakers. FCL are of different types and these include transformer coupled bridge fault current limiter (BFCL), solid-state FCL, and the superconducting FCL [81]- [85].

## 3.4.4. Magnetic Energy Recovery Switch (MERS)

As shown in Figure 3.12, the MERS is similar to the circuit configuration of a single-phase full-bridge inverter with a dc capacitor and four reverse conductive semiconductor switches. The difference with the MERS to a single-phase full-bridge converter is the smaller dc-link capacitor.

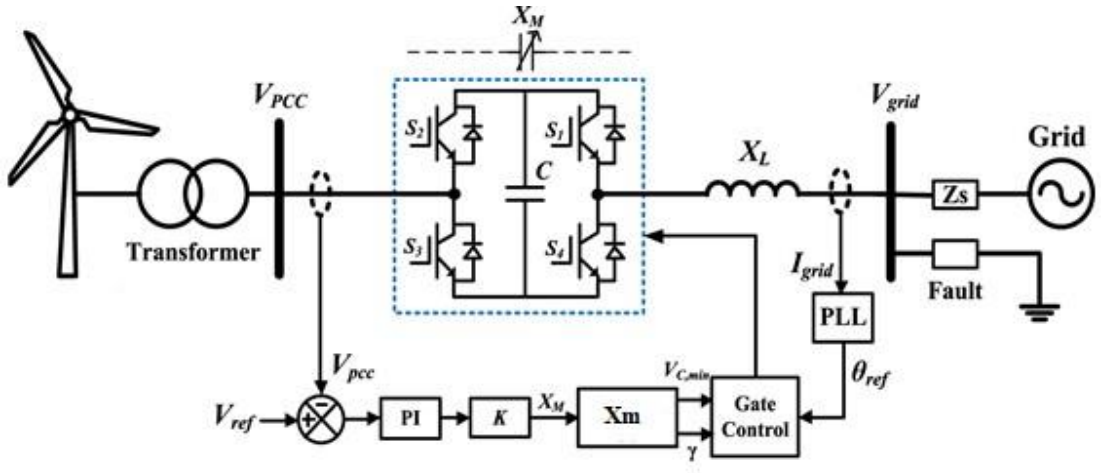


Figure 3.12. Circuit configuration of a MERS

The MERS when compared to pulse width modulation converters have fewer losses since they are synchronously switched to the line frequency, which is very important in high wind applications. The MERS acts as a variable series compensator between the power grid and the main transformer of the wind farm by compensating for reactive power and controlling the wind turbine terminal voltage thereby improving the LVRT capability of the FSWT [86]-[88]. Characteristics of MERS such as double voltage-current operating range, zero current turn-ons, and a lower current conduction period of each switch make the MERS an attractive alternative option for reactive power compensation in a FSWT wind farm [88].

### 3.4.5. The Series Dynamic Braking Resistor (SDBR)

This is designed to eliminate or reduce the need for reactive power compensation devices by the installation of a resistor in series between the WT and grid to improve the terminal voltage of the FSWT. Under a fault condition, the SDBR is used in active power balance between the electrical and mechanical sides of the WT [89], [90]. The installation of the resistor in series between the WT and grid improves the electrical power and torque of the FSWT wind system during a fault condition [91], [92]. The resistor allows the evacuation of the generator's active power, it also creates a voltage drop that leads to boosting the terminal voltage of the generator.

## 3.5. Hybrid Connected Devices

In addition to the above-discussed methods, there have been other proposed techniques that combine the series and shunt topologies. The technologies are sometimes referred to as hybrid connected solutions. These techniques include the unified power quality conditioner (UPQC) [93] – [95] and the unified compensation system (UCS) [96].

The UPQC is a combination of both the series and shunt VSC for improving voltage sag, harmonics, dynamic active and reactive power regulation, linked by a common DC link. This allows for a bidirectional flow of active power and provision of the needed additional VAR when a grid fault condition occurs preventing the over-speeding of the FSIG rotor. The shunt VSC provides the additional needed VAR during voltage reduction while the series VSC provides for the lack of voltage to prevent over-speeding of the FSIG rotor.

A major setback of the UPQC is the huge capital cost required to install this device because of the two converters required. To solve the problem associated with cost, a novel combination of the UPQC and a resistive superconducting fault current limiter (SFCL) was proposed in [93], shown

in Figure 3.13. However, this proposed strategy has a setback of the need for a properly coordinated control scheme between the UPQC and the SFCL.

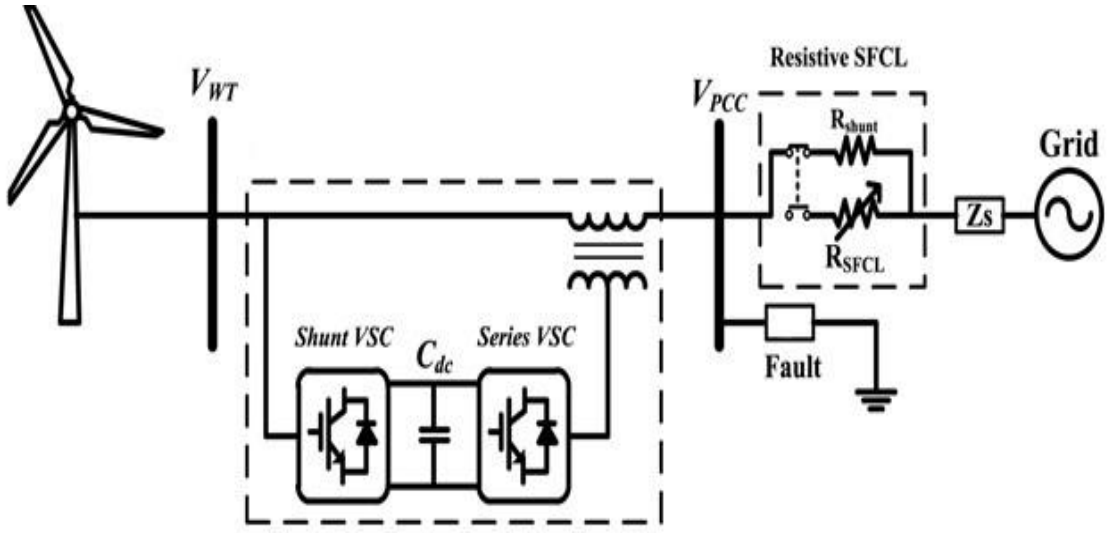


Figure 3.13. UPQC and SFCL connected to a FSWT system

The UCS in a normal operating condition behaves like the STATCOM, supporting reactive power regulation through the shunt connection. Under a fault condition, the UCS automatically switches to the series grid connection from the shunt connection to compensate for voltage, keeping the FSWT at its rated stator voltage. Figure 3.14 depicts the configuration of a UCS connected to a WT terminal. The drawback of the UCS is the high conduction losses of the series bypass switch.

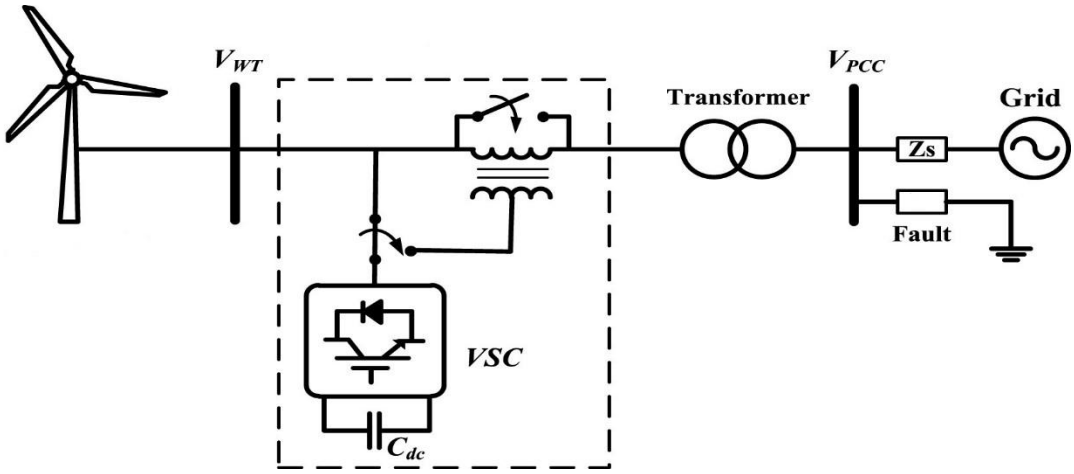


Figure 3.14. UCS configuration connected to a WT terminal

## 3.6. Integrated Gate-Commutated Thyristor (IGCT)

The IGCT is an emerging technology of semi-conductor devices used as self-commutated reactive power compensators. These devices are gate-controlled turn-off switches that turn off like a transistor but conduct like a thyristor, with low conduction losses. The application of the IGCT requires that the semiconductor can block high voltages in the kV range. Key advantages of the IGCT include but are not limited to cost-effectiveness, standardization and simplicity. It is also important to note that the IGCT can adapt to multiple applications and can operate over temperature ranges of -40 degrees Celsius to 140 degrees Celsius.

## 3.7. Technical Comparison of FACTS

A comparative analysis of the SVC and TCSC is presented in [97]. It was observed that during wind speed fluctuations, the SVC offers better reactive power compensation to the FSWT wind system to maintain its transient stability while the TCSC can effectively promote the terminal voltage of the FSWT and enhance FRT in severe three phases fault currents. Though the SVC and TCSC both have sophisticated components, they both have relatively simple control structures.

In comparison to the SVC and other FACTS devices, the STATCOM provides a faster response time and better performance at reduced voltage levels. This makes the STATCOM the most extensively used solution for the enhancement of the FRT of the FSWT wind system [20]. The response time however does not affect voltage support or transient stability improvement. Since power electronics are utilized in the STATCOM rather than capacitors and reactors, the STATCOM has a slightly smaller footprint than the SVC.

Comparing the SVC and SDSC in [98], the research showed that there is better performance with the SVC during the occurrence of a fault condition with minor voltage reduction at the terminal of the WT while the SDSC can adjust the voltage to the rated value quicker during a severe grid fault condition.

The UPQC and UCS compared to other FACTS devices have superior performance because they can provide both shunt and series compensation. However, these devices have a higher overall cost and control complexity due to the presence of two converters. Compared to the UPQC, the UCS however has a lesser control complexity because only one of the converters is grid-connected at a time. In [89], research shows that the SDBR can dissipate active power, however, lacks reactive power control ability. Therefore, it cannot minimize the power and voltage fluctuations of the FSWT. The SFCL and BFCL both have simpler control structures that have proven their ability to improve the transient stability and LVRT capability of the FSWT system. The BFCL however requires a costly and special transformer to connect the three-phase diode bridge in series with the wind power system.

## 3.8. Chapter Summary

A review of the various devices available for reactive power support and improving voltage stability of a grid-connected FSWT wind system has been carried out. Table 3.1 presents a technical comparison of each of these devices discussed in the previous sub-sections.

Table 3.1 Summary of reactive power compensation devices

| **Device** | **Advantage** | **Limitation** |
|---|---|---|
| **STATCOM** | Rapid response to grid disturbance and less disturbance compared to other FACTS devices.<br><br>They do not contribute to short circuit currents. | Limited power capability without any energy storage.<br><br>Output voltage magnitude cannot be independently controlled in a steady state.<br><br>Cannot supply active power.<br><br>Needs to be cut off during high voltage drops.<br><br>Arbitrary reactive current allocation. |
| **SVC** | Provides continuous voltage control.<br><br>Voltage stability in a weak wind power system.<br><br>Simple control structure. | Generates unstable voltage oscillations as a result of its fast response.<br><br>Reactive power control is voltage-dependent. |
| **SDSC** | Low loss level.<br><br>Can perform with very high currents for a long time. | Low efficiency for low voltage conditions.<br><br>Slow response to a grid fault condition. |

| | | |
|---|---|---|
| **TCSC** | Useful for fault current limitation and voltage unbalance.<br><br>Variable capacitive reactance.<br><br>A suitable solution for offshore wind applications.<br><br>Simple control structure. | Produces undesirable resonance.<br><br>Injects harmonics into the wind power system. |
| **FCL** | Useful for high voltage dips.<br><br>Minimizes rotor speed variations.<br><br>Automatically detects fault current.<br><br>Fast action on limiting fault current.<br><br>Low conduction losses. | Unable to effectively control reactive power.<br><br>Requires a high recovery time.<br><br>Requires a large scale coupling transformer.<br><br>Undesirable saturation of DC reactance. |
| **MERS** | Low switching losses.<br><br>Effective for large scale wind applications. | Less robust control. |
| **SDBR** | Low maintenance and high reliability.<br><br>Mechanical active power mitigation | Unable to control reactive power.<br><br>Cannot dampen voltage fluctuations. |
| **DVR** | Controllable reactive power supply.<br><br>Fast voltage recovery. | Active power absorption.<br><br>Inability to endure long time steady-state voltage unbalance fault due to its limited DC link. |

| | | |
|---|---|---|
| **UPQC** | Provides fast reactive power compensation.<br><br>Long critical clearance time.<br><br>Increases the voltage safety margin of the LVRT curve. | Lack of a properly coordinated control scheme between the UPQC and SFCL.<br><br>Requires a huge DC-link capacitor.<br><br>Absorbs active power. |
| **UCS** | Supports both series and shunt compensation with one converter. | High conduction losses. |

From the available literature, the following conclusions can be made:

- The STATCOM is regarded as the most commonly used device for reactive power support and voltage stability in wind power systems. This is because the STATCOM has greater performance, more flexibility in dynamic control ability, and a better transient stability margin during the occurrence of a grid fault [20].
- A major setback of the STATCOM is the possibility of excessive reactive power support and arbitrary reactive current allocation during the occurrence of a grid fault condition. The result of this over-compensation is a further increase in the cost of the wind system due to the difficulty in determining the rated capacity of the STATCOM.
- The STATCOM has a limited power capability in the absence of additional energy storage. The energy storage, therefore, adds extra cost to the wind energy system.

To solve the problem of reactive current allocation and extra cost associated with the STATCOM, this thesis proposes a hybrid wind system that utilizes the full rated GSC of a PMSG wind system installed alongside the FSIG system. A current allocation principle that utilizes the GSC of the

PMSG to provide the needed reactive power support required by the FSIG-WT during a grid fault condition is proposed. The proposed method eliminates the need for an external auxiliary device such as the STATCOM, guaranteeing cost savings on the part of the wind power system operator and improving grid voltage during a fault condition while providing the required reactive power needed by the FSIG-WT system.

The concept of a hybrid wind energy system is discussed further in Chapter 4.

The contributions and parts of this chapter have been published in the paper

**O. Apata and D. T. O. Oyedokun, "Novel Reactive Power Compensation Technique for Fixed Speed Wind Turbine Generators," 2018 IEEE PES/IAS PowerAfrica, Cape Town, 2018, pp. 628-633, DOI: 10.1109/PowerAfrica.2018.8521131.**

# Chapter 4

# Hybrid Wind Power Systems

As established in Chapter 3, FSIG based wind systems need adequate reactive power support to function properly. Various research has been carried out for designing devices and technologies that can provide the required reactive support needed by the FSWT system. The STATCOM has been identified as the most commonly used device for reactive power support and voltage stability in wind power systems. This is because of the greater performance, more flexibility in dynamic control ability, and a better transient stability margin of the STATCOM during the occurrence of a grid fault. As identified in Chapter 3, the STATCOM has a limitation of excessive reactive power support and arbitrary reactive current allocation during the occurrence of a grid fault condition. Also, the need for additional energy storage to improve the power capability of the STATCOM leads to an increased cost of the wind power system.

To solve these problems associated with the STATCOM, this thesis proposes a strategy that eliminates the need for the STATCOM or any additional FACTS devices for reactive power and voltage support in the FSWT wind system. This chapter, therefore, introduces the concept of hybrid wind systems for improved voltage stability and reactive power compensation in WT systems. In comparison to wind farms operating with a single type of WT, a hybrid wind farm operating with multiple types of WT generators can utilize the operational characteristics of the different WTs to improve system stability and performance leading to a better techno-economic operation of the wind farm. The different components of the individual wind turbines are modelled using the MATLAB software and the different simulations have been carried out in the Simulink simulation environment of the MATLAB software.

# 4.1. Introduction to Hybrid Wind Power Systems

There have been various proposals on ways of improving the land area power density of wind farms. One of such recently proposed approaches is the co-location of WTs to improve wind farm efficiency and increase total power production [99]. During a network unbalance, the behaviour of a connected power grid can improve by compensating for unbalanced voltage using distributed energy sources based on pulse width modulation converters [100]. This implies that the performance of a wind power system can improve if installed alongside distributed energy resources. Recent studies in [17], [24], [101], and [102] have also shown that wind power systems can be installed side by side for improved performance and efficiency. There have been various researches carried out on hybrid renewable energy systems comprising of WTs and other renewable energy sources such as photovoltaic systems [103]-[105], however, these systems are beyond the scope of this research. This research focuses on a hybrid wind farm without considering other renewable energy sources.

A hybrid wind power system, therefore, is a wind power system that consists of two sub-wind farms connected in parallel at PCC and grid-connected by a transmission line. A hybrid wind farm can therefore be a combination of a VSWT and a FSWT or two VSWT wind systems. Based on the above submission, this research has identified three possible configurations of a hybrid wind farm [106] - [115]. These are:

- DFIG-PMSG wind conversion system
- DFIG-FSIG wind conversion system
- PMSG-FSIG wind conversion system

A hybrid wind farm system consisting of PMSG- and DFIG-based wind power systems has more flexible control than any other type of hybrid wind farm because of the advantage of the power

converters of the WTs. This can lead to improved performance of the wind power system, even in abnormal grid conditions. The Rudong 150 MW offshore wind farm consisting of both PMSG and DFIG wind turbines is an example of a DFIG-PMSG hybrid wind conversion system.

Researches carried out in [109], [110], [113] and [116] have shown that the DFIG wind system can be installed side by side with the FSIG wind system. The various studies have shown that the voltage at PCC in a DFIG-FSIG hybrid wind farm can be supported effectively with control of the DFIG wind system to provide reactive power support to the FSIG wind system and effectively the entire hybrid wind farm. However, the support provided by the DFIG wind system for reactive power compensation in the FSIG system is restricted due to the partially rated power converters of the DFIG based wind farm. This means that during a network unbalance, the DFIG based wind farm has a limited effect on improving the operational performance of a hybrid wind consisting of the FSIG based wind farm and DFIG wind system. Its compensation ability also varies with output power, generator speed the transmission network impedance.

In comparison to the DFIG wind system with partially rated converters, the PMSG-WT utilizes full-scale power converters in the transmission of wind power to the power grid. This gives the PMSG wind system a more efficient advantage of terminal voltage and strong reactive power support capability [117] – [118]

A unique characteristic of the PMSG-WT system is its ability to control a wider operating region for various control targets. With a coordinated control of the PMSG-WT during grid faults, the operational performance of a nearby DFIG or FSIG based wind system can be improved. This characteristic of the PMSG-WT makes it more ideal than the DFIG for a hybrid wind configuration with the FSIG system. This research work, therefore, focuses on a hybrid configuration of a PMSG-FSIG wind power system. The power electronic converters of the PMSG are utilized in ensuring adequate reactive power compensation for the FSIG system by a proposed coordinated

control strategy. The major advantage of a hybrid wind system is the possibility of ensuring voltage stability and effective reactive power control without the need for external support devices.

## 4.2. Hybrid Wind Farm Topology

The block diagram representation of the hybrid wind farm is shown in Figure 4.1. The wind system is developed and modelled in the Simulink environment of the MATLAB software, using an aggregate modelling approach. The number of WTs shown in Figure 4.1 is for illustration purposes as the wind farm can consist of n types of WTs with an output of n MW depending on the requirement of the hybrid wind farm. The modelled hybrid wind farm consists of a 20 MW FSIG wind system and a 10 MW PMSG wind system both connected in parallel at the PCC and grid-connected via a transmission line. In steady-state conditions, both wind farms operate normally at their rated capacity. The modelling of the individual wind farms making up the hybrid wind farm is further discussed in the sub-sections below.

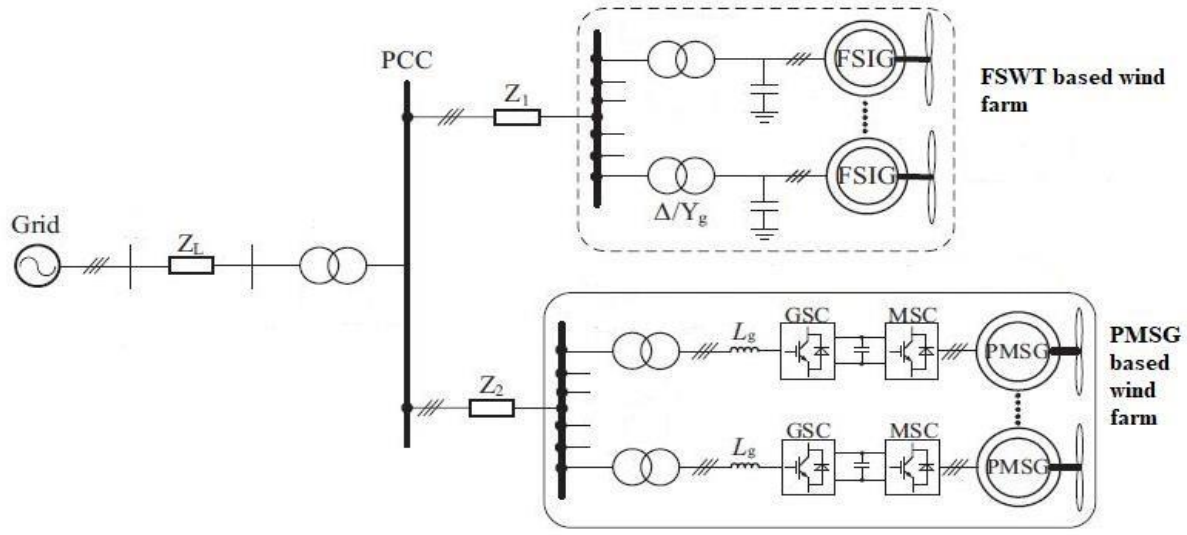


Figure 4.1. Configuration of a hybrid wind farm consisting of FSWT and PMSG wind system.

## 4.3. FSIG –Based Wind Farm

The equivalent circuit of the FSIG in the direct (d)-quadrature (q) axis is shown in Figure 4.2(a) and (b). All the electrical parameters and variables are referred to the stator and all rotor and stator quantities are in the d-q axis reference frame. In modelling the wind generator of the FSWT, certain assumptions have been taken into consideration:

- The q-axis is assumed to lead the d-axis by 90 degrees in the direction of rotation.
- The q- component of the stator voltage is chosen as the real part of the bus bar voltage and d-component is selected as the imaginary part.
- The stator current is assumed to be positive when flowing from the generator.
- The equations are based on the synchronous reference of the generator.

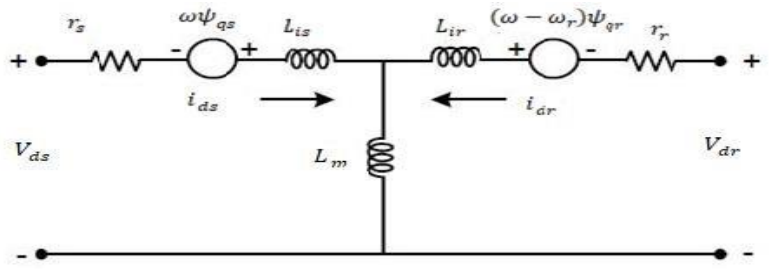


(a) d-axis

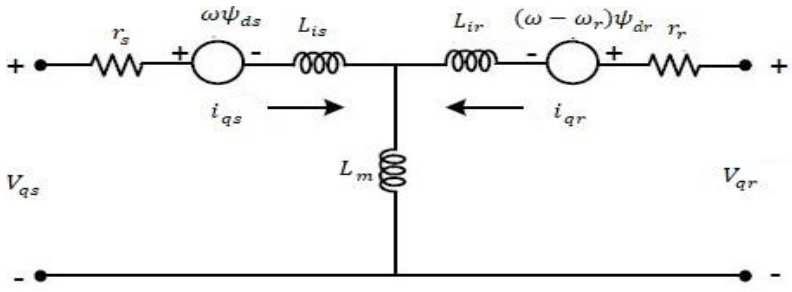


(b) q-axis

Figure 4.2. Equivalent circuit of the FSIG in the d-q axis reference frame

The relationship between the fluxes and currents in the d-q reference frame, the rotor voltage, and stator voltage is represented by the following set of equations.

$$V_{ds} = r_s i_{ds} - \omega_s \psi_{qs} + \frac{d}{dt}\psi_{ds} \quad (4.1)$$

$$V_{qs} = r_s i_{qs} + \omega_s \psi_{qs} + \frac{d}{dt}\psi_{qs} \quad (4.2)$$

$$V_{dr} = r_r i_{dr} - (\omega_s - \omega_r)\, \psi_{qr} + \frac{d}{dt}\psi_{dr} \quad (4.3)$$

$$V_{qr} = r_r i_{qr} + (\omega_s - \omega_r)\, \psi_{dr} + \frac{d}{dt}\psi_{qr} \quad (4.4)$$

(4.5) – (4.8) represents the stator and rotor flux linkages

$$\psi_{ds} = L_s i_{ds} + L_m i_{dr} \quad (4.5)$$

$$\psi_{qs} = L_s i_{qs} + L_m i_{ds} \quad (4.6)$$

$$\psi_{dr} = L_r i_{dr} + L_m i_{ds} \quad (4.7)$$

$$\psi_{qr} = L_r i_{qr} + L_m i_{qs} \quad (4.8)$$

The stator and rotor inductances is given as

$$L_s = L_{is} + L_m \quad (4.9)$$

$$L_r = L_{ir} + L_m \quad (4.10)$$

$V_{ds}$, $i_{ds}$, $\psi_{ds}$, $V_{qs}$, $i_{qs}$, $\psi_{qs}$, $\psi_{ds}$ represents voltage components of the d-q axis, stator currents, and flux while d-q axis voltage components, rotor current, and flux are given as $V_{dr}$, $V_{qr}$, $i_{qr}$, $i_{dr}$, $\psi_{qr}$,

$\psi_{dr}$, $r_s$ and $r_r$ represents stator and rotor windings resistance respectively. The magnetizing inductance is represented as $L_m$, $\omega_s$ is the synchronous speed of the generator, $\omega_r$ represents the rotor speed, the rotor and stator currents are represented by $i_{dqs}$ and $i_{dqr}$ respectively. The generator electromagnetic torque is represented by

$$T_e = 1.5p\ (\psi_{ds} i_{qs} - \psi_{qs} i_{ds}) \tag{4.11}$$

Where the number of poles is represented by p. The generated active power $P_{FSIG}$ and consumed reactive power $Q_{FSIG}$ represented in the d-q axis are given as

$$P_{FSIG} = V_{ds} i_{ds} + V_{qs} i_{qs} \tag{4.12}$$

$$Q_{FSIG} = V_{qs} i_{ds} - V_{ds} i_{qs} \tag{4.13}$$

A simplified equivalent circuit of the FSWT wind farm with grid line parameters is shown in Figure 4.3. This is important to analyze how the parameters of the network influence the behaviour of the FSWT wind farm.

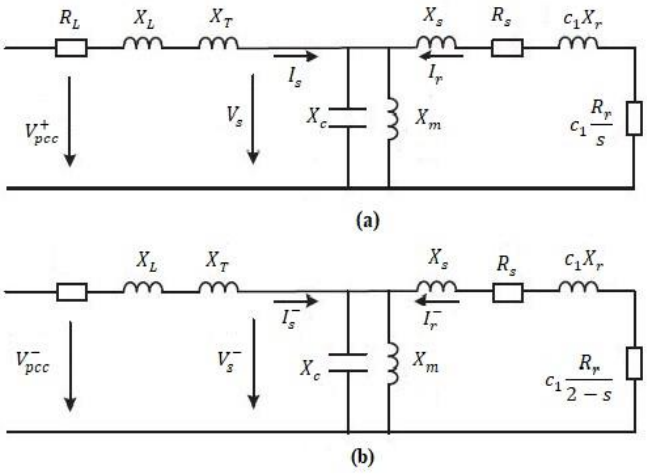


Figure. 4.3 (a) Simplified equivalent positive sequence circuit of FSWT based wind farm with grid line parameters (b) Simplified equivalent negative sequence circuit with grid line parameters.

From Figure. 4.4, the positive and negative sequence mathematical model of the FSWT based wind farm is developed as follows

$$V_{pcc}^{+} = [R_L + j(X_L + X_T)]\, I_s\, V_s \tag{4.14}$$

$$V_{pcc}^{-} = [R_L + j(X_L + X_T)]\, I_S^{-}\, V_s^{-} \tag{4.15}$$

Where

$$V_s = jX_c//m\,(I_s + I_r^{+}) =$$

$$-[(R_s + c_1\frac{R_r}{s}) + j(X_s + c_1X_r)]I_r \tag{4.16}$$

$$V_s^{-} = jX_c//m\,(I_s^{-} + I_r^{-}) =$$

$$-[(R_s + c_1\frac{R_r}{2-s}) + j(X_s + c_1X_r)]I_r^{-} \tag{4.17}$$

$c_1$ is a correction factor and can be expressed as $1 + \frac{X_s}{X_m}$.

$V_{pcc}^{+}$ is the grid voltage of PCC, $V_s$ is the FSIG stator voltage, the slip of the FSIG is given as $s$ while $I_s$ and $I_r$ are the stator and rotor currents of the FSIG. $X_T$, $X_m$ and $X_L$ represent the short circuit reactance, magnetizing reactance, and grid line reactance between the PCC and FSIG wind farm respectively.

The rotor of the FSIG is expressed as $\frac{d\omega}{dt} = \frac{1}{2H_m}(T_m - T_e)$ (4.18)

Where the shunt reactance of $X_c$ and $X_m$ is given as $X_c//m = X_cX_m/X_c + X_m$. The mechanical and electromagnetic torque is given as $T_m$ and $T_e$ respectively, $H_m$ represents the constant of inertia. The average electromechanical torque of the FSWT is a combination of both the positive and negative torques. During a grid fault condition, the average electromagnetic torque $T_e$ of the FSWT based wind farm is represented as

$$T_e = T_e^+ + T_e^- \quad (4.19)$$

Depending on the degree of the grid voltage sag, the acceleration of the FSWT rotor can be more serious.

## 4.3.1. Transient Behavior and Power Characteristics of the FSWT Wind System

In steady-state, at the rated slip of $S_N$ the FSWT wind farm is stable at point a of the torque slip curve shown in Figure 4.4. When a grid fault condition occurs, the working point of the wind farm moves from point a to point b causing the rotor of the FSWT to accelerate excessively because of the unbalance between the electromagnetic and mechanical torques. Since the FSWT wind farm is not equipped with an external compensating device like the STATCOM, it is important to establish a critical clearing time $t_{ct}$ that determines if the wind farm will be disconnected from the grid if the fault condition is not cleared. The working point of the FSWT wind farm will change from point f to point e if the fault condition is eliminated at point f. This means the fault clearance time defined as $t_f$ is equal to the critical clearing time $t_{ct}$.

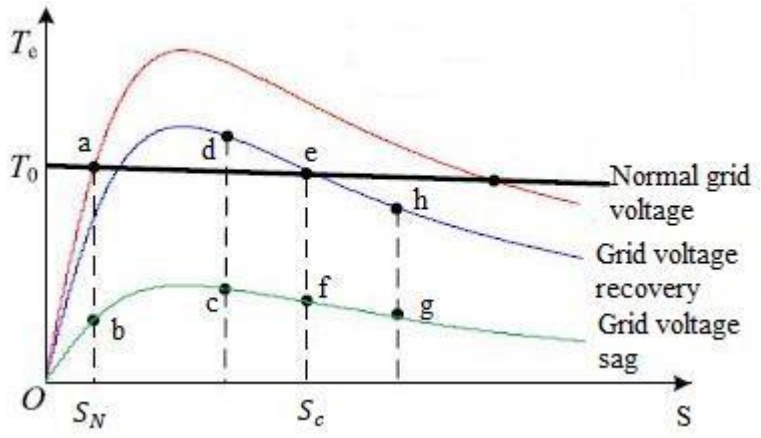


Figure. 4.4. FSIG wind farm torque-slip curve

At this point, the slip of the FSWT wind farm is represented by $S_c$ which is the critical slip. If the fault clearance time $t_f$ is less than the critical clearing time $t_{ct}$, the grid fault is cut off at point c and the working point of the FSWT wind farm moves from point c to point d while the rotor speed can be increased to a point of stability e ensuring that the wind farm can successfully ride through the fault. However if $t_f$ is greater than $t_{ct}$, the fault condition is cut off at point g while the working point of the wind farm moves from point g to point h. This causes the rotor speed of the FSIG to increase continuously causing the FSIG based wind farm to trip.

In the presence of a grid fault condition, the PCC voltage level impacts the critical clearing time of the FSIG wind farm. To extend the critical clearing time of the wind farm to fulfil the conditions for a successful fault ride through, the PMSG based wind farm is used to improve the voltage amplitude at PCC. From Figure. 4.2, the PCC equivalent impedance of the FSIG wind farm consisting of the network parameters is determined and expressed in (4.20) and (4.21),

$$R_{pcc} = R_L + \frac{(s^2 R_s + sR_r)X_c // m^2}{(sR_s+R_r)^2 + s^2 (X_s + X_r + X_c // m)^2} \tag{4.20}$$

$$X_{pcc} = X_L + X_T + \frac{(sR_s+R_r)^2 X_c // m}{(sR_s+R_r)^2 + s^2(X_c // m + X_s + X_r)^2} + \frac{s^2(X_s + X_r)(X_c // m + X_s + X_r)X_c // m}{(sR_s+R_r)^2 + s^2 (X_s + X_r + X_c // m)^2} \tag{4.21}$$

From (4.20) and (4.21), it is seen that resistance and reactance of the FSWT based wind farm are dependent on the slip. Both the equivalent impedance and inductive component gradually decrease as the rotor speed and slip increase causing the resistive components to initially experience an increase then decrease. Ignoring all electrical transients, the reactive and active power of the FSIG wind farm is therefore expressed as

$$Q_{FSWT} = V_{PCC}^2 \frac{X_{pcc}}{R_{pcc}^2 + X_{pcc}^2} \tag{4.22}$$

$$P_{FSWT} = V_{PCC}^2 \frac{R_{pcc}}{R_{pcc}^2 + X_{pcc}^2} \tag{4.23}$$

From (4.22) and (4.23), it is observed that the power characteristics of the FSIG wind farm are dependent on the PCC voltage and slip.

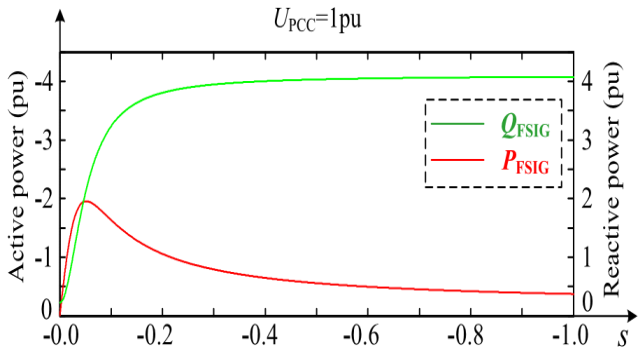


Figure 4.5. Power-slip curve of the FSIG wind farm

As seen in Figure 4.5, the WT active power initially increases then decreases while the reactive power shows a corresponding increase with an increase in the slip of the FSIG. As a result of the grid fault condition, the rotor of the FSWT experiences an increase in speed that causes it to deviate from the synchronous speed. This causes the FSWT wind farm to require large amounts of reactive power during and after the grid fault condition, this could deteriorate the voltage quality of the wind farm at PCC. However, with the appropriate control of the PMSG based wind farm as proposed in this research work, the required reactive power needed to successfully ride through the grid fault ride condition is obtained and the PCC voltage improved.

# 4.4. PMSG-Based Wind Farm

The equivalent circuit shown in Figure 4.7 represents the PMSG-based wind farm.

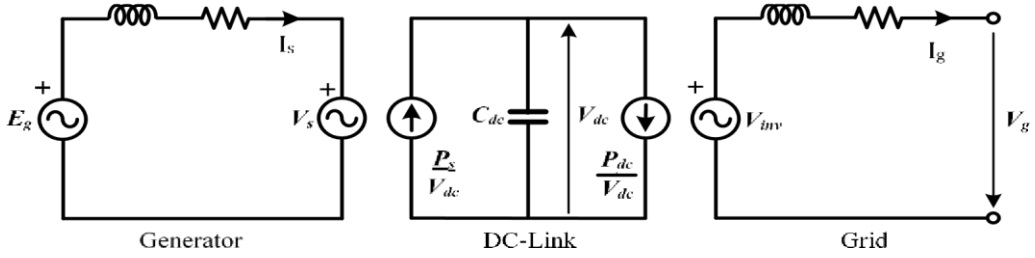


Figure. 4.6. PMSG based wind turbine equivalent circuit

Since the WT generator of the PMSG wind system is directly coupled to the rotor, its electrical angular frequency $\omega_e$ is determined from the number of generator poles $n_p$ and mechanical rotor speed $\omega_r$.

$$f_e = {}^{n_p}/_{2}\ f_r = {}^{n_p}/_{2}\ {}^{\omega_r}/_{2\pi} \tag{4.24}$$

$$\omega_e = 2\pi f = {}^{n_p}/_{2}\ \omega_r \tag{4.25}$$

Where $f_r$ and $f_e$ are the rotor angular frequency and electrical angular frequency of the WT generator, respectively. The stator coil flux distribution is sinusoidal since it is assumed that the distributed magnetic flux surrounding the wind generator air gap is sinusoidal. This implies the electromotive force is also sinusoidal and the generated induced voltage $E_g$ from the permanent magnets is expressed as

$$E_g = 2\pi f_e \psi_m = \omega_e \psi_m \tag{4.26}$$

Where $\psi_m$ is the stator coil flux linkage

The three-phase quantities $abc$ of the PMSG in the $abc$ frame or stationary frame are transformed into orthogonal values in the stationary $\alpha\beta$ frame through Clarke transformation as shown in Figures 4.7 and 4.8. Since these values are still ac values in the $\alpha\beta$ frame, a proportional-resonant (PR) converter is used to minimize or eliminate the tracking error at the fundamental frequency.

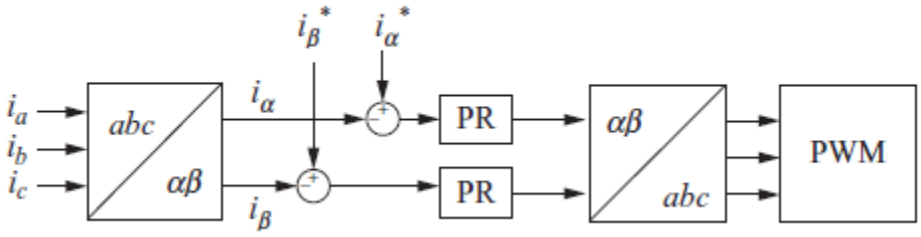


Figure 4.7. Current control mode in the stationary frame.

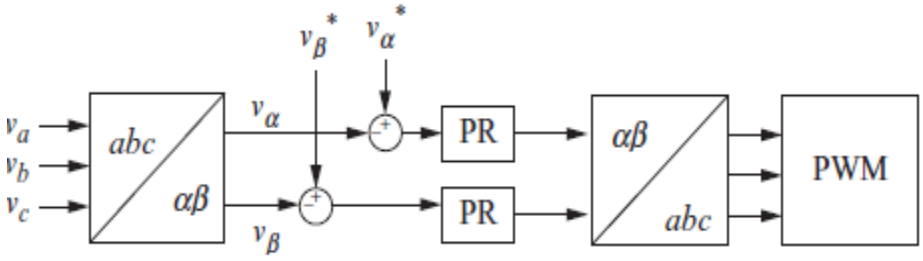


Figure 4.8. Voltage control mode in the stationary frame.

The feedback voltage or current, as shown above, are transformed into $\alpha\beta$ control frame. The controller outputs are then transformed back to the $abc$ frame to generate the required PWM signals. It is important to state that the active and reactive components in the $\alpha\beta$ control frame are coupled for power generation. From the instantaneous reactive power theory [119], the active and reactive power is expressed in the $\alpha\beta$ control frame respectively as

$$P = V_\alpha i_\alpha + V_\beta i_\beta \; ; \; Q = V_\beta i_\alpha + V_\alpha i_\beta \tag{4.27}$$

From (4.27) the desired output control reference is derived. The Park transform is then used in converting the $\alpha\beta$ components in the $\alpha\beta$ frame to a rotating reference frame, otherwise referred to as the $dq$ frame. Figure 4.9 illustrates the phasor diagram of $abc$ and $dq$ reference frames. In the synchronous reference frame, the q-axis of the PMSG is ahead of the d-axis by 90 degrees when considering the direction of rotation.

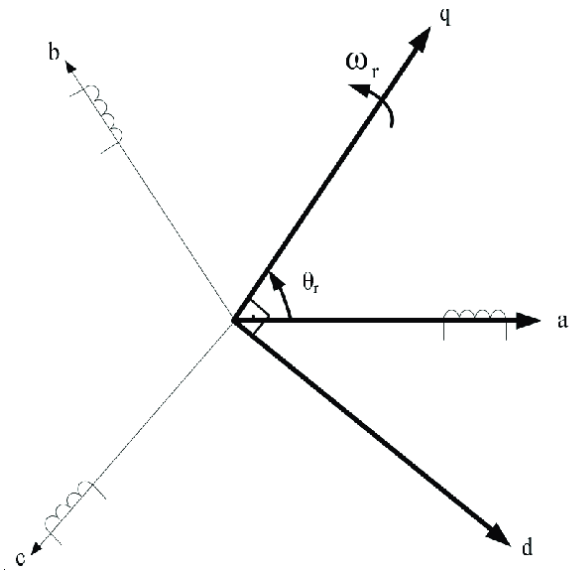


Figure 4.9. $abc$-$dq$ axis representation

In the $dq$ reference frame, the ac quantities are transformed by Park transformation into dc. To implement the current and voltage control of the PMSG in the synchronous frame, the Clark transformation in Figure 4.7 and Figure 4.8 is modified as shown in Figure 4.10 by replacing the PR controller and Clark transformation with proportional-integral (PI) controllers and the Park transformation block.

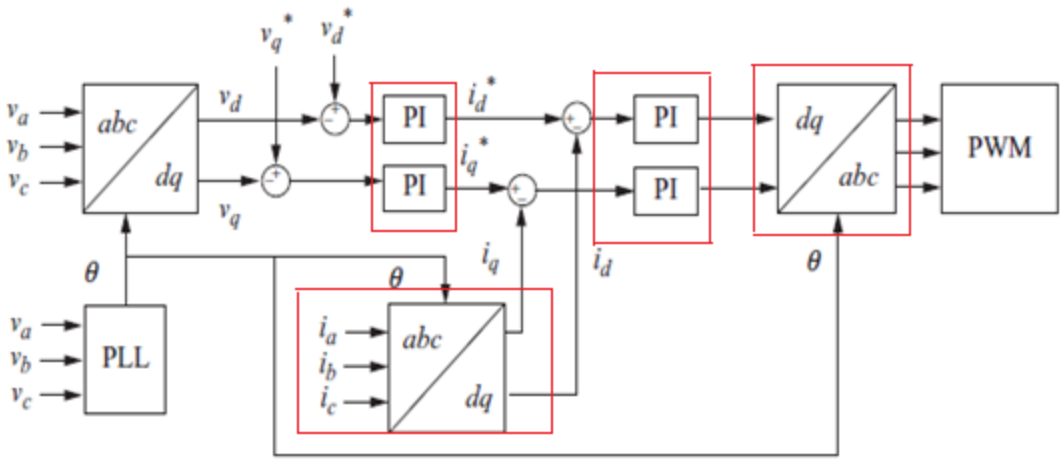


Figure 4.10. Voltage and current control in the synchronous frame

The PI controller is used to regulate the three-phase feedback voltages after being transformed into the $dq$ frame and the outputs are used for the current reference, where the three-phase feedback currents are then transformed to $dq$ frame and also controlled. The outputs of the controller are then inverse transformed back to the $abc$ frame and fed into the PWM module to generate the converter voltage.

By adapting the space vector theory in [120], the stator voltage equations in the $dq$-axis can be developed and expressed as:

$$\begin{pmatrix} V_{ds} \\ V_{qs} \end{pmatrix} = -r_s \begin{pmatrix} i_{ds} \\ i_{qs} \end{pmatrix} - \frac{d}{dt} \begin{pmatrix} \psi_{ds} \\ \psi_{qs} \end{pmatrix} + \omega_e \begin{pmatrix} 0 & -1 \\ 1 & 0 \end{pmatrix} \begin{pmatrix} \psi_{ds} \\ \psi_{qs} \end{pmatrix} \tag{4.28}$$

$r_s$ is the stator winding of the generator, $V_{ds}$ and $V_{qs}$ is d-q axis stator voltage components respectively, $i_{ds}$, $i_{qs}$, $\psi_{ds}$, $\psi_{qs}$ are the d-q axis current and flux components respectively. Aligning the generator d- axis along with the rotor flux position, the flux linkages of the stator can be expressed as

$$\begin{pmatrix}\psi_{ds}\\ \psi_{qs}\end{pmatrix} = \begin{pmatrix}L_s + L_{dm} & 0\\ 0 & L_s + L_{qm}\end{pmatrix}\begin{pmatrix}i_{ds}\\ i_{qs}\end{pmatrix} + \begin{pmatrix}\psi_m\\ 0\end{pmatrix} \quad (4.29)$$

The stator winding leakage inductance is represented by $L_s$ while the magnetizing inductances of the d - q axis are represented by $L_{dm}$ and $L_{qm}$ respectively. Substituting (4.29) into (4.28), the stator voltage equation becomes:

$$\begin{pmatrix}V_{ds}\\ V_{qs}\end{pmatrix} = -r_s\begin{pmatrix}i_{ds}\\ i_{qs}\end{pmatrix} - \frac{d}{dt}\begin{pmatrix}L_{ds}i_{ds}\\ L_{qs}i_{qs}\end{pmatrix} + \omega_e\begin{pmatrix}-L_{qs}i_{qs}\\ L_{ds}i_{qs} + \psi_m\end{pmatrix} \quad (4.30)$$

Where $L_{ds} = L_s + L_{dm}$, $L_{qs} = L_s + L_{qm}$

In steady-state condition, equation (4.30) is reduced to

$$\begin{pmatrix}V_{ds}\\ V_{qs}\end{pmatrix} = \begin{pmatrix}-r_s & -\omega_e L_{qs}\\ \omega_e L_{ds} & -r_s\end{pmatrix}\begin{pmatrix}i_{ds}\\ i_{qs}\end{pmatrix} + \begin{pmatrix}0\\ \omega_e\psi_m\end{pmatrix} \quad (4.31)$$

The stator active and reactive power are expressed as:

$$P_s = V_{ds}i_{ds} + V_{qs}i_{qs} \quad (4.32)$$

$$Q_s = V_{qs}i_{ds} - V_{ds}i_{qs} \quad (4.33)$$

The active and reactive power delivered to the grid are expressed as

$$P_g = V_{dg}i_{dg} + V_{qg}i_{qg} \quad (4.34)$$

$$Q_s = V_{qs}i_{ds} - V_{ds}i_{qs} \quad (4.35)$$

By a further simplification of (4.31), the steady-state stator d-q axis currents are obtained as

$$i_{sq} = \frac{-V_{sd}}{\omega_e L_{qs}}, \quad i_{sd} = \frac{V_{sq} - \omega_e\psi_m}{\omega_e L_{ds}} \quad (4.36)$$

## 4.5. PMSG Control Strategy

The control system block diagram of the PMSG-WT system is represented in Figure 4.11, it consists of the wind generator connected to back-to-back converters that are composed of a machine side converter (MSC) and a grid-side converter (GSC), a DC-link and two controllers (machine side controller and grid side controllers). The MSC is responsible for the conversion of the three-phase AC voltages of the PMSG into DC voltage, and it is connected to the stator of the PMSG. The rotor speed of the generator is measured from the rotor of the wind turbine while all the outputs of the sensors are directly imputed into the controller of the machine side as input signals, used in voltage reference control of the MSC during modulation.

The GSC is grid-connected by a step-up transformer, grid voltage and current are both detected on the transformer high voltage side respectively. The DC capacitor detects the DC voltage $V_{dc}$, and the grid side controller is responsible for controlling the voltage reference of the GSC. During the grid fault incidence, the DC voltage $V_{dc}$ may experience a significant increase as a result of power unbalance between the MSC and GSC. For both converters, the triangle signal is chosen as the carrier wave of pulse wave modulation (PWM) operation, and the carrier frequency of the PWM is set to 1.65 kHz for both converters.

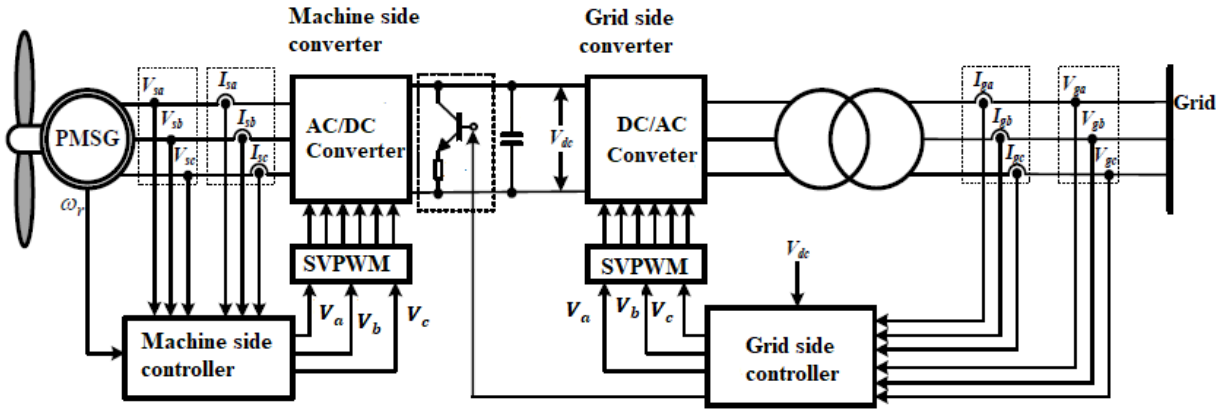


Figure 4.11. Block diagram of PMSG-WT control.

# 4.5. 1. Machine Side Control

There are two main control techniques for the PMSG's machine side converter as reported in [30], which are the Direct Torque Control (DTC) and Field Oriented Control (FOC). This thesis uses the FOC and is implemented in the synchronously rotating reference frame. The FOC is preferred in this thesis as the control algorithm for the generator side converter because of the convenience of the control of the spatial orientation of the permanent magnet flux. The phasor diagram of the FOC is shown in Figure 4.12. Conventional control of the machine side converter is shown in Figure 4.13. The PMSG utilizes an inner current loop and an outer reactive power loop. The inner current loop outputs a q-axis current reference $i_{sq}^{*}$. This loop ensures that the q-component of the measured current reaches the q-axis current reference while the d-component of the measured current reaches the d-axis current reference $i_{sd}^{*}$ [120] - [122], and the outer reactive power loop depends entirely on the controllers of the d- and q- current loop. The conventional control strategy generates a d-or q-

axis voltage that is based on the error signals of the d-or-q-axis current. Under a normal grid voltage condition, the MSC adopts the traditional control method.

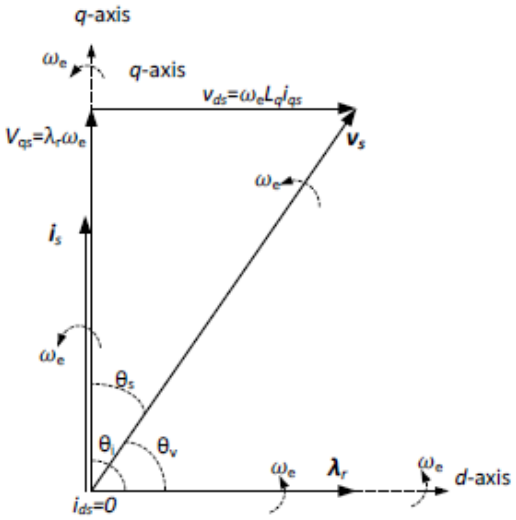


Figure 4.12. Phasor diagram of the FOC

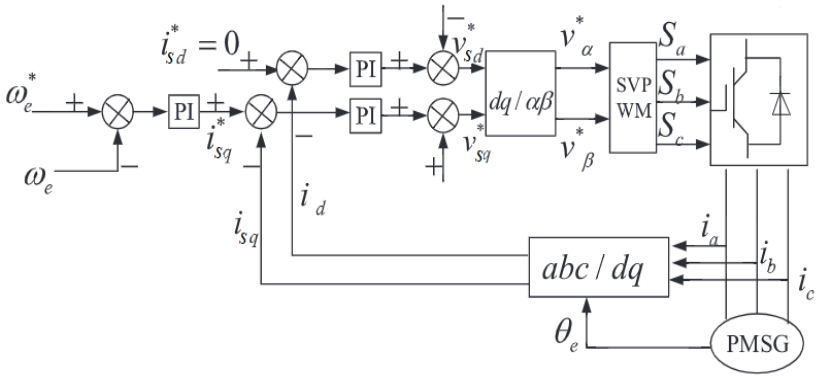


Figure 4.13. Conventional control of Machine side converter

The proposed controller structure for the MSC of the PMSG is presented in Figure 4.14. Unlike the conventional control that utilizes the d-or q-axis current error in generating the d- or q-axis voltage, the proposed MSC control strategy uses the actual current signal at the d-and q-axis loop of the

controller to generate the d-axis and q-axis currents $i_{sd}$ and $i_{sq}$, respectively, which are in turn used to compute the d-and q voltages $V_{sd}$ and $V_{sq}$, expressed in (4.37) and (4.38), derived from (4.30).

$$V_{sd} = -\left(r_s i_{sd} + L_d \frac{di_{sd}}{dt}\right) - \omega_e L_q i_{sq} \tag{4.37}$$

$$V_{sq} = -\left(r_s i_{sq} + L_q \frac{di_{sq}}{dt}\right) + \omega_e L_d i_{sd} + \omega_e \psi_f \tag{4.38}$$

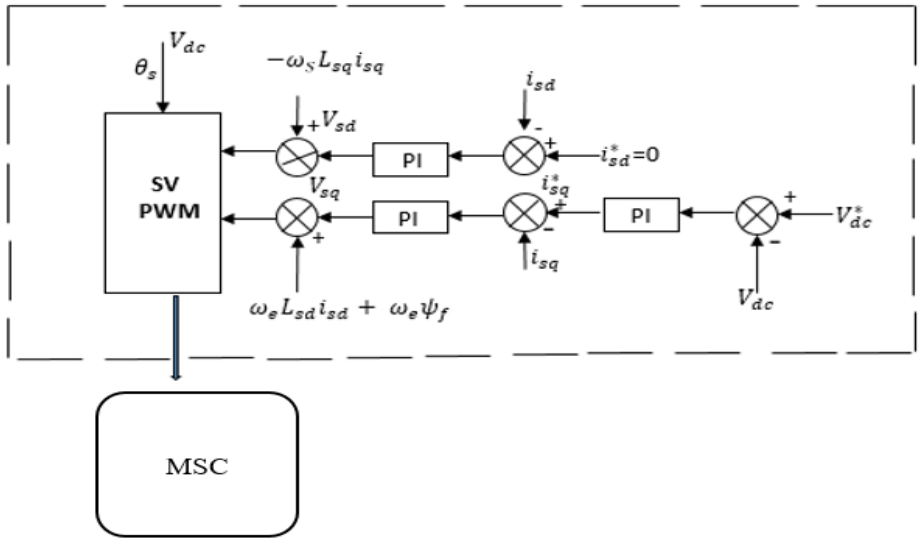


Figure 4.14. Machine side controller system

The focus of the machine side converter is to ensure the stability of the DC link voltage of the converter. The DC link voltage is determined by the differential between the extracted active power by the MSC and the power output of the GSC. The PI controller is used in deriving the reference current, $i^*_{sq}$, on the q-axis. During the fault period, the rotational speed of the generator may become uncontrollable. Pitch control is therefore activated to limit the speed of the generator.

It is important to point out that the proposed control ensures that the reference current on the d-axis is adjusted if its amplitude exceeds the rated current, this way the turbine generator is prevented

from exceeding the rated current at any given time. This is achieved by modifying the current reference, $i_{sd}^{*}$, on the d-axis and keeping the reference current, $i_{sq}^{*}$, on the q-axis unchanged to effectively maintain the control of the wind turbine. The current control loop of the controller in the d-q axis is expressed as

$$V_{sd} = \left(K_{p1} + {K_{p1}}/{\tau_i S}\right)(0 - i_{sd}) - \omega_s L_s i_{sq} \tag{4.39}$$

$$V_{sq} = \left(K_{p1} + {K_{p1}}/{\tau_i S}\right)(0 - i_{sq}) + \omega_s L_s i_{sq} + \omega_s \psi \tag{4.40}$$

Where $\tau_i$ and $K_{p1}$ are integral time constants and proportional coefficients of the PI controllers.

## 4.5.2. Grid Side Control

The GSC of the PMSG is modelled in the synchronously rotating reference frame with grid voltage orientation (4.41) and (4.42), adapted from [120].

$$\mathrm{V_{gd}} = \mathrm{v_{gd}} - \mathrm{R_g i_{gd}} - \mathrm{L_g}\frac{\mathrm{di_{gd}}}{\mathrm{dt}} + \omega \mathrm{L_g i_{gq}} \tag{4.41}$$

$$\mathrm{V_{gq}} = -\mathrm{R_g\, i_{gq}} - \mathrm{L_g}\frac{\mathrm{di_{gq}}}{\mathrm{dt}} - \omega \mathrm{L_g i_{gd}} \tag{4.42}$$

The average active power, $P_{g-av}$ and average reactive power $Q_{g-av}$ of the PMSG based wind farm are presented as

$$1.5\,(V_{gd}\ i_{gd} + V_{gq}\ i_{gq}),\ 1.5\,(V_{gd}\ i_{gq} - V_{gq}\ i_{gd}) \text{ respectively.} \tag{4.43}$$

Where $V_g$ represents the terminal voltage of the PMSG based wind farm and $i_g$ represents the AC current of the GSC. The terminal voltage of the PMSG wind farm is represented by $V_g$ , the voltage and current of the AC side are represented by $v_g$ and $i_g$ respectively, the synchronous rotating angular speed is represented by ω, the total inductance is given as $L_g$, $R_g$ represents the line resistor while the subscripts d and q represent the components of the d-and q-axis components respectively.

The primary control target of the GSC in this research is the stabilization of the PMSG-FSIG hybrid wind system, ensuring that the active power of the PMSG is stably and reliably transferred to the grid, maintaining and improving the grid voltage during a fault condition, and compensating the reactive power demand of the FSIG- based wind system. The block diagram of the grid side controller system is shown in Figure 4.15.

By implementing an active power limit control strategy, the capacity of the GSC is used to improve the LVRT ability of the FSIG based wind farm by providing the required reactive power.

Just like the MSC, this control strategy is also based on and implemented in the $dq$ rotating reference frame, having the same rotational speed as the grid voltage. The three-phase voltages and currents are transformed from the $abc$ reference frame to the $dq$ rotating reference frame using the Park transformation and, the phase angle of the grid side $\theta_g$ is extracted by a phase-locked loop (PLL). By transforming the grid voltages from the $abc$ reference frame to $dq$ rotating reference frame using the Park transformation, $V_{gd}$ is set to constant while $V_{gq}$ is set to zero. This way, the active and reactive power are both delivered to the grid and controlled separately by the $d$- and q- axis currents $i_{gd}$ and $i_{gq}$ respectively.

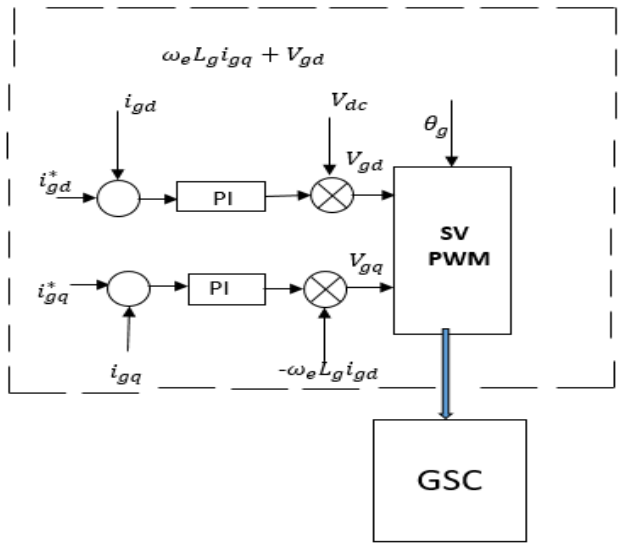


Figure 4.15. Grid side controller system

For a balance between the generated active power and active power delivered to the grid, $V_{dc}$ is maintained constant. The current reference signal $i^*_{gd}$ on the d-axis is determined from the output of the DC-voltage controller while the current reference signal on the q-axis, $i^*_{gq}$ is obtained to keep the grid terminal voltage constant at 1 pu. $i^*_{gd}$ is kept unchanged to ensure that dc-link voltage is controlled effectively while $i^*_{gq}$ is modified to provide the reactive power demand. The d-q axis current control loop of the controller is expressed as

$$V_{gd} = -\left(K_{p1} + {K_{p1}}/{\tau_i S}\right)\left(i^*_{gd} - i_{gd}\right) + \omega_e L_e i_{gq} + V_{gd} \tag{4.44}$$

$$V_{gq} = -\left(K_{p1} + {K_{p1}}/{\tau_i S}\right)\left(i^*_{gq} - i_{gq}\right) - \omega_e L_e i_{gd} \tag{4.45}$$

Where $\tau_i$ and $K_{p1}$ are integral time constants and proportional coefficients of the PI controllers.

## 4.5.3. Phase-Locked Loop (PLL)

The transformation of the three-phase grid voltage from the $abc$ frame into the $dq$ synchronous frame is made possible by the phase-locked loop (PLL) of the control scheme of the PMSG. The PI controller controls the $q$-axis current by suppressing it to zero to ensure the grid voltage is aligned to the $d$-axis, ensuring that the decoupling of the $dq$ axis is consequently achieved. The output of the PI controller alongside the integrator then generates the grid voltage phase angle, which is delivered back as the input of the Park transformation. Figure 4.16 shows the schematic of the PLL. The phase detector measures the phase difference between input and output signals and then passes the signal through a low pass filter that generates an error signal which drives a voltage controlled oscillator to generate the output signal, as shown in the schematic in Figure 4.16.

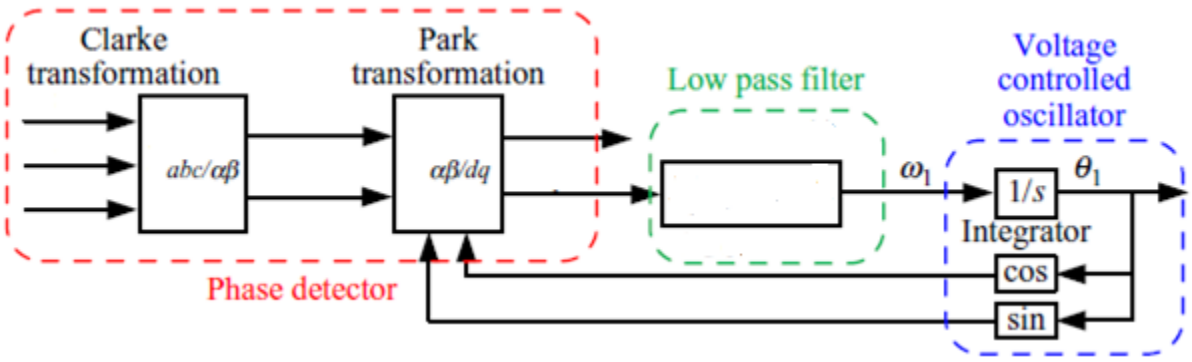


Figure 4.16. PLL for grid integration

In designing the PI controller of the PLL, a linear modelling approach is used. Therefore, the angular frequency of the PLL is represented as

$$\omega = \frac{d\theta}{dt} = K_f \,.\, E_m \sin\delta \tag{4.46}$$

The filter gain is represented as $K_f$, $\delta$ is the phase difference. $\delta$ is linearized and (4.46) is further expressed as (4.47) in the linearized form.

$$\omega = K_f E_m \delta \tag{4.47}$$

Therefore (4.46) is represented as shown in Figure 4.17. The rotor angle and rotor speed can be estimated by tuning the PLL using the design procedure as reported in [123].

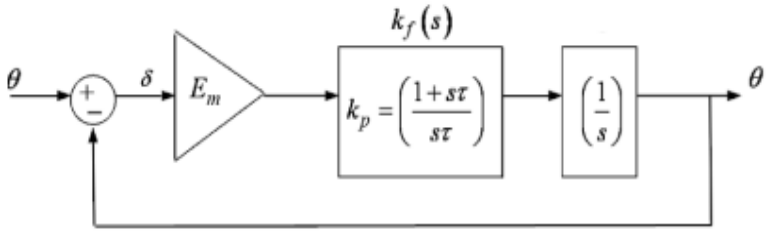


Figure 4.17. A linearized model representation of the PLL

## 4.5.4. Space Vector Pulse Width Modulation (SVPWM)

The SVPWM control scheme is implemented by a double control loop, an inner current loop and the outer control loop. The outer loop is responsible for adjusting the $d$-axis current for the control of active power, thus ensuring that there is a direct injection of power from the converter into the grid. In the same way, the reactive power is controlled by the inner loop control through the PI controller by regulating the $q$ axis current. The target of the SVPWM is to approximate the reference voltage vector by turning the power switches either ON or OFF. The reference signal is modified according to the operating conditions of the PMSG wind system in every sampling period, to improve the power quality of the AC outputs. A two-level voltage source inverter (VSI) is used for transforming the DC power to AC power. This is shown in Figure 4.18. The IGBT power switches, $Q_1$ to $Q_6$ are controlled by the switching signals $a, a', b, b', c$ and $c'$ to set the ON and OFF switching states

respectively. The VSI operates in two zero states and six active states, and a triangular carrier wave is employed. The frequency of the SVPWM generator is set at 1.6kHz.

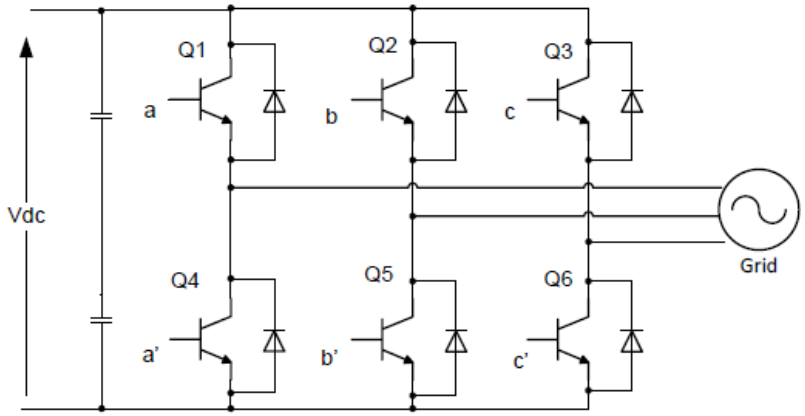


Figure 4.18. Two-level voltage source inverter.

## 4.6. Operation of the Hybrid Wind Farm

As indicated in Section 4.2 of this Chapter, the hybrid wind farm consists of a 20 MW FSIG wind system and a 10 MW PMSG wind system. The sub-wind farms are parallel connected at the PCC by a 35 kV short transmission line, and the hybrid wind farm is connected to the power grid via a 110 kV transmission line. The mechanical torque output of the PMSG wind turbine is effectively reduced when the rated power is reached by a simple pitch control modelled into the control system. Figure 4.19 shows the control scheme block diagram of the hybrid wind farm consisting of the PMSG- and FSIG wind turbine, and Figure 4.20 presents the relationship between the turbine output power and its generator speed, for different wind speeds. The parameters used for the PMSG and FSIG based wind farms are shown in Tables 4.1 and 4.2 respectively.

**Table 4.1. PMSG-WT parameters**

| **Parameters** | **Values** |
|---|---|
| Rating | 10 MW |
| Generator Voltage | 690V |
| Stator resistance | 0.006 pu |
| Reactor resistance | 0.013 pu |
| Frequency | 50Hz |
| Stator leakage reactance | 0.125 pu |
| Reactor inductance | 0.179 pu |
| D-axis inductance | 0.95 pu |
| Q-axis inductance | 0.75 pu |
| Inertia constant | 0.62 H |
| DC-link voltage | 1100 V |

**Table 4.2. FSIG parameters**

| **Parameters** | **Values** |
|---|---|
| Rating | 20 MW |

| | |
|---|---|
| Generator Voltage | 690V |
| Stator resistance | 0.0049 pu |
| Reactor resistance | 0.004 pu |
| Frequency | 50Hz |
| Stator leakage reactance | 0.125 pu |
| Reactor inductance | 0.179 pu |
| Magnetizing inductance | 6.80 pu |
| Inertia constant | 5.0 H |

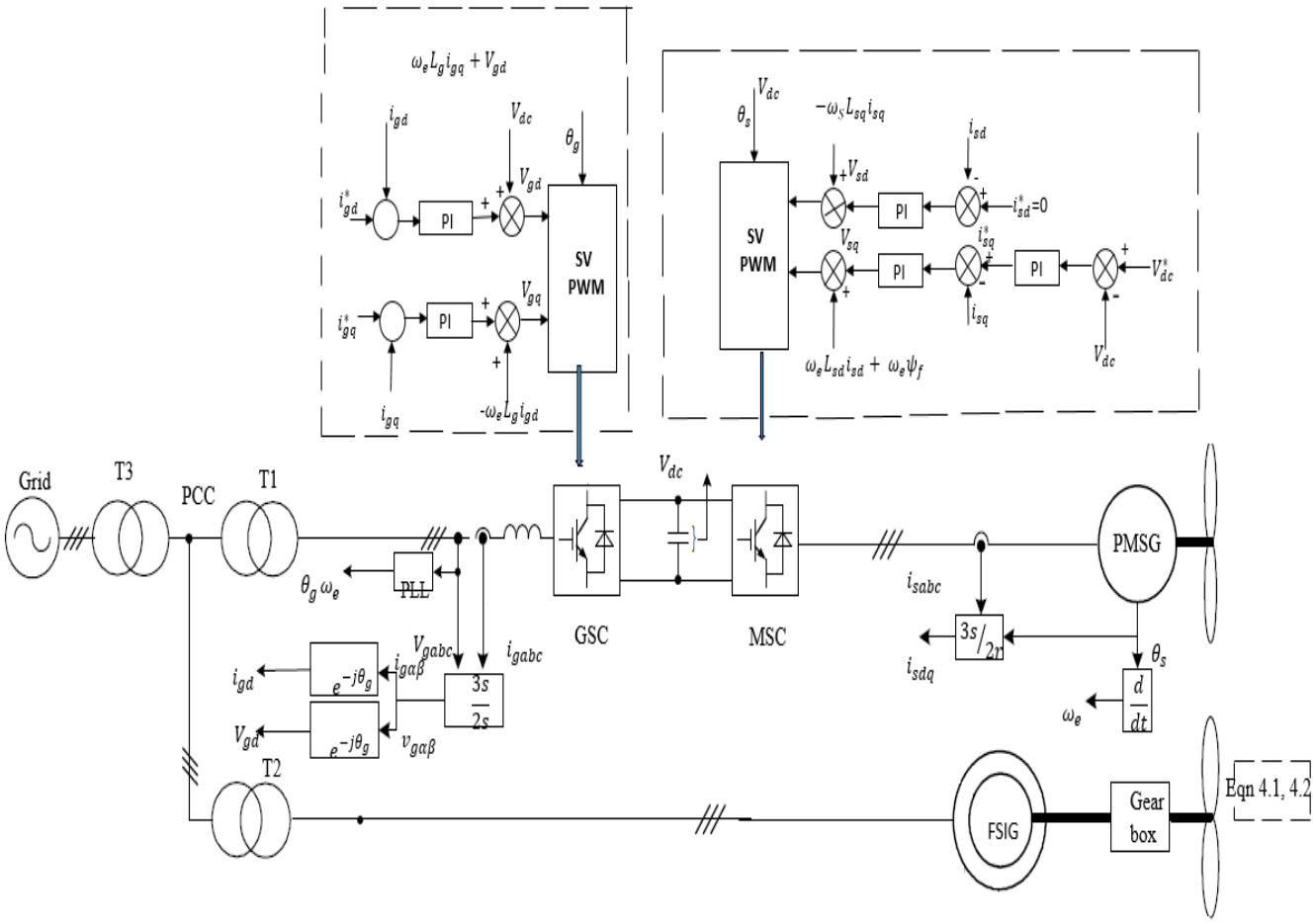


Figure 4.19. Schematic diagram of the proposed control scheme for the hybrid wind farm.

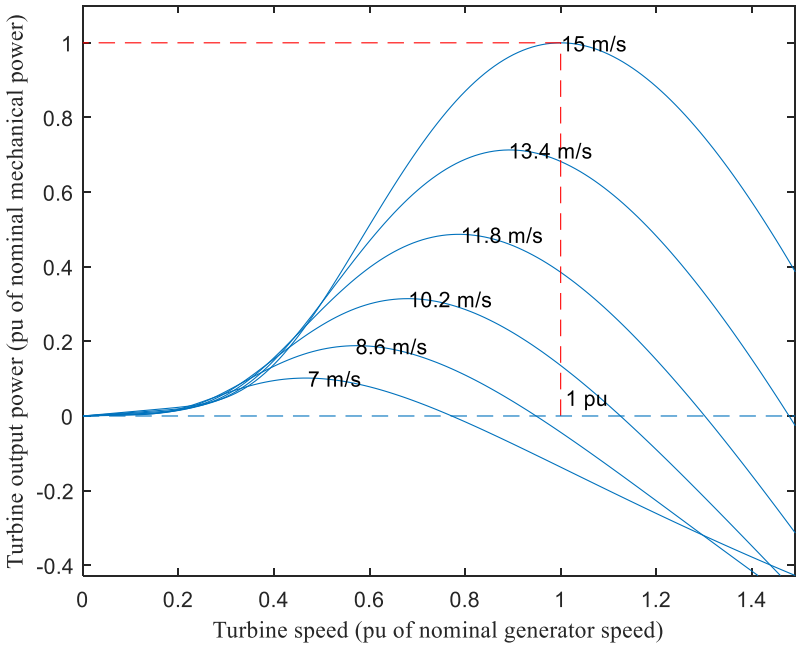


Figure 4.20. Turbine output power vs generator speed

As seen from Figures 4.21 to 4.28, the FSIG-and PMSG-wind farms both operate as normal under steady-state conditions. Both wind systems generate an output power of 1 pu of rated power. The generator speed of the PMSG is kept at 1 pu, while the rotor speed of the FSIG varies between 1 pu and 1.005 pu and DC voltage is set at 1100V. The rotor speed of the FSIG is assumed to be proportional to the wind speed at maximum aerodynamic efficiency at low speeds and equal to the rated rotor speed at high wind speeds. In a steady state, the GSC of the PMSG is controlled for active power by regulating the rotor speed. This is however dependent on mechanical time constraints. During grid normal operation, the power from the MSC is equal to that of the GSC, ignoring power loss. Accordingly, the DC voltage is maintained at a rated value.

However, under transient conditions, an unbalance occurs between the input mechanical torque of the FSIG and output electromagnetic torque as a result of the grid voltage sags. This unbalances in torque results in the over-speeding of the FSIG rotor causing as indicated in Chapter 3, causing it to

lose its stability, and resulting in the disconnection of the FSIG from the power network. Also, there is a need for large consumption of reactive power by the FSIG while the rotor operates at a high slip, this can lead to further grid voltage collapse during fault recovery. This characteristic of the FSIG makes it impossible for the FSIG wind system to be able to inject the needed reactive power required to fulfil the conditions of the grid code during a grid fault condition without additional auxiliary devices.

The GSC of the PMSG is controlled to provide the minimum required reactive power needed for the FSWT to successfully go through a grid voltage condition. When a fast electrical transient occurs, like a grid fault condition, the rotor speed regulation of the PMSG is temporarily neglected and the reactive power is used in supporting the grid during voltage sag. For the hybrid wind system under investigation, during a grid fault condition, the flexible low voltage ride-through capability of the GSC of the PMSG is taken advantage of, by modifying the GSC to transiently inject nominal reactive power for the support of the FSIG wind system. The current components $i_{gd}$ and $i_{gq}$ are both controlled to ensure voltage stability and provide the required reactive power needed by the nearby FSIG-wind system.

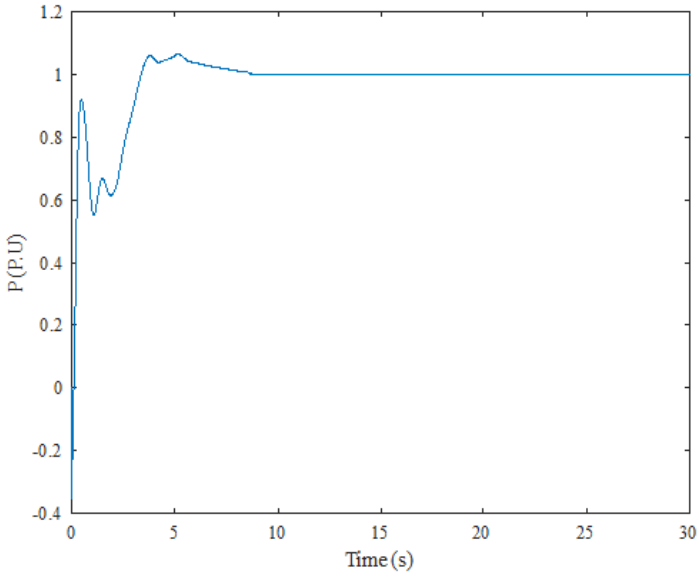


Figure 4.21. Output active power of PMSG wind farm

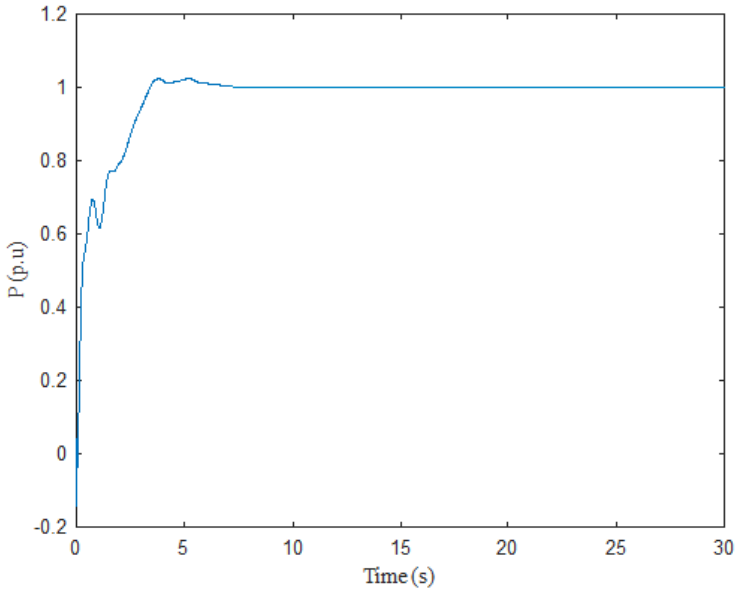


Figure 4.22. The output power of FSIG wind farm

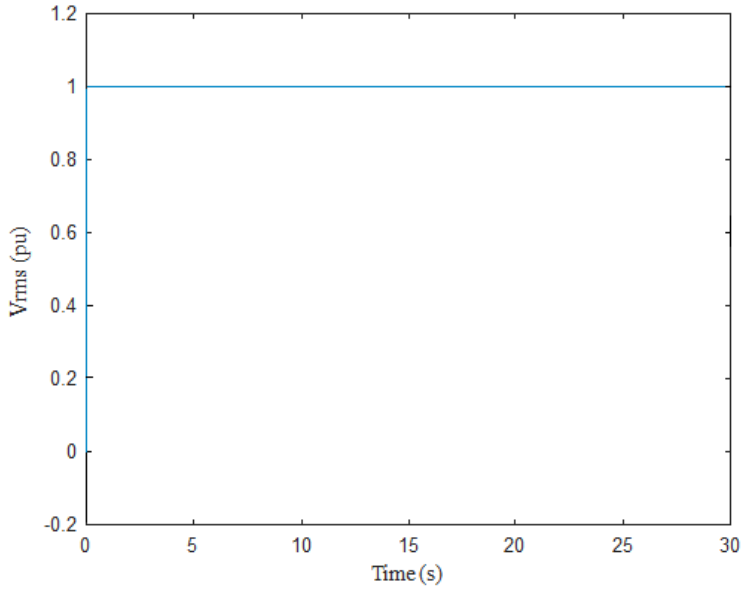


Figure 4.23. Grid  voltage of hybrid wind farm

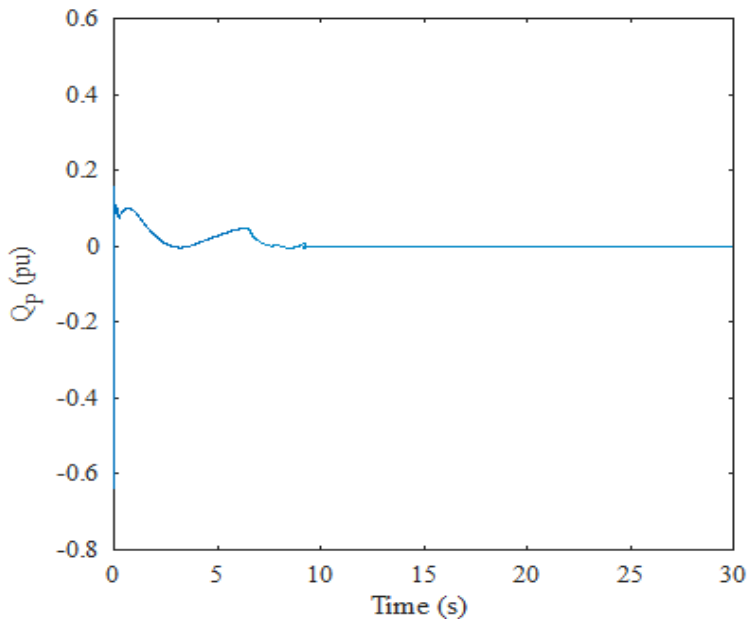


Figure 4.24. Reactive power output of PMSG wind farm

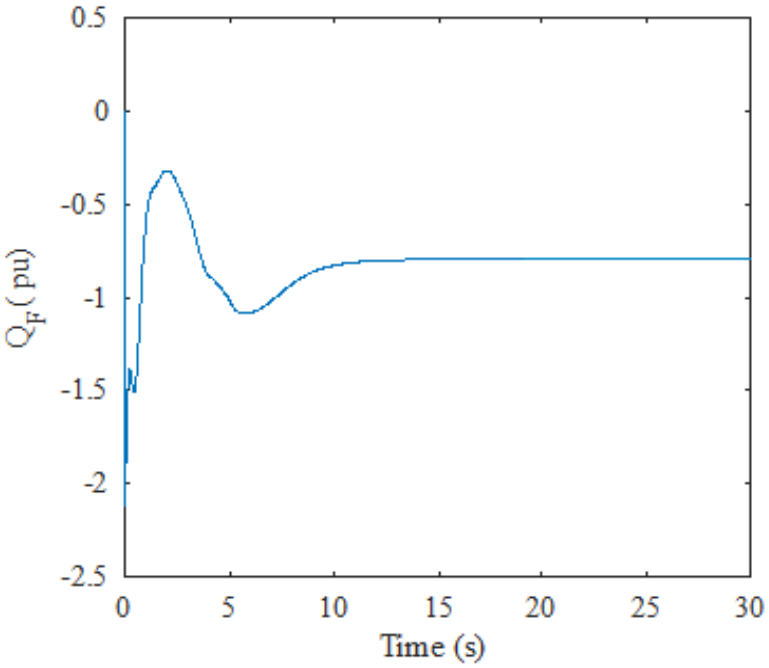


Figure 4.25. Reactive power output of the FSIG wind farm

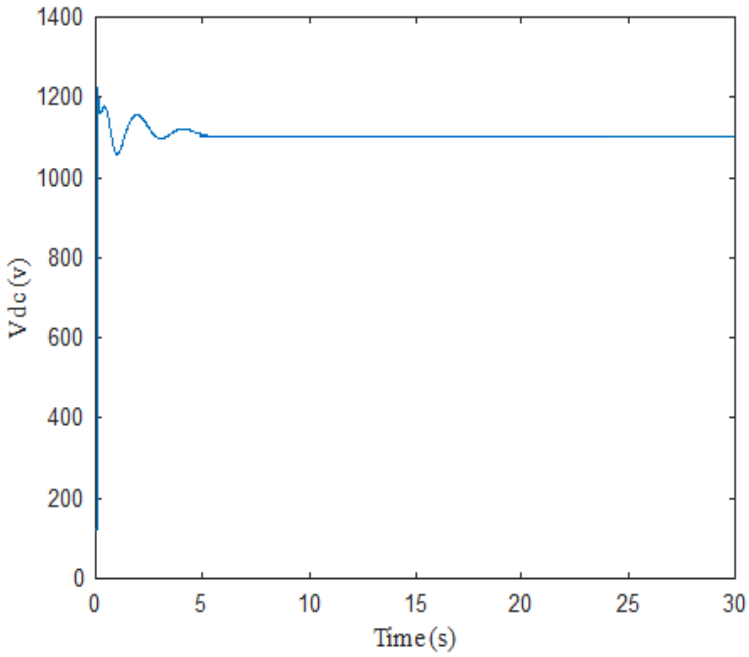


Figure 4.26. DC link voltage

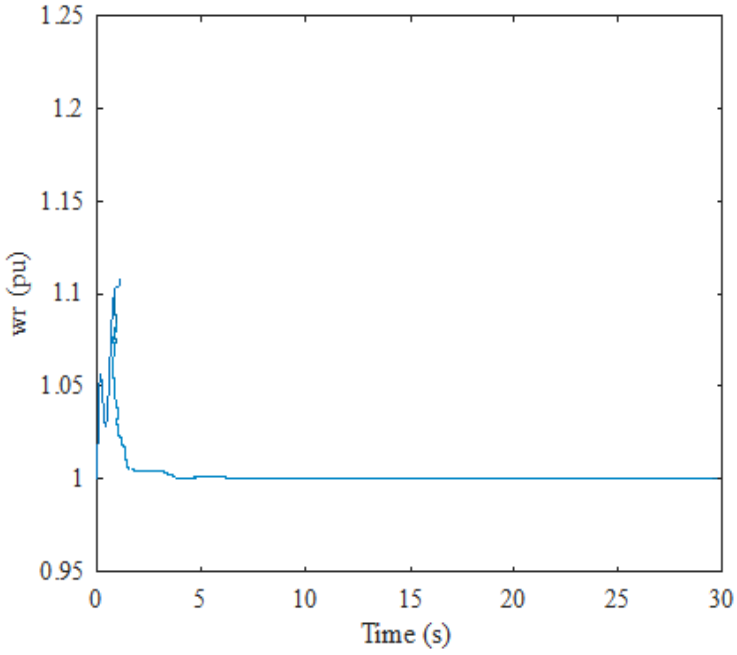


Figure 4.27. Rotor speed of the PMSG

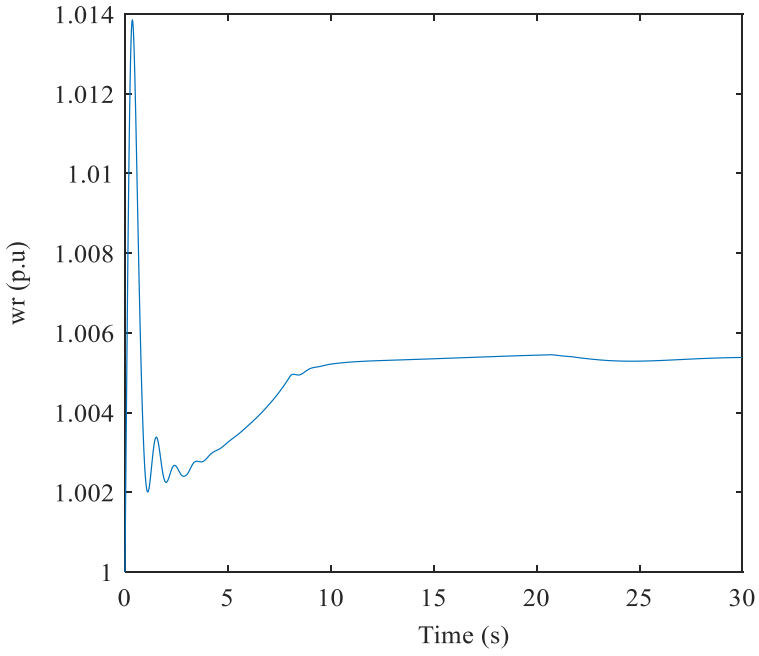


Figure 4.28. Rotor speed of the FSIG

## 4.7. Chapter Summary

This chapter has presented an introduction to hybrid wind energy systems. Three different configurations for hybrid wind power systems have been identified. These are the

- DFIG-PMSG wind conversion system
- DFIG-FSIG wind conversion system
- PMSG-FSIG wind conversion system.

Though the DFIG is popular with wind installations, however, the support provided by the DFIG wind system for reactive power compensation in a hybrid wind system is restricted due to the partially rated power converters of the DFIG based wind farm. This means that during a network unbalance, the DFIG based wind farm has a limited effect on improving the operational performance of a hybrid wind system which consists of a FSIG based wind farm

Unlike the DFIG, the PMSG wind system is regarded as a better option for a hybrid wind system. This is because the PMSG operates with fully rated power converters and can control a wider operating region for various control targets. A unique characteristic of the PMSG-WT system is its ability to control a wider operating region for various control targets. With a coordinated control of the PMSG during grid faults, the operational performance of a nearby DFIG or FSIG based wind system can be improved. This characteristic of the PMSG-WT makes it more ideal than the DFIG for a hybrid wind configuration with the FSIG system.

The mathematical modelling of the individual wind farms that make up the hybrid wind farm is presented and the chapter concludes by presenting the operation of the hybrid wind farm. The proposed coordinated control strategy for the hybrid wind system is discussed further in Chapter 5.

The contributions and parts of this chapter have been published in the paper

**Apata, O., and D. T. O. Oyedokun. "A Mathematical Approach To Hybrid Wind Farm Modelling." 2020 IEEE PES/IAS PowerAfrica. IEEE, 2020.**

# Chapter 5

# Development of Proposed Hybrid Solution for Reactive Power Compensation in the FSIG Wind System

This chapter presents a proposed coordinated control strategy for a hybrid wind farm consisting of the PMSG-wind farm and FSIG- wind farm under a grid fault condition. The proposed strategy is based on a novel principle of reactive current allocation in the GSC, that is implemented for the PMSG wind farm to support the reactive power need of the FSIG wind farm and provide the maximum reactive power required for grid voltage support of the hybrid wind farm. The subsections below describe the development of the proposed strategy.

## 5.1. Reactive Current Limit Determination

To determine the current allocation procedure for the reactive current of the PMSG wind system, it is important to determine the reactive current limit of the PMSG based wind system to avoid the possibility of injecting an overcurrent of reactive current which can subsequently result in the wind system disconnecting from the grid by the protection relay. Since the PMSG based wind system is controlled in the grid-voltage-oriented reference frame [124], its output active and reactive powers respectively are expressed as shown in (5.1).

$$P_P = V_{g\_P} i_{gd\_P} \; ; Q_{PMSG} = V_{g\_P} i_{gq\_P} \tag{5.1}$$

Where $V_{g\_P}$ represents the voltage at the terminal of the PMSG based wind farm, $i_{gd\_P}$ and $i_{gq\_P}$ represents the currents of the GSC in the d- and q- axis of the PMSG wind system respectively.

In other to determine the reactive current limit for the GSC, there is a need to specify the grid code requirements with regards to grid voltage and reactive power compensation during a fault occurrence. Figure 5.1 illustrates the voltage-time profile of the South African grid code, showing

the voltage ride-through requirements for wind generators [125]. The South African grid code requires that if grid voltage drops to 0 pu the wind system should be able to remain connected to the grid for 0.15 seconds without disconnecting and the grid voltage to recover to at least 0.85pu in 2 seconds. During a fault, the delivery of reactive power is given higher priority than active power to support the voltage over maintaining active power production. However, in [126], it was shown that depending on network and wind farm configuration, a fault condition does not necessarily lead to a zero voltage at the grid. A relatively simple calculation indicates that the corresponding voltage dip at lower voltage levels, near the terminals of the wind turbine, is likely to be somewhat above 15%. This thesis has therefore adopted the lowest grid voltage to be 15% instead of 0% as indicated in the South African grid code.

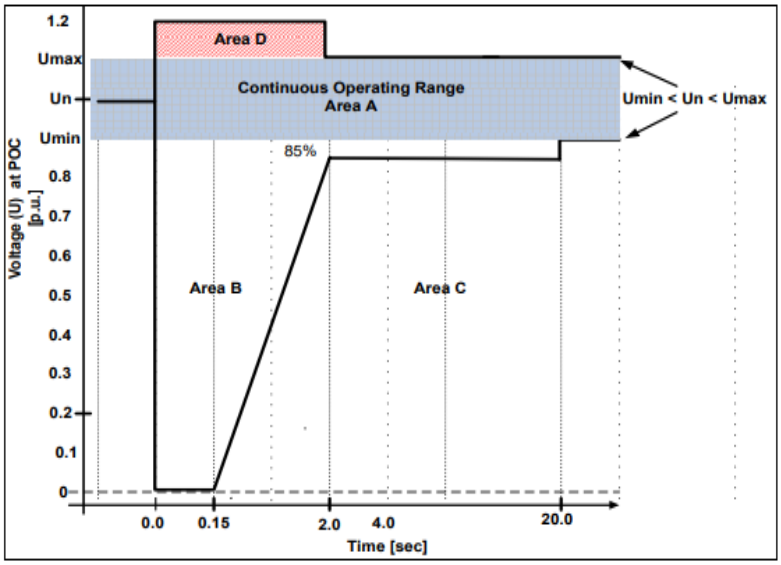


Figure 5.1. Voltage ride through requirements for wind generators [127]

The grid code requires that the grid-connected wind farm must be able to provide appropriate reactive currents $I_Q$ required by the wind farm under a grid fault condition and the per-unit value of $I_Q$ must satisfy the conditions

$$I_Q \geq 1.5\,(0.9 - V_G)I_r,\ 0.2\ \text{pu} \leq V_G \leq 0.9\text{pu} \tag{5.2}$$

Where $V_G$ is the per-unit value of the terminal voltage of the grid-connected wind farm and $I_r$ is the rated current of the wind farm. From (5.2) it can be inferred that the minimum reactive current required by a wind farm during a grid fault condition is $1.5\,(0.9 - V_G)I_r$. From the grid code requirement, it can be deduced that the maximum reactive current, $i_{gqmax}$, of the GSC should be less than the maximum allowable current $i_{gmax}$.

$$i_{gqmax} \leq i_{gmax} \tag{5.3}$$

To prevent the GSC from exceeding the rated current, the $d$-axis current, $i_{gd}$, is kept unchanged to maintain voltage control of the dc-link while the $q$-axis current $i_{dq}$ is modified to satisfy the reactive power need of the wind system. Considering the current capacity of the GSC in the PMSG, the output reactive current limit of the GSC is calculated as:

$$i_{gqmax} = \sqrt{(i_{gmax})^2 - (i_{gd})^2} \tag{5.4}$$

The allowable maximum current amplitude of the GSC, $i_{gqmax}$, is set at 1.1 pu. Based on (5.4), and since $i_{gqmax}$ of the GSC is larger than the stator capacity of the FSIG, more reactive current is supplied by the PMSG based wind farm during the grid faults conditions. The detailed control process to achieve (5.4) is shown in Figure 5.2. $P_g$, and $P^*$ are the actual and reference values of the active power output of the PMSG respectively, $Q_g$, and $Q^*$ are the actual and reference values of the reactive power output of the PMSG respectively. The amplitudes of $i_{gd}^*$ and $i_{gq}^*$ are limited according to the maximum current rating of the converter. It is important to point out that by controlling $i_{gd}^*$ to provide more reactive current reference $i_{gq}^*$ in the GSC for reactive power support in the FSIG-based wind system, the PMSG during the fault duration will have its output power reduced momentarily while the DC voltage rises momentarily.

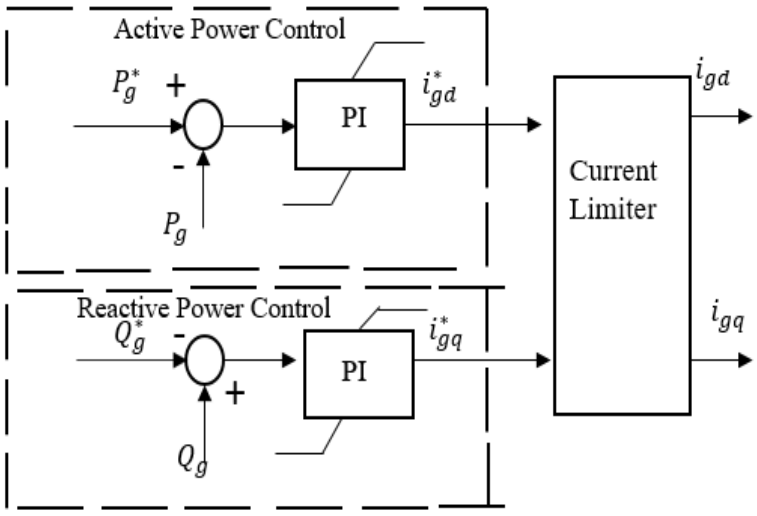


Figure 5.2. Current limiter control process

## 5.2. Proposed Current Allocation and Coordinated Control Strategy for the Hybrid Wind Farm

A current allocation strategy in the PMSG wind system is developed based on the converter capacity and current capability of the GSC to provide the required reactive power needed by the FSIG-based wind farm during the grid fault condition. Based on the current allocation strategy, coordinated control of the hybrid wind farm consisting of a PMSG -based wind farm and FSIG-based wind farm is developed. With this approach, the GSC capacity of the PMSG is utilized efficiently for the LVRT capability enhancement of the FSIG-based wind farm.

### 5.2.1 Proposed Current Allocation Strategy

Based on the requirement of the grid code and the requirement of (5.2), the GSC current limit as expressed in (5.4) is modified and becomes

$$i_{gqmax} = \sqrt{I_{gmax}^2 - (\frac{P_P}{V_g})^2} \geq 1.5\,(0.9 - V_G)I_r \quad (5.4)$$

The GSC controller changes the priorities of the real and reactive current when the terminal voltage drops below the defined value of 0.9 p.u. In normal operation, high priority is given to the DC-link voltage regulation. However, during a fault, high priority is given to the voltage control. A flowchart of the proposed current allocation strategy in the GSC of the PMSG is shown in Figure 5.3 while Figure 5.4 presents the current allocation strategy of the GSC in the PMSG-based wind farm. When a grid fault occurs on the hybrid wind farm system, the proposed control mechanism checks the network parameters of the FSIG based wind system to see if there is provision to fulfil the requirements of the grid code and to determine the minimal reactive power need of the FSIG wind system. During the grid fault, depending on the severity of the fault type and level of voltage sag, the transient component appears in the stator flux of the FSIG causing an overvoltage and overcurrent in the FSIG based wind system. During the low voltage period, the reference value of the reactive current $i_{gq}^*$ is set as the required minimum reactive current of the low voltage condition to meet the grid-connected wind farm code. Taking into consideration the maximum allowable current of the GSC in the PMSG wind system, the PMSG based wind farm can immediately deploy the proposed control strategy when the grid fault occurs, independently setting the active and reactive current reference values. Based on the current reference values, the converters are regulated by the PI controllers and the operational performance of the hybrid wind farm is significantly improved during the grid faults.

Depending on the condition of the hybrid wind farm when the grid fault condition occurs, the current components $i_{gd}$ and $i_{gq}$ are controlled to pass through a current limiter to get the maximum allowable current $I_{gmax}$. The current limiter is a set point that determines the maximum allowable

current references allowed to pass through. The reference currents are limited to protect the switching power electronic components of the power converter. The resulting current references, $i^*_{gd}$ and $i^*_{gq}$, are then transformed into the relevant reference frame for the control of the GSC converter in providing the required reactive and active power.

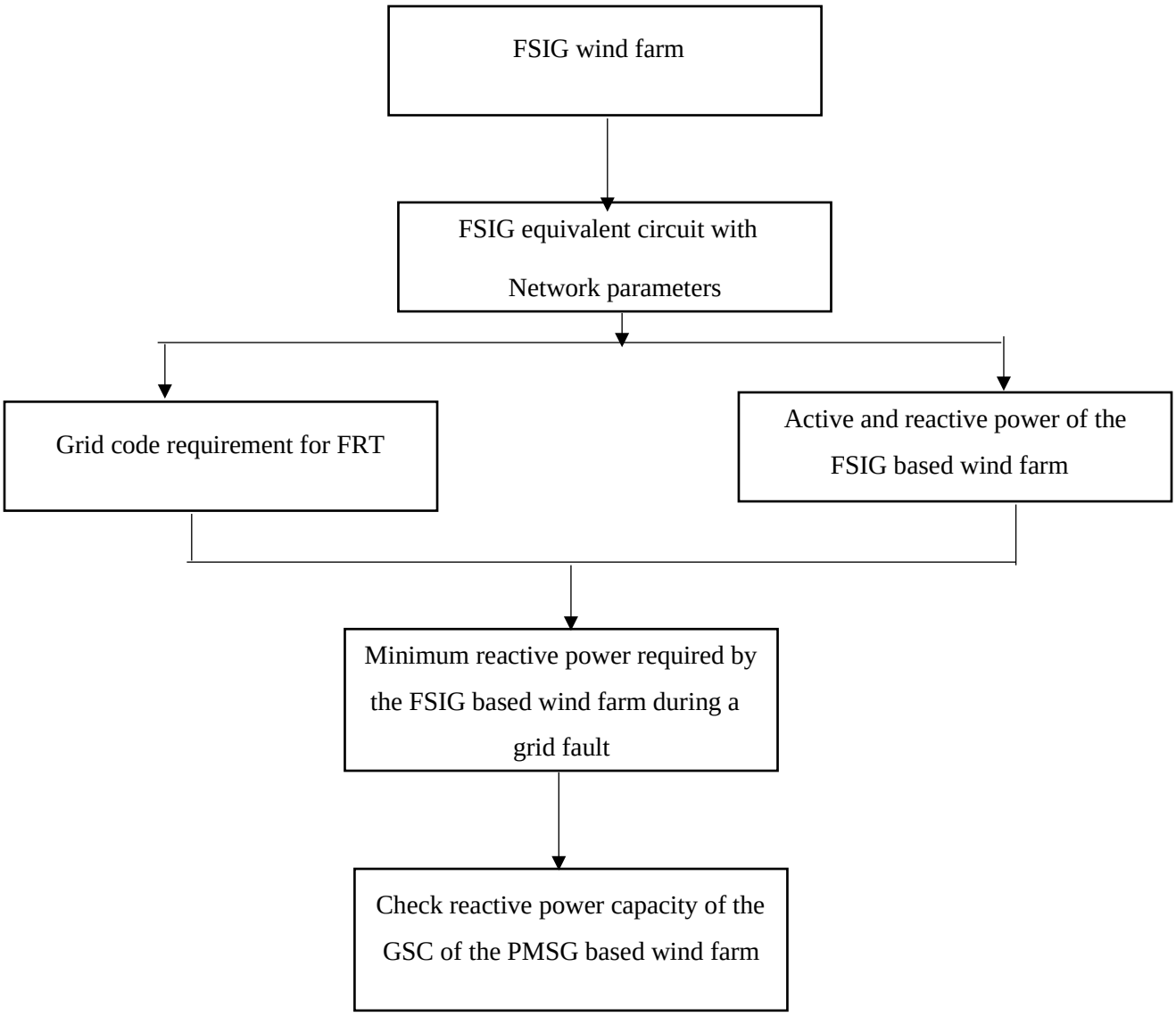


Figure 5.3. Flow chart of reactive power determination in the FSWT

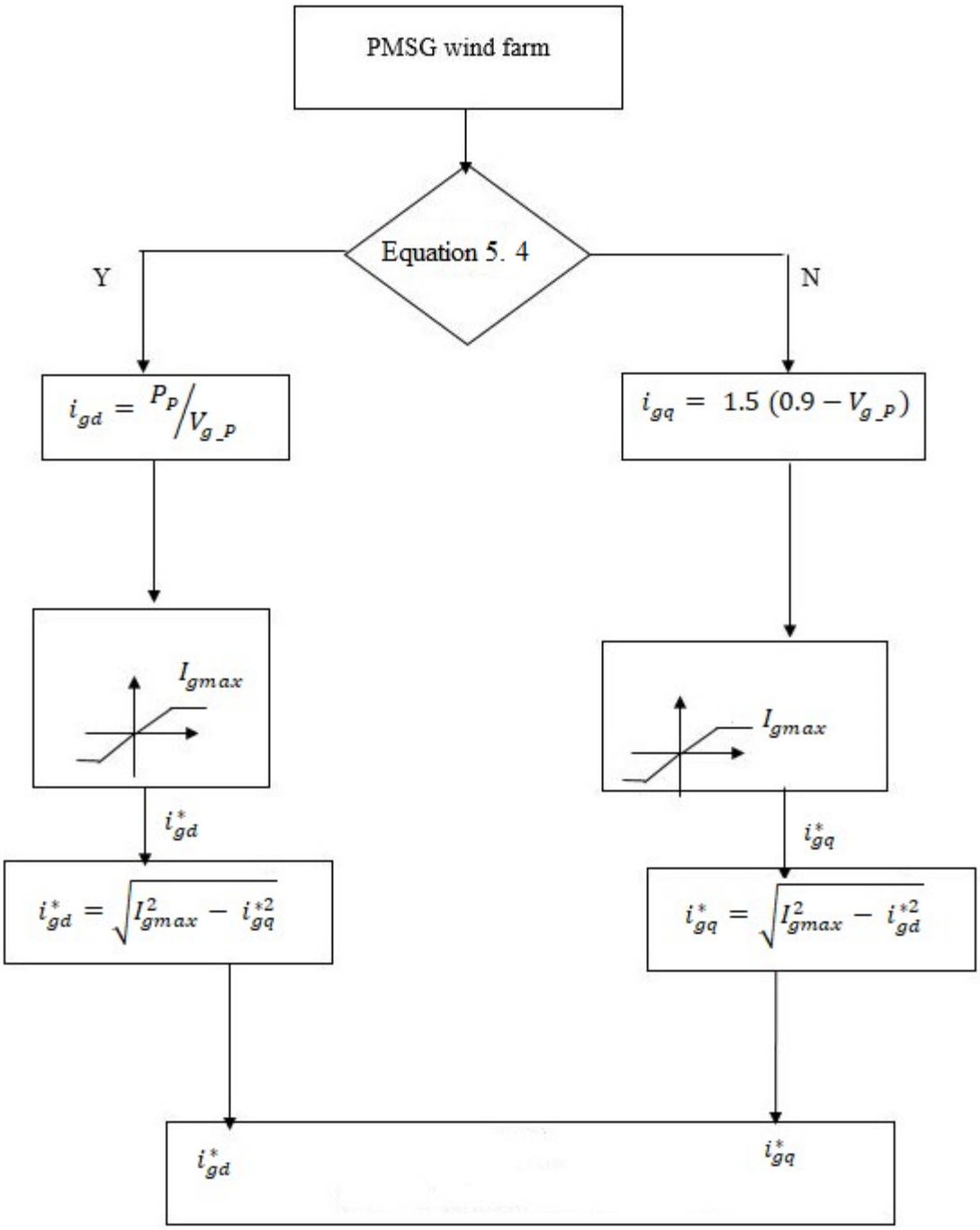


Figure. 5.4. Proposed current allocation strategy of GSC in PMSG

## 5.3. Chapter Summary

Building on the modelling of the hybrid wind farm and power characteristics of the FSIG-based wind farm as described in Chapter 4, in this chapter, the reactive current limit of the GSC of the PMSG is deduced. This is necessary to determine the maximum allowable current references allowed to pass through. The reference currents are limited to protect the switching power electronic components of the power converter.

During normal grid conditions, the individual wind farms are controlled to operate as normal while under a grid fault condition, the control priority is focused on the reactive current reference $i^*_{gq}$, which is set to the maximum allowable current $I_{gmax}$ of the GSC for reactive power support of the FSWT-based wind farm while the control priority of the q-axis reactive current $i^*_{sq}$ of the MSC is changed to maintain the stability of the DC bus.

A novel reactive current allocation strategy is proposed and applied in designing a coordinated control strategy of the hybrid wind farm consisting of the PMSG and FSWT-based wind farms respectively. The reactive current component of the GSC of the PMSG is controlled based on the reactive current allocation strategy to provide reactive power support to the FSWT-based wind farm without the installation of additional auxiliary devices, and support grid voltage recovery of the hybrid wind farm. The active current component is also controlled to improve the output active power of the FSWT wind system. The results from the proposed control strategy are presented in Chapter 6.

# Chapter 6

# Simulation Protocol, Results, and Discussions

This chapter presents the simulation of the modelled hybrid wind farm consisting of the PMSG- and FSIG-based wind farms connected to the grid at PCC. The hybrid wind farm is simulated, observing the grid voltage and behaviour of the FSIG based wind farm with and without the proposed strategy. The simulations have been carried out in the Matlab/Simulink environment. The simulation results and relevant discussions are therefore presented.

## 6.1. Simulation Protocol

To verify the validity of the proposed control scheme and theoretical analysis, a hybrid wind farm that comprises the PMSG-based wind farm and an FSIG-based wind farm has been modelled and simulated in the Simulink environment of MATLAB. The aggregate modelling approach is selected because simulation time can be reduced significantly without compromising the validity of the results. The parameters used for the PMSG and FSIG based wind farms are shown in Tables 4.1 and 4.2 respectively. The simulated system has the same configuration as the one shown in Figure 4.1 and the control model of the hybrid wind system developed in Matlab Simulink has been described in Figure 4.19.

## 6.2. Steady-State Operation of the Hybrid Wind Farm

The steady-state operation of the wind system is described in Figure 4.21 to Figure 4.28, in steady-state, the individual wind farms are controlled to operate as normal since there is no voltage sag on the grid as both the PMSG and FSIG-based wind farms respectively are controlled to supply maximum active power. It is also observed that the rotor of the FSIG-based wind farm operates

within the range of its rated speed of between 1 pu to 1.005 pu while the hybrid wind farm operates in a steady state.

When the individual sub-wind farms of the hybrid wind farm operate in a steady-state, there is no voltage sag on the grid voltage of the hybrid wind farm. Therefore the grid voltage of the hybrid wind farm operates as normal.

## 6.3. Transient State Operation of the Hybrid Wind Farm Without Proposed Reactive Power Support Strategy

To verify the correctness of the proposed method and the theoretical analysis carried out, different fault scenarios such as the single-line-to ground fault (LG), line-to-line fault (LL), double-line-to-ground fault (LLG) and a balanced 3-phase (LLL)line-to-line-to line fault are introduced into the wind power system at t = 20 seconds, lasting for 0.2 seconds, taking into consideration the requirement of the grid code.

### 6.3.1. Single-Line-to-Ground (LG) Fault

A single line-to-ground fault is introduced into the wind system without any reactive power support provided for the FSIG wind system. Figure. 6.1 shows the impact of the grid fault on grid voltage. The grid fault condition impacts the grid voltage at PCC leading to sag in voltage levels, the grid voltage of the hybrid wind farm drops to 0.40 p.u. As analysed in Section 4.3.1, the rotor of the FSIG-based wind farm accelerates excessively above the rated speed, as seen in Figure. 6.2, because of the unbalance between the electromagnetic and mechanical torques which occur as a result of the sag in grid voltage level leading to large absorption of reactive power from the grid by the FSIG-based wind farm to stay grid-connected while the active power

at the FSIG-based wind farm drops to 0.62 p.u after the fault duration, shown in Figure 6.3 and Figure 6.4 respectively.

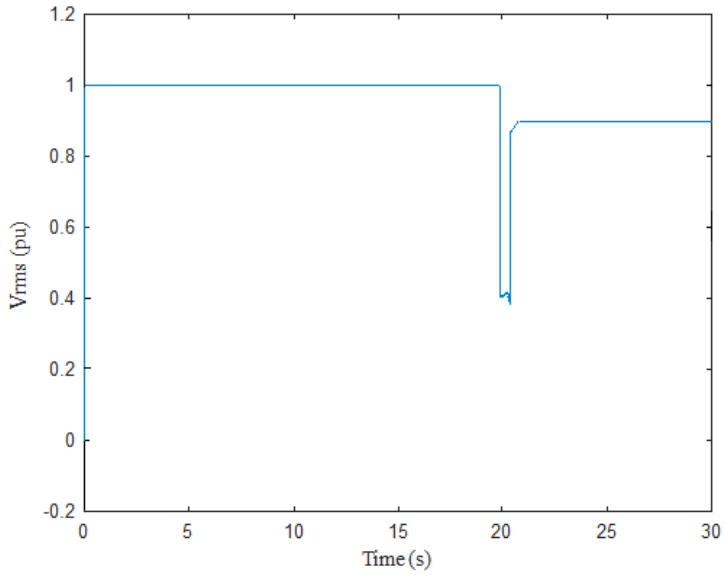


Figure 6.1. Grid voltage of hybrid wind farm

The absorption of a large amount of reactive power from the grid by the FSIG-based wind farm without adequate support validates the theoretical analysis of the transient behaviour of the FSIG-based wind system carried out in section 4.3.1. It is seen from Figure 6.2 that the rotor speed of the FSIG is within its rated speed before the introduction of the fault condition at t=20s. Without adequate reactive power support, there is a high chance the rotor speed of the FSIG-based wind farm being will continue to accelerate excessively causing the FSIG wind farm to be disconnected from the grid during the grid fault condition. The rotor behaviour of the PMSG based wind system is shown in Figure 6.5. It can be seen that the grid fault also causes the rotor of the PMSG to experience a form of momentary overspeeding, however, due to the compensating ability of the PMSG, unlike the rotor of the FSIG, the rotor of the PMSG stabilizes after the duration of the fault without it affecting the safe operation of the PMSG system. The active power of the PMSG drops to 0.58 pu during the fault. The GSC of the PMSG

supplies 0.26 p.u reactive power to the PMSG wind farm while the grid fault occurs as seen in Figure 6.6. It is observed that the PMSG wind farm immediately returns to its rated value in Figure 6.7 as soon as the fault condition is cleared while the DC-link voltage rises slightly and recovers back to 1100 V.

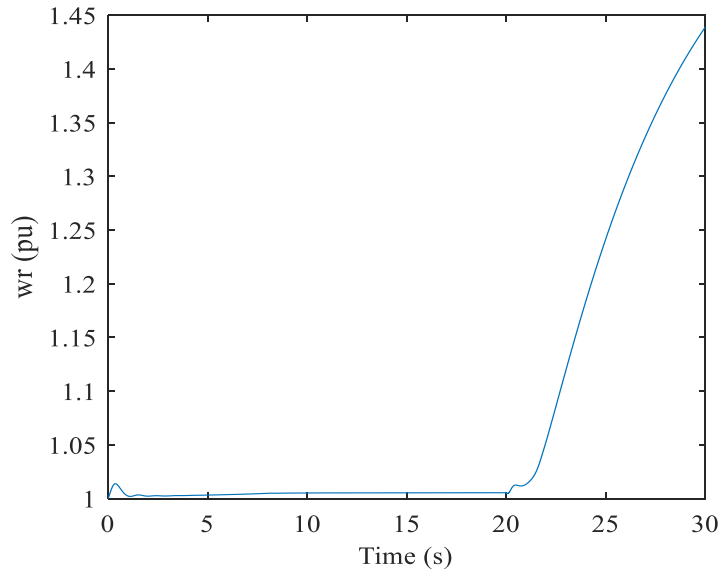


Figure. 6.2. Rotor speed of FSIG-based wind farm

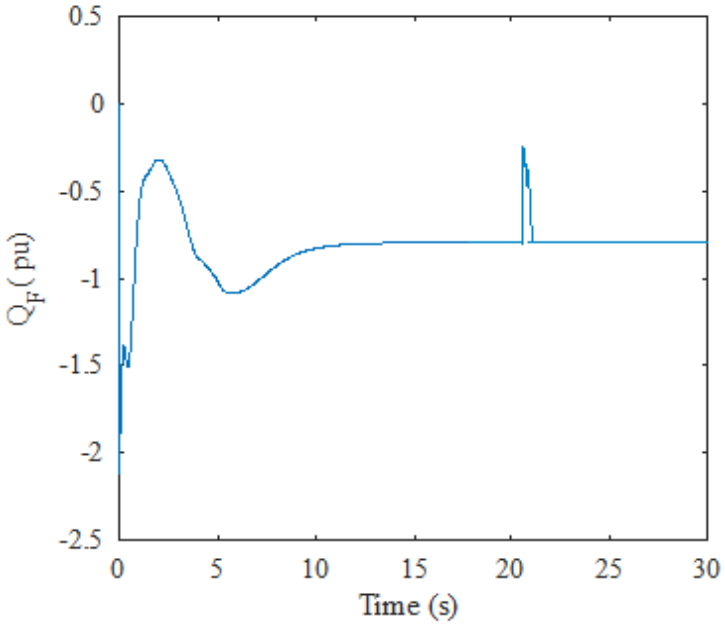


Figure. 6.3. Absorbed reactive power by FSIG-based wind farm

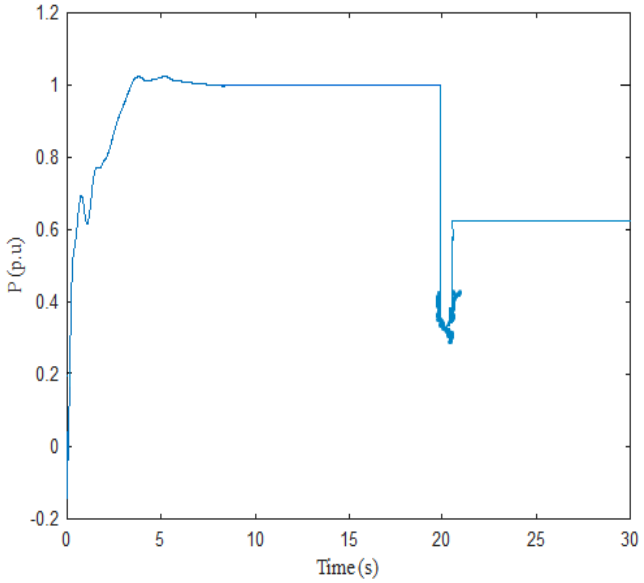


Figure. 6.4. Output active power of FSWT-based wind farm

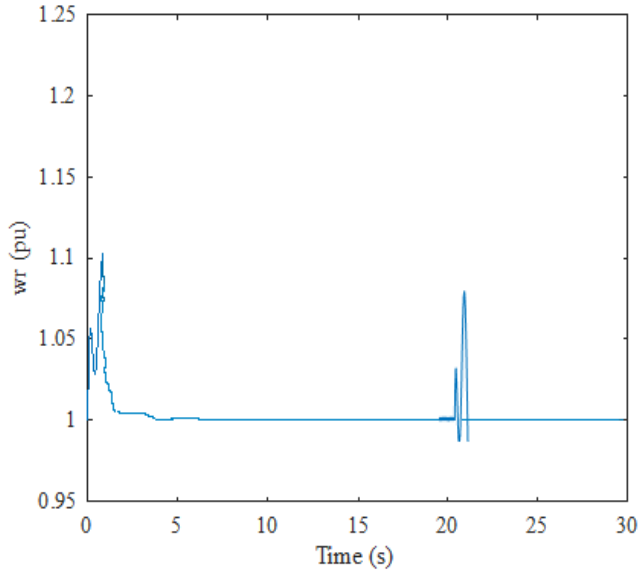


Figure. 6.5. Rotor speed of PMSG based wind farm

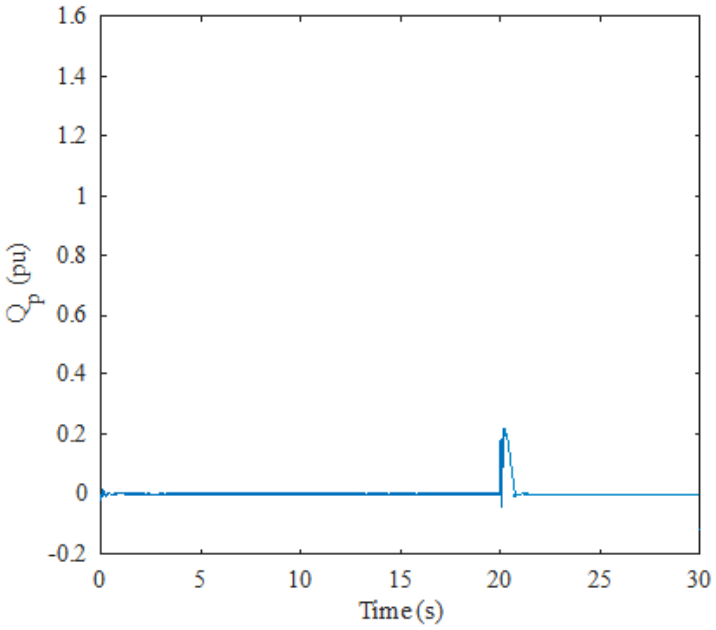


Figure. 6.6. Reactive power output of the PMSG wind farm

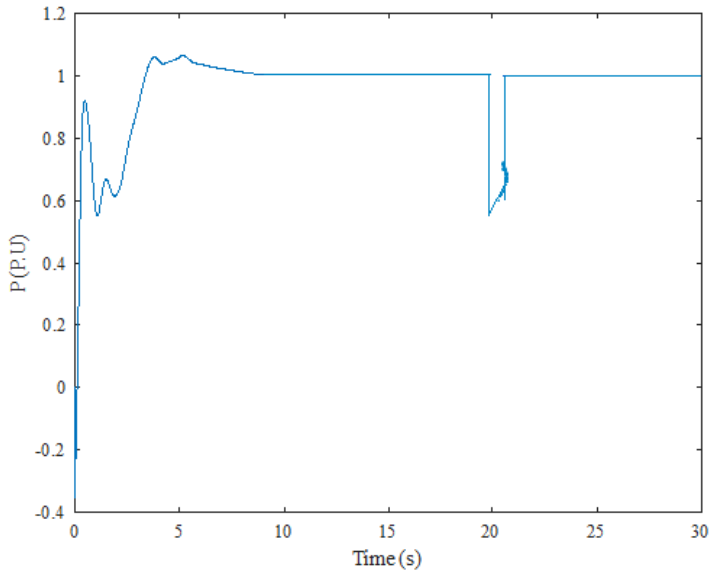


Figure. 6.7. Outpower active power of PMSG-based wind farm

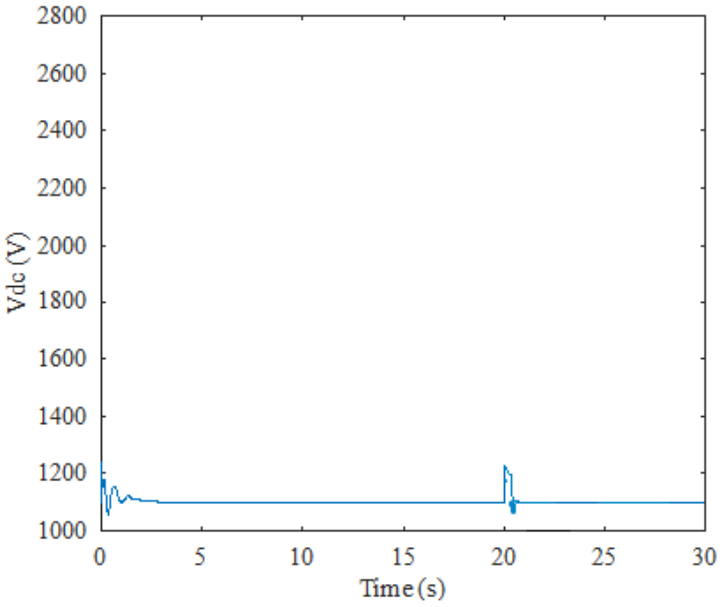


Figure. 6.8. DC-Link voltage

## 6.3.2. Double-Line-to-Ground (LLG) Fault

Figure 6.9 presents the simulation result of the grid voltage of the hybrid wind farm when a double-line-ground (LLG) fault is applied to the hybrid wind system. The fault condition on the grid affects the grid voltage of the hybrid wind farm, causing it to drop to 0.361 p.u. Similarly, the low voltage condition on the grid also affects the FSIG-based wind farm and its rotor experiences the same behavioural pattern shown in Figure 6.2 causing it to absorb large amounts of reactive power from the grid to remain grid-connected as shown in Figure 6.10. Also, as observed in Figure 6.11, the total output active power of the FSIG-based wind farm drops to 0.58 p.u and the severity of the grid fault can be noticed in both the dip in grid voltage and the active power of the FSIG wind system. The rotor of the PMSG based wind system experiences overspeeding as shown in Figure 6.12 and stabilizes thereafter the grid fault. The active power of the PMSG drops to 0.53 pu during the fault, shown in Figure 6.13. The GSC of the PMSG

supplies 0.285 p.u reactive power to the PMSG wind farm while the grid fault occurs as seen in Figure 6.14. It is observed that the PMSG wind farm immediately returns to its rated value as soon as the fault condition is cleared.

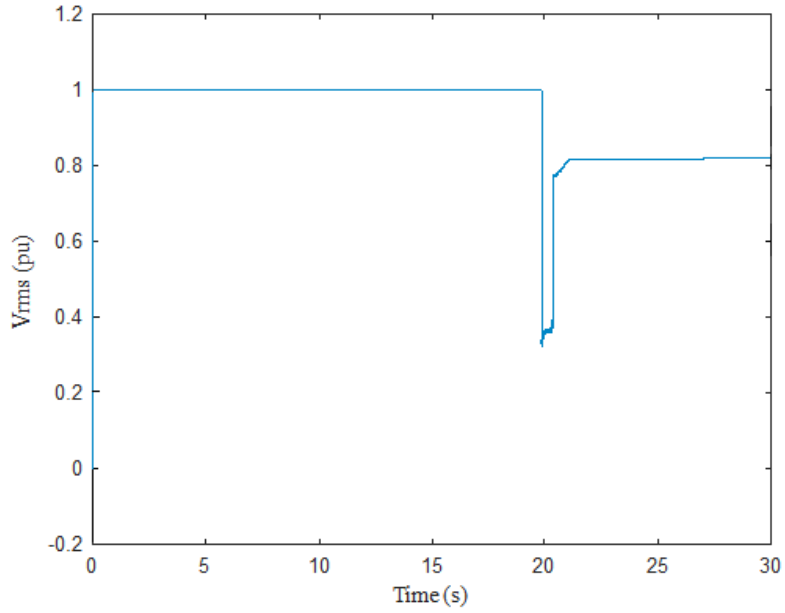


Figure. 6.9. Grid voltage of hybrid wind farm

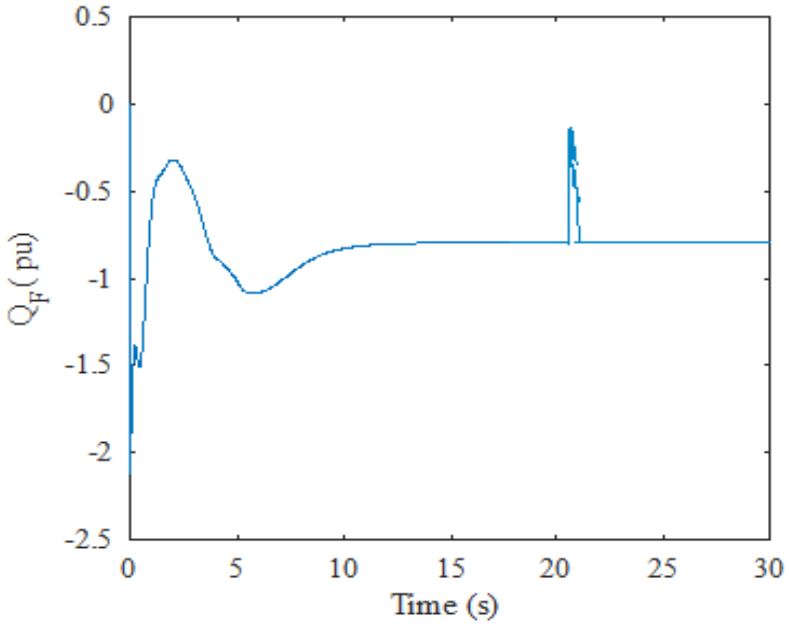


Figure. 6.10. Absorbed reactive power by FSIG-based wind farm

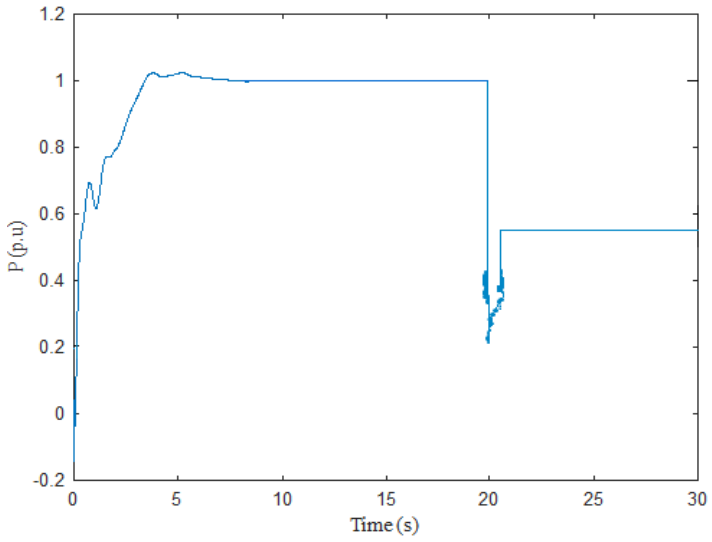


Figure. 6.11. Output active power of FSIG-based wind farm

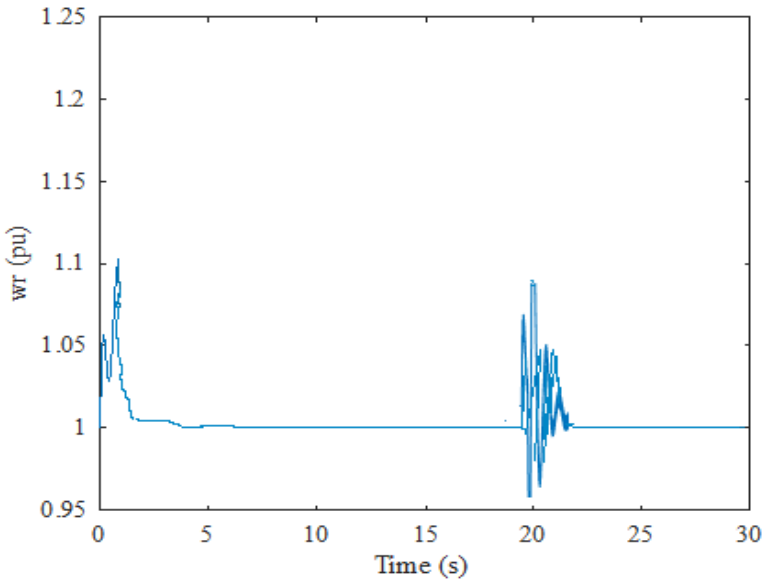


Figure 6.12. Rotor speed of PMSG

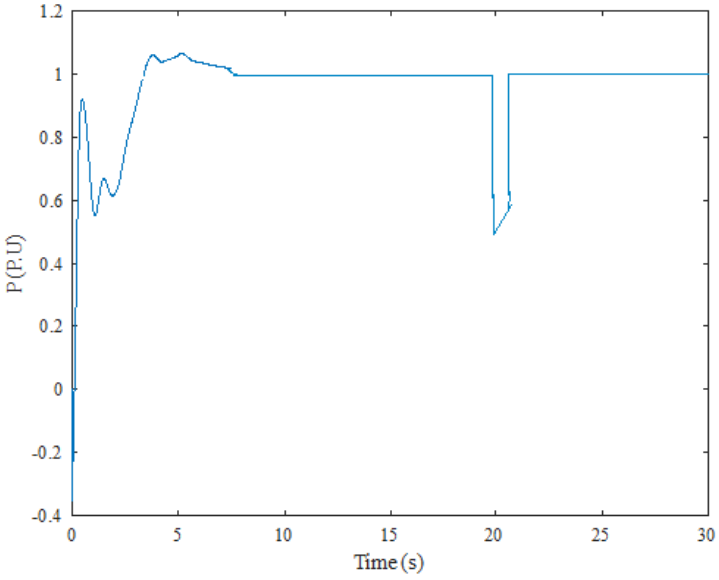


Figure. 6.13. Output active power of PMSG-based wind farm

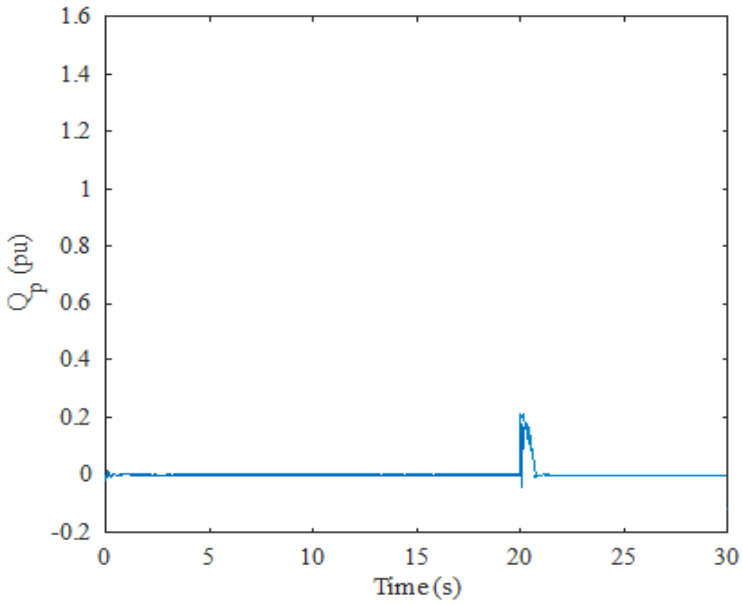


Figure 6.14. Reactive power output of the PMSG wind farm

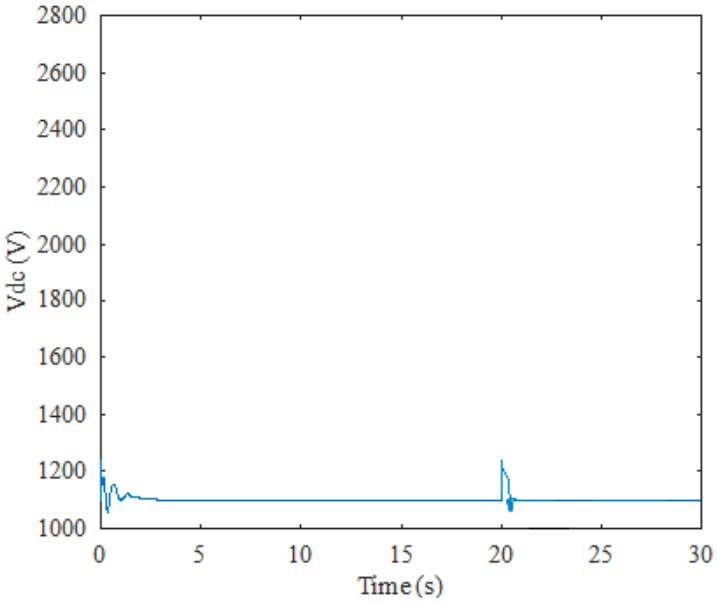


Figure 6.15. DC-link voltage

## 6.3.3. Line-to-Line (LL) Fault

Figure 6.16 shows the simulation result of the hybrid wind farm when a line-to-line (LL) fault is introduced into the system. It can be seen that the grid voltage experiences a sag causing the voltage at the grid to drop to 0.38 pu during the grid fault. Without the reactive power compensation provided by the PMSG-based wind farm during the grid fault, the rotor of the FSIG-based wind turbine experiences a sustained acceleration resulting from the unbalance between the mechanical torque and electromagnetic torque. Consequently, the FSIG-based wind farm absorbs a large amount of reactive power which causes further deterioration of the grid voltage at PCC. Comparing Figure 6.9 and Figure 6.16, it can be seen that the impact of the line-to-line fault on the grid is less severe when compared to the double-line-to ground fault. The lack of reactive power compensation also impacts the performance of the FSIG-based wind turbine as seen in the simulation result of Figure 6.18. The active power of the FSIG-based wind systems dips to 0.24 pu during the fault

occurrence and recovers to 0.60 pu post fault. The response of the PMSG-based wind system to the line-to-line fault is shown in Figures 6.19 to 6.22. The active power of the PMSG drops to 0.56 pu during the fault, shown in Figure 6.19. The GSC of the PMSG supplies 0.28 p.u reactive power to the PMSG wind farm while the grid fault occurs as seen in Figure 6.21.

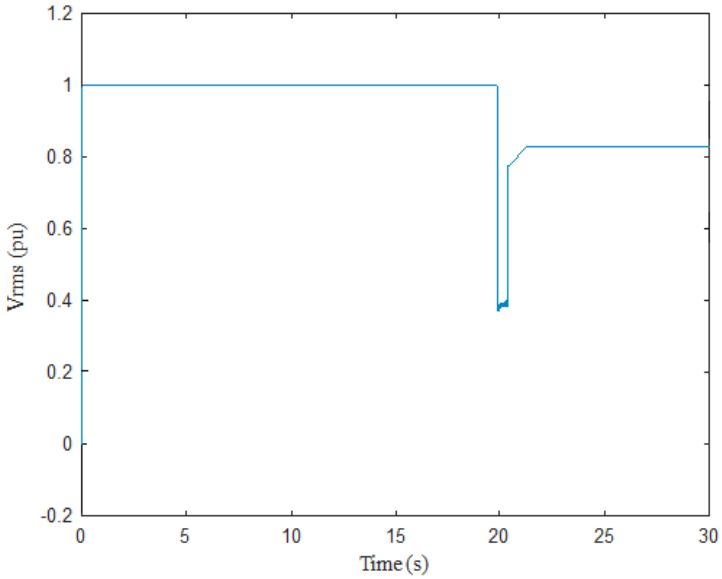


Figure. 6.16. Grid voltage of the hybrid wind farm

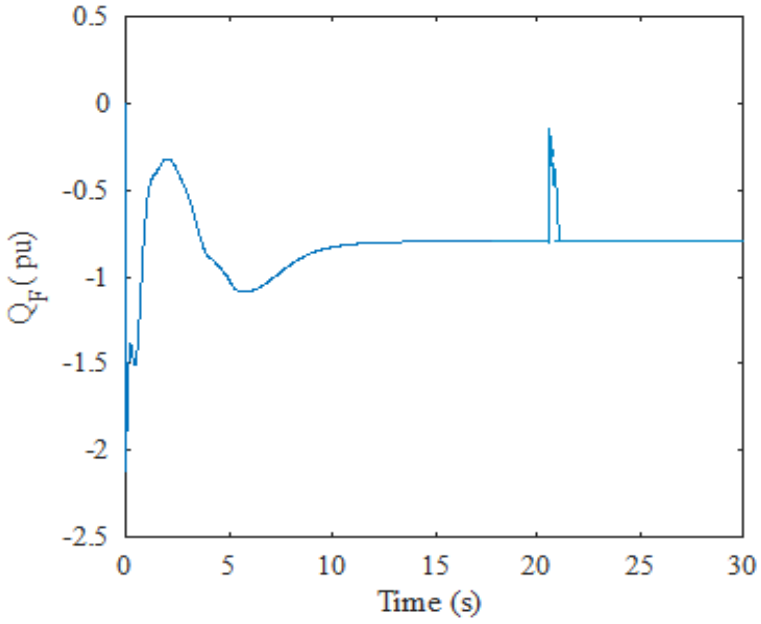


Figure 6.17. Reactive power output of the PMSG wind farm

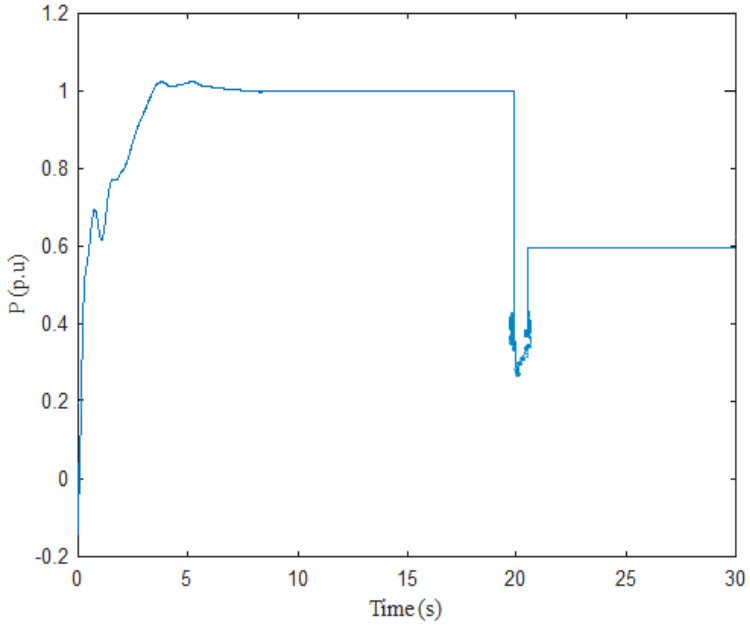


Figure 6.18. Output active power of FSIG-based wind farm

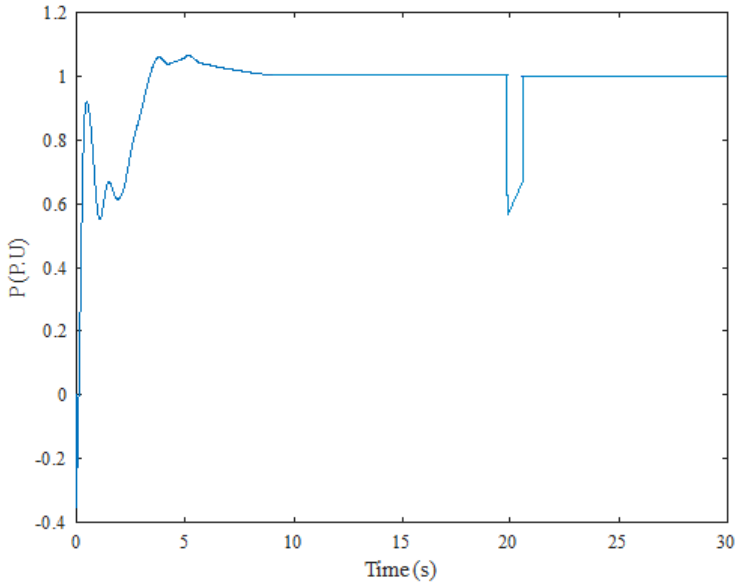


Figure 6.19**.** Output active power of PMSG-based wind farm

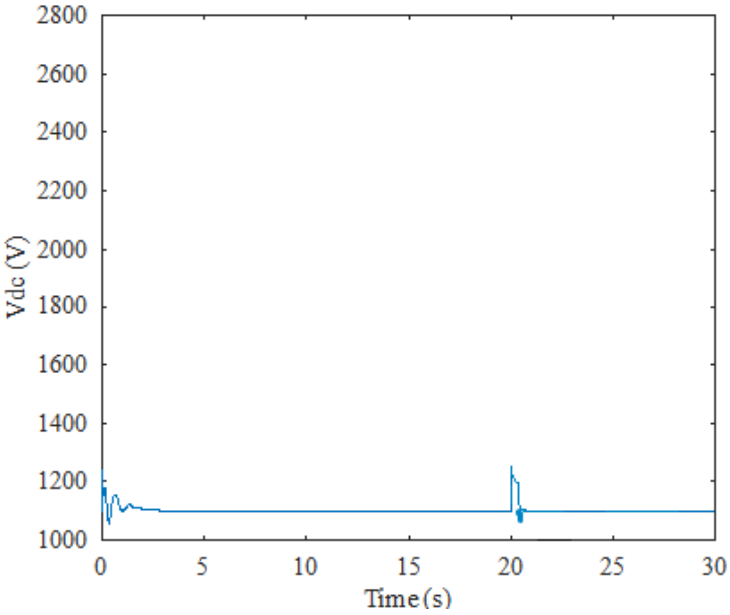


Figure 6.20. DC-link voltage

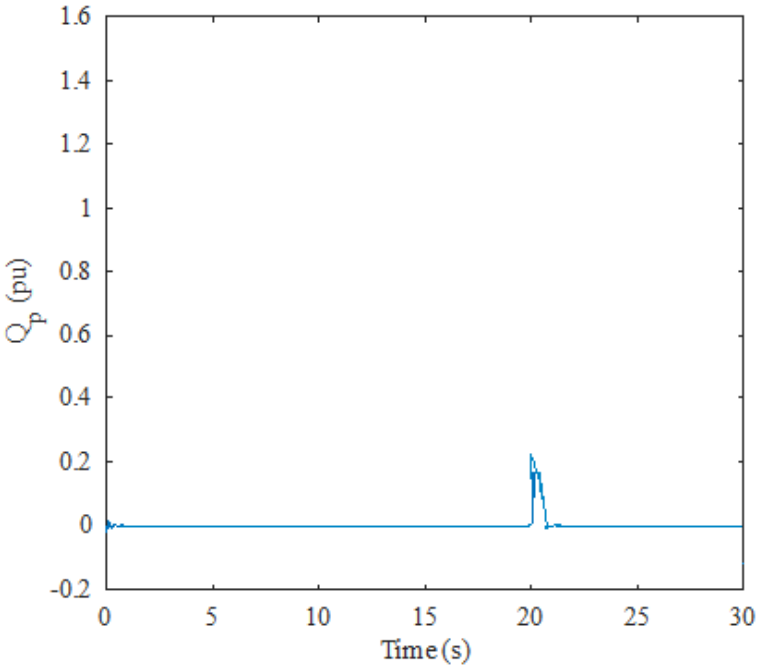


Figure 6.21. Reactive power output of the PMSG wind farm

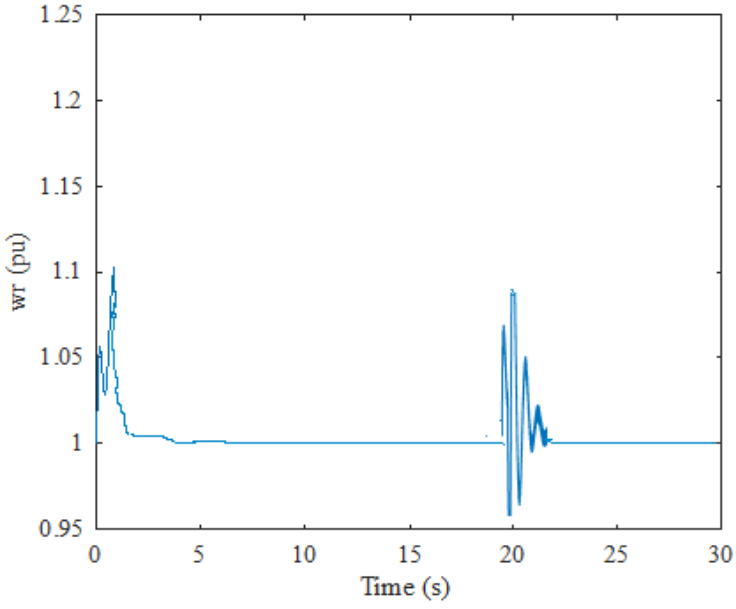


Figure 6.22. Rotor speed of PMSG

## 6.3.4. Balanced 3-Phase Fault (LLL)

Figures 6.23 to 6.29 represent simulation results of a balanced three-phase (LLL) grid fault condition introduced into the hybrid wind system without reactive power compensation. As observed from Figure 6.23, and in comparison to Figures 6.1, 6.9 and 6.16, this fault type is the most severe on the wind power system. Figure 6.23 shows that grid voltage experiences a dip to 0.32 pu. Just like the previously introduced fault conditions, the voltage sag on the grid causes the rotor of the FSIG to be out of synchronization due to the unbalance between the mechanical and electromagnetic torques. The grid fault causes the FSIG based wind turbine to absorb reactive power from the grid and the active power of the FSIG based wind turbine drops to 0.2 pu as shown in Figures 6.24 and 6.25 respectively. The response of the PMSG based wind turbine to the three-phase grid fault is shown in Figures 6.26 to 6.29.

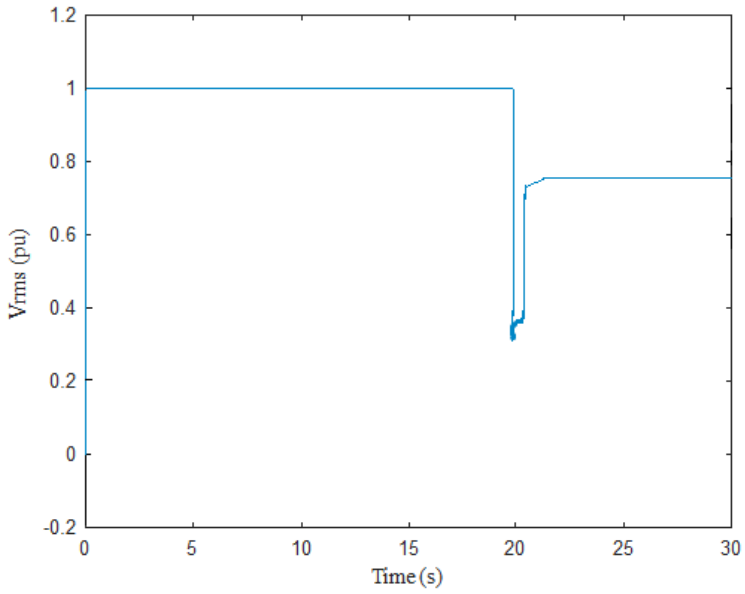


Figure 6.23. Grid voltage of the hybrid wind farm

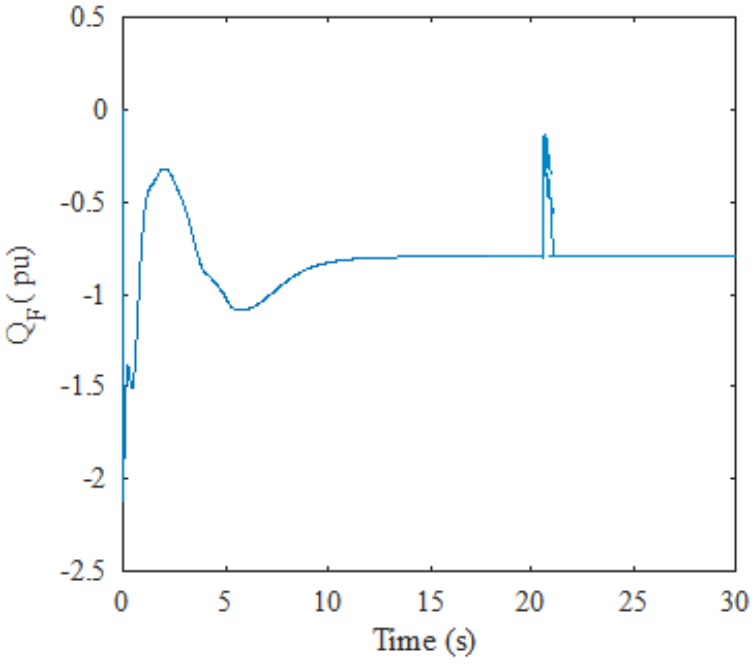


Figure 6.24. Reactive power output of the FSIG wind farm

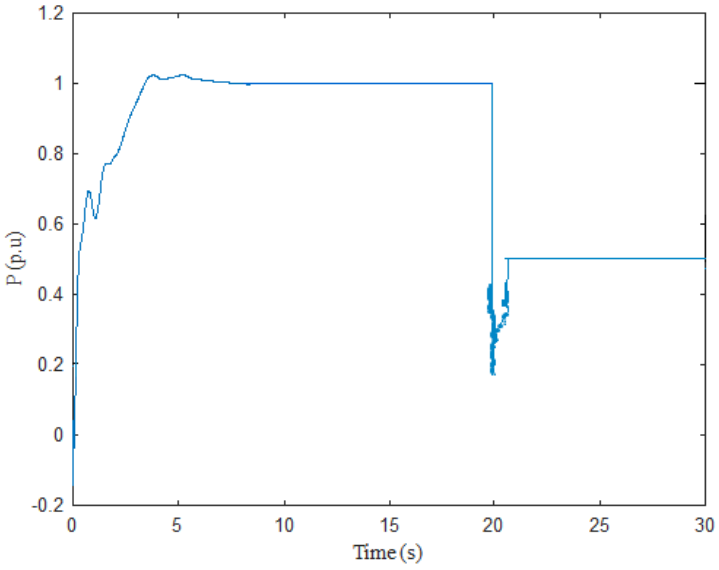


Figure 6.25. Output active power of FSIG-based wind farm

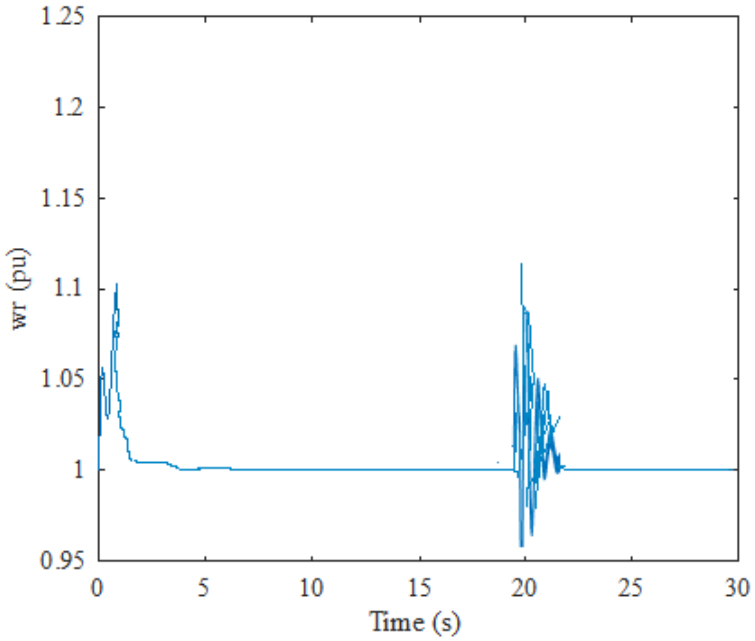


Figure 6.26. Rotor speed of PMSG

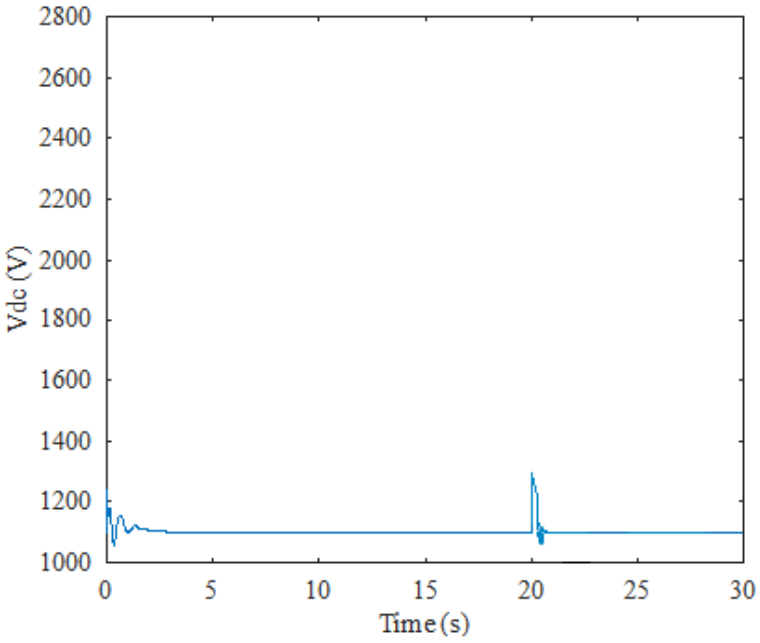


Figure 6.27. DC-link voltage

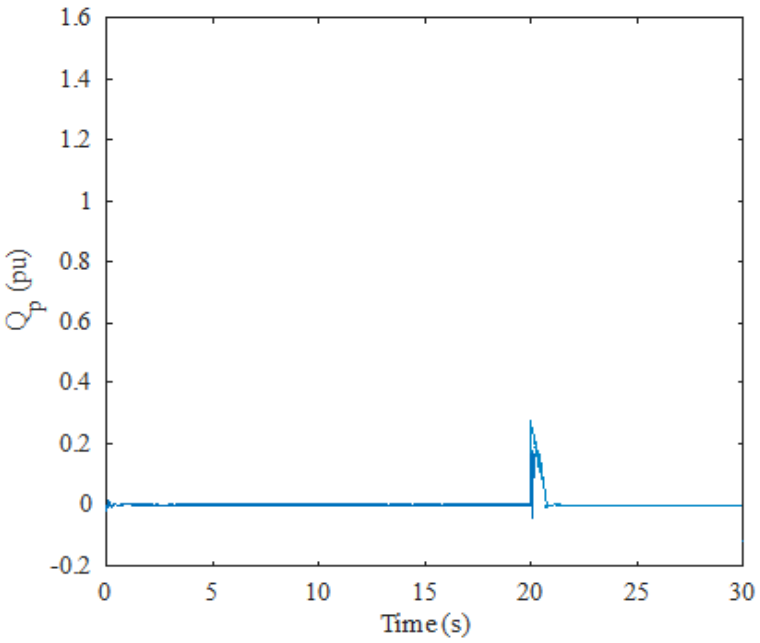


Figure 6.28. Reactive power output of the PMSG wind farm

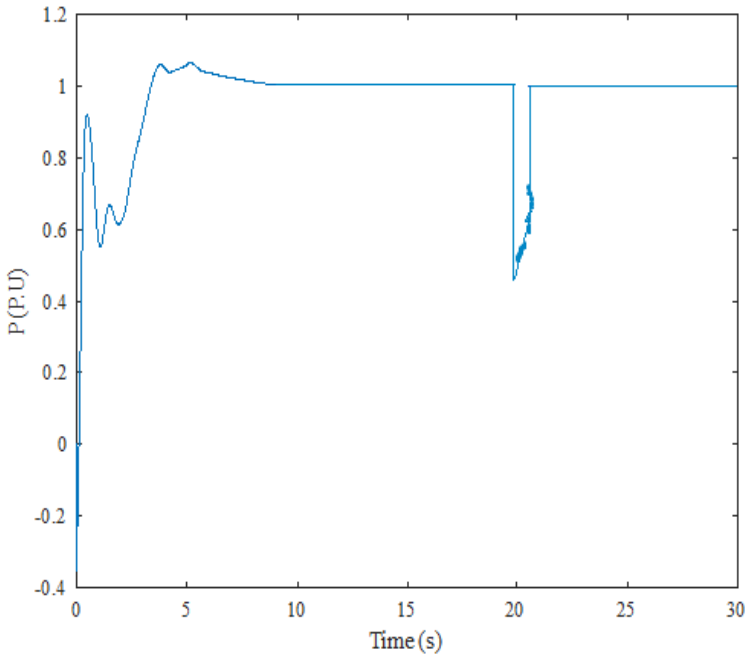


Figure 6.29. Output active power of PMSG-based wind farm

# 6.4. Transient State Operation of the Hybrid Wind Farm With Proposed Reactive Power Support Strategy

The proposed coordinated control of the hybrid wind farm is implemented with the different grid faults discussed in Section 6.3 to observe the response of the hybrid wind system to the different fault scenarios.

With the proposed current allocation strategy and coordinated control of the reactive and active current references of the GSC in the PMSG, appropriate reactive power support is provided to the FSIG-based wind farm and the voltage profile of the hybrid wind farm is improved. Under normal conditions, the GSC works at unity power factor mode, that is $i_q^*$ is set to 0, this means no reactive power is injected into the grid from the GSC as observed in Figure 4.24. Based on (5.2), rather than unity power factor control, the GSC is utilized to provide reactive power support, in other words, the priority of the GSC is set to the Q-priority mode. The reference control variables of the GSC are altered to provide reactive support to the grid under the fault conditions discussed in Section 6.3. Figure 6.30 shows the operation of the GSC control in both normal and fault modes.

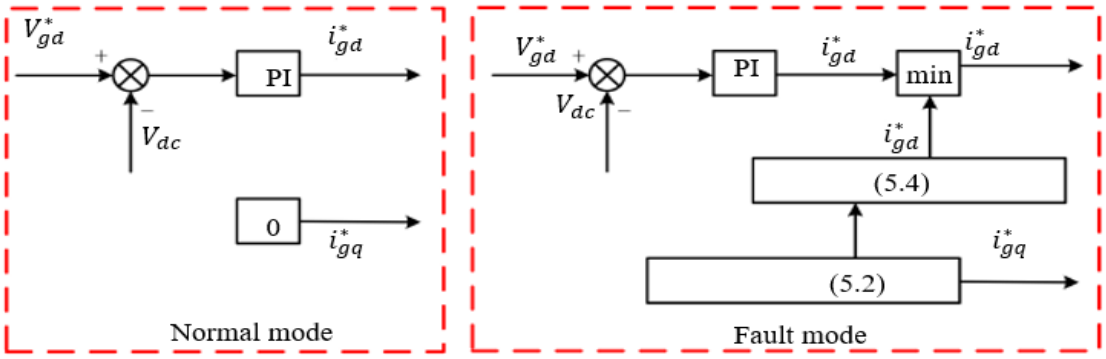


Figure 6.30. Operation of the GSC in normal and fault modes

During the initial stage of the fault condition, the protection system of the FSWT-wind system is triggered to prevent the overcurrent of the rotor circuit, since the FSIG- based wind farm is appropriately supported by the PMSG based wind farm. Based on the proposed coordinated control of the PMSG and FSIG, the reactive current reference $i_{gq}^{*}$ , of the GSC in the PMSG is controlled to provide the required reactive current for reactive power support in the FSIG-based wind system during the duration of the grid fault condition. When the grid voltage sags, the reactive current of the GSC is given higher priority than the active power injected into the grid as analysed in Chapter 5. The active current reference $\mathrm{i}_{\mathrm{gd}}^{*}$ of the current component $i_{gd}$ is limited and controlled to provide the required reactive support by improving $i_{gq}^{*}$ of the reactive power component $i_{gq}$, thereby improving the reactive power profile of the FSIG based wind system and simultaneously improving the active power output of the FSIG-based wind farm.

## 6.4.1. Single-Line-to-Ground (LG) Fault

With the proposed coordinated control, when a single line-to-ground fault is introduced into the wind system at t = 20 seconds, it can be seen from Figure 6.31 that there is an improvement in the depth of voltage sag on the grid from 0.40 pu to 0.428 pu while the fault condition lasts. The grid voltage of the hybrid wind farm is also restored to the normal grid voltage level. As shown in Figure 6.6, the PMSG can fulfil the conditions of the grid code during the fault condition by generating 0.26 pu of reactive power. However, in Figure 6.32, by control of the GSC, the PMSG generates 0.30 pu of reactive power to support the grid voltage recovery. The extra capacity of the GSC is used in providing the required reactive power needed by the FSIG-based wind turbine to fulfil the requirement set out in (5.2).

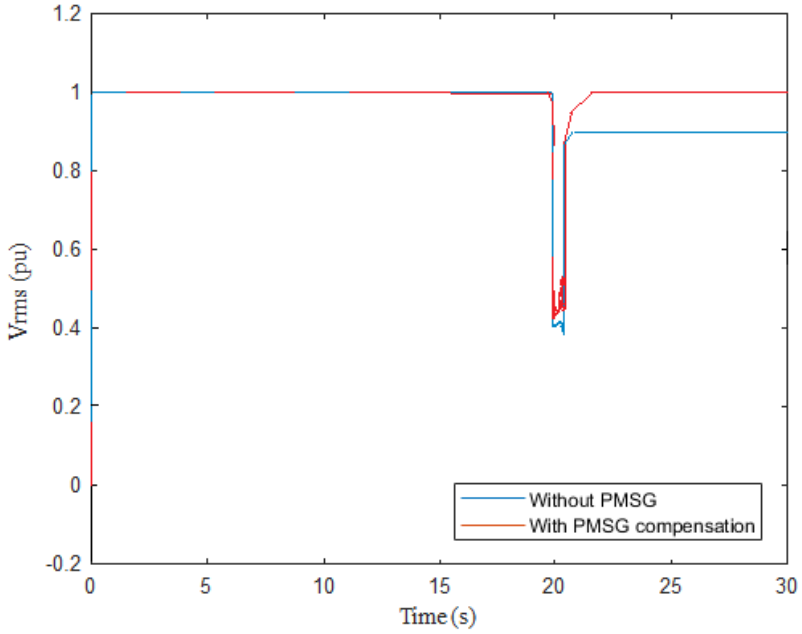


Figure 6.31. Grid voltage of hybrid wind farm

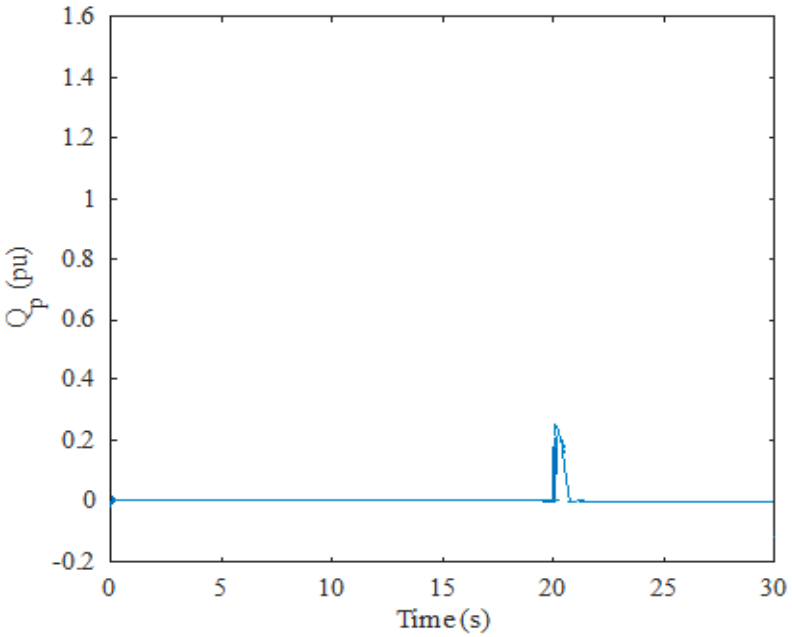


Figure 6.32. Reactive power output of PMSG wind farm.

The performance and output power quality of the FSIG-based wind farm is also improved effectively. When compared to Figure 6.2 where the rotor of the FSIG loses synchronism and over speeds due to the unbalance between the electromagnetic torque and mechanical torque

when a grid fault occurs without appropriate voltage and reactive power support for the FSIG-based wind turbine system, Figure 6.33 shows the rotor of the FSIG begins to decelerate and returns to its rated speed as a result of the reactive power support provided by the PMSG during the grid fault condition. The FSIG-based wind turbine returns to its rated operating point and the reactive power profile is also improved as seen in Figures 6.34 and 6.35 respectively. However, the PMSG based wind farm experiences a momentary decrease in its output power to 0.849 p.u and then returns to its rated output power, shown in Figure 6.36 and validates the analysis done in Chapter 5.

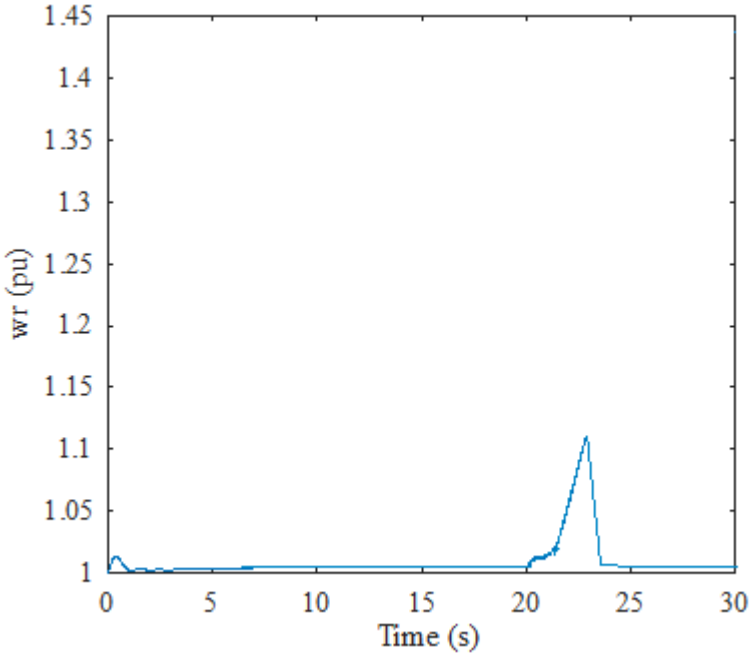


Figure. 6.33. Rotor speed of FSIG

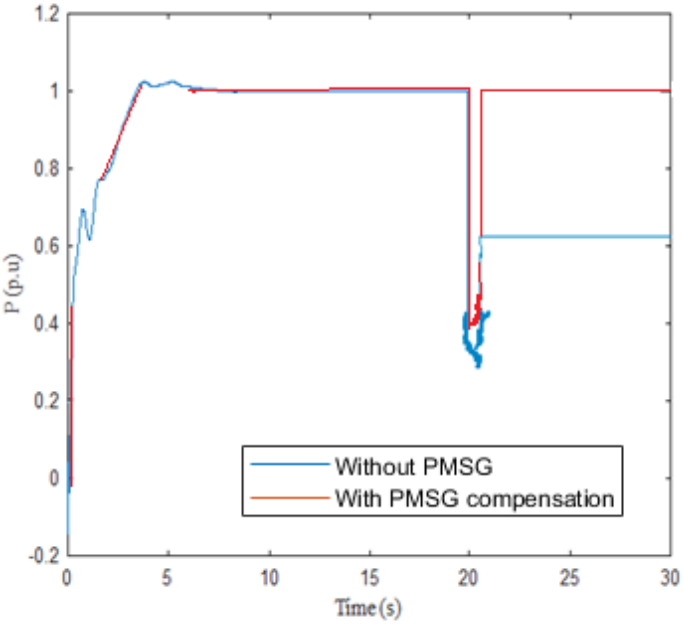


Figure 6.34. output of FSIG based wind farm

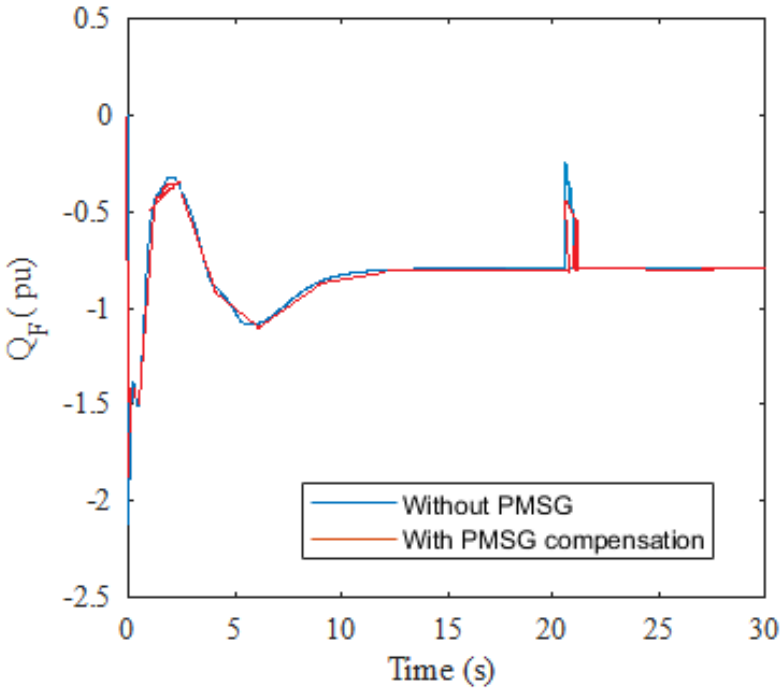


Figure 6.35. Reactive power of the FSIG based wind farm

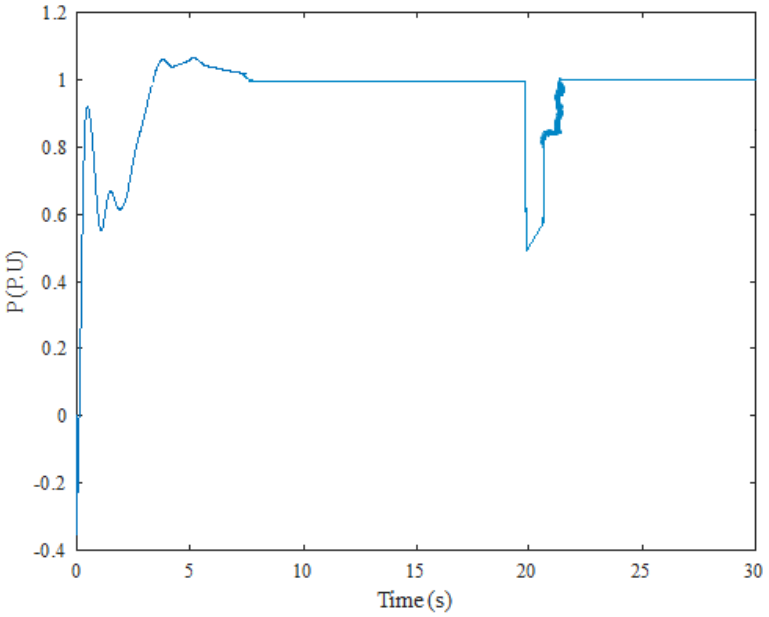


Figure 6.36. Output power of PMSG

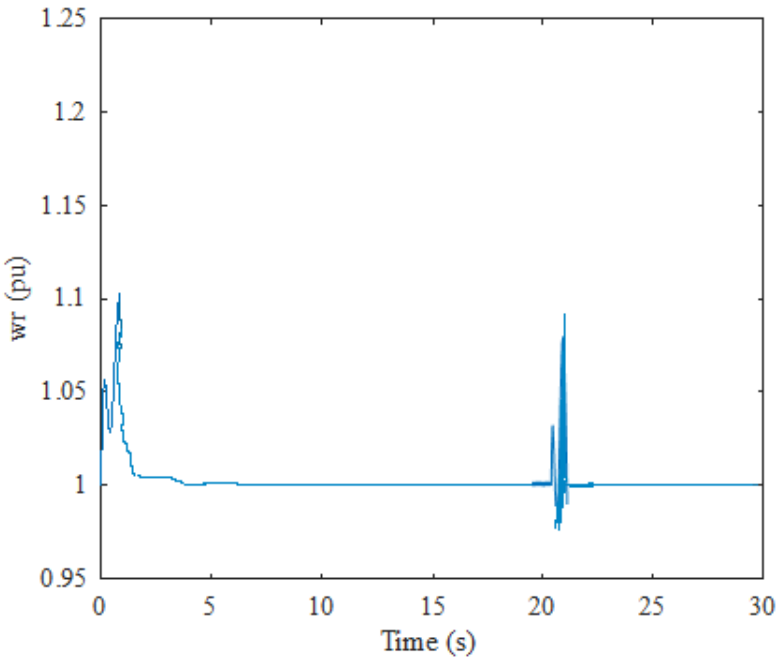


Figure 6.37 Rotor speed of PMSG

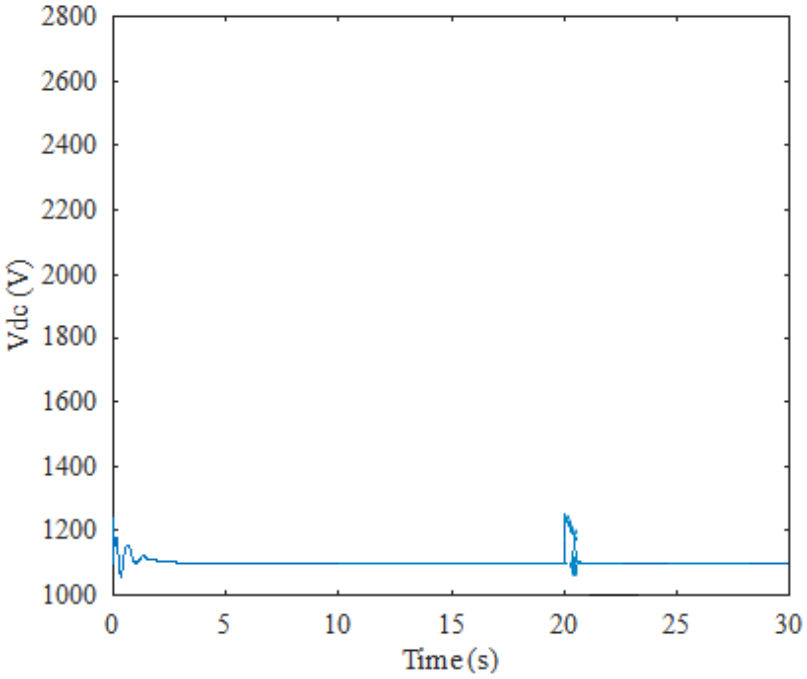


Figure 6.38 DC-link voltage

## 6.4.2. Double-Line-to-Ground (LLG) Fault

Figure 6.39 shows an improvement in the grid voltage of the hybrid wind system when the proposed coordinated control is implemented during a double-line-to ground fault (LLG). It can be seen that the grid voltage is improved and the depth of the sag is reduced while the grid voltage is restored to the normal grid voltage level pre-fault condition. As shown in Figure 6.40, the PMSG can fulfil the requirements of the grid code during the fault condition by generating 0.34 pu of reactive power. The extra capacity provided by the GSC is used in providing the required reactive power needed by the FSIG-based wind turbine to fulfil the requirement of the grid code. Figure 6.41 shows a deceleration of the FSIG rotor after the grid fault with the support of the PMSG, returning to its rated speed and the FSIG can return to its rated operating point

with an improved reactive power profile as shown in Figures 6.42 and 6.43 respectively. Due to the limiting of active power, the PMSG based wind farm experiences a decrease in its output power to 0.78 p.u as illustrated in Figure 6.44 before returning to its rated output power.

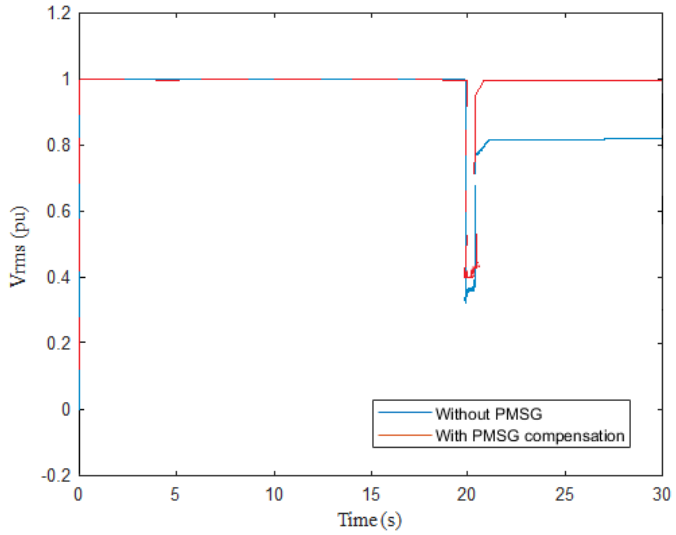


Figure 6.39 Grid voltage of hybrid wind farm

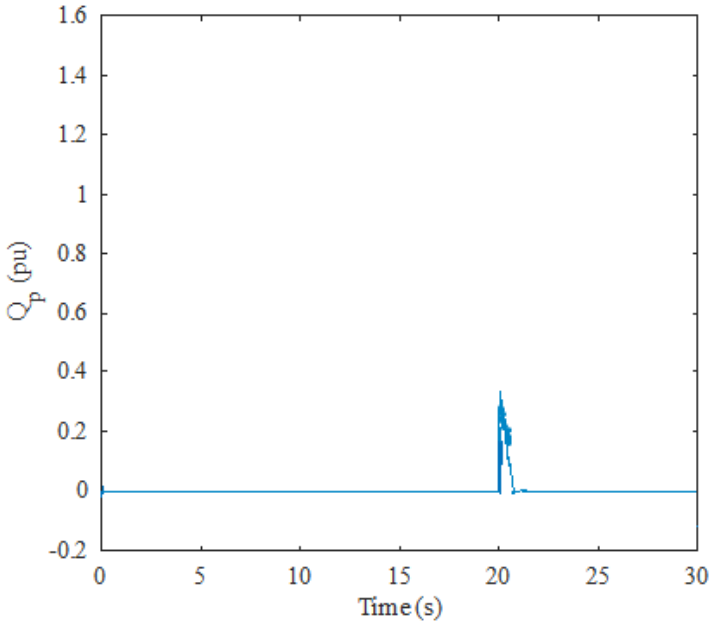


Figure 6.40 Reactive power output of PMSG wind farm.

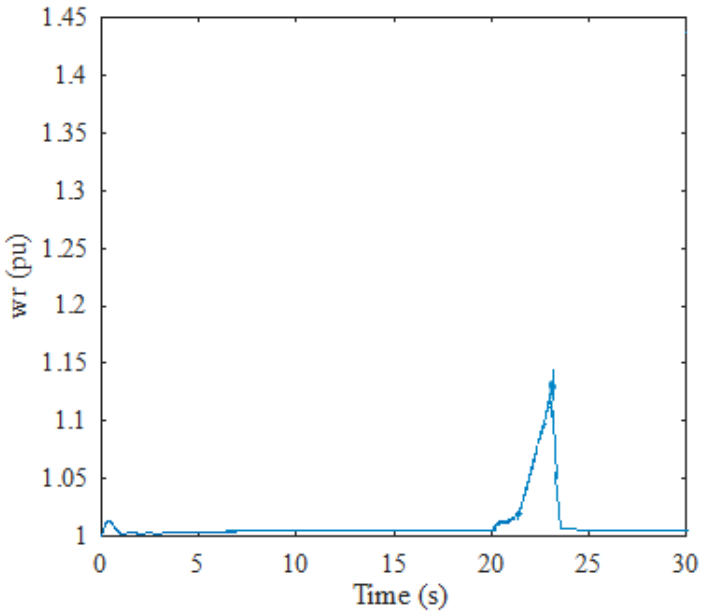


Figure 6.41 Rotor speed of FSIG

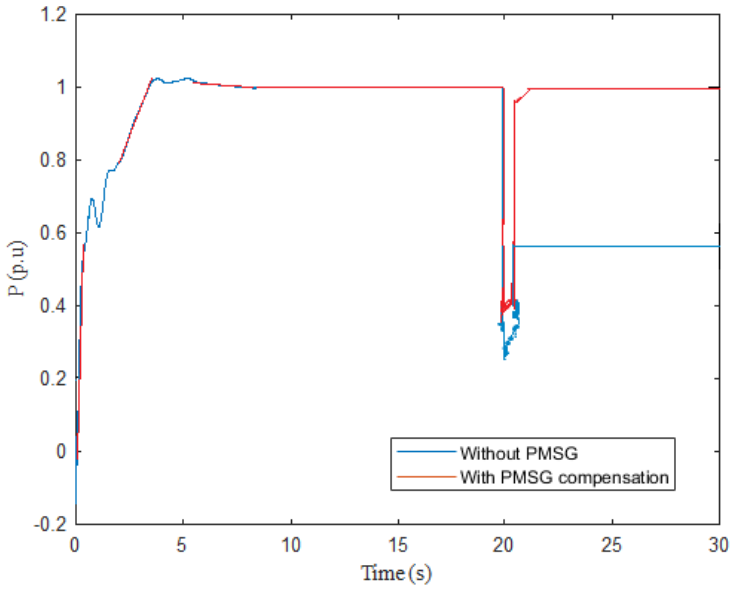


Figure 6.42 output of FSIG based wind farm

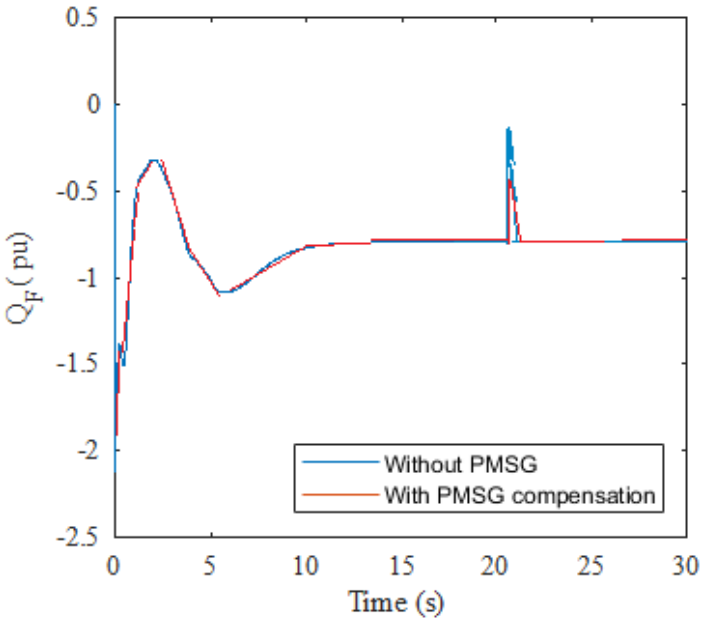


Figure. 6.43 Reactive power output of FSIG wind farm.

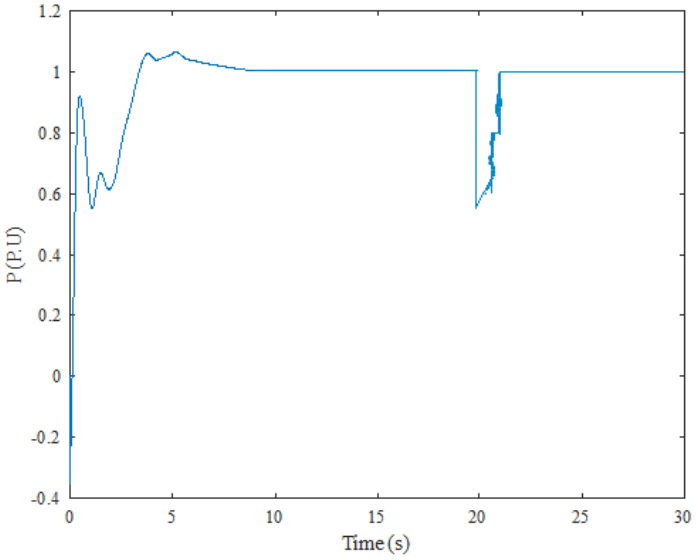


Figure. 6.44. Output active power of PMSG based wind farm

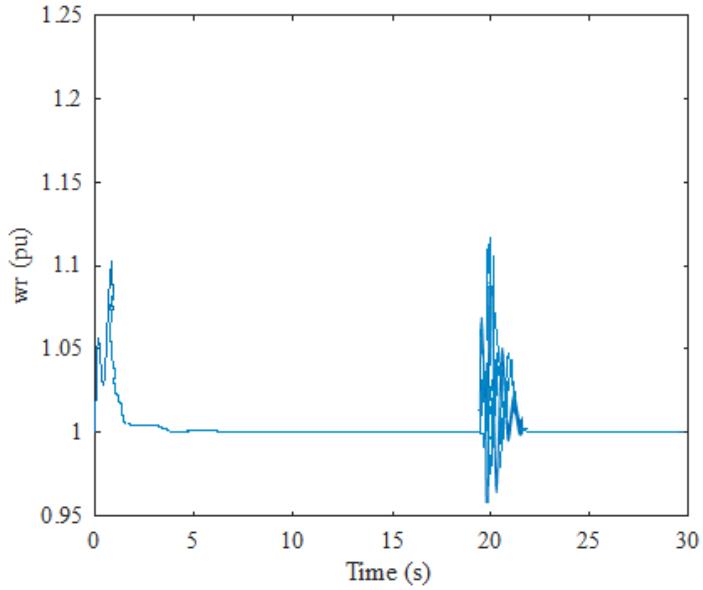


Figure. 6.45 Rotor speed of PMSG

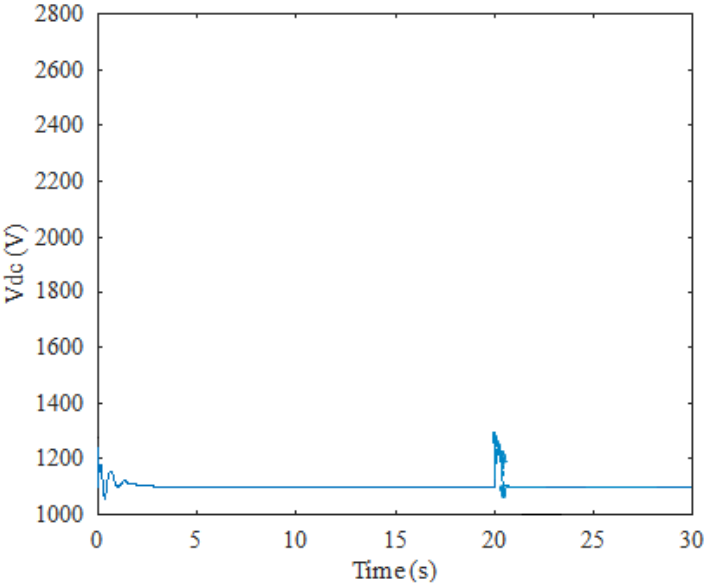


Figure 6.46 DC-link voltage

## 6.4.3. Line-to-Line (LL) Fault

Figure 6.47 shows an improvement in the grid voltage of the hybrid wind system when the proposed coordinated control is implemented during a line-to-line fault (LL). It is seen that the

grid voltage is improved and the depth of the sag is reduced while the grid voltage is restored to the normal grid. As shown in Figure 6.48, the PMSG can fulfil the requirements of the grid code during the fault condition by generating 0.315 pu of reactive power. The generated extra capacity provided by the GSC is used in providing the required reactive power needed by the FSIG-based wind turbine to fulfil the requirement of the grid code. Figure 6.49 shows the rotor behaviour of the FSIG after the grid fault with the support of the PMSG, returning to its rated speed while the FSIG-based wind turbine returns to its rated operating point with an improved reactive power profile as shown in Figures 6.50 and 6.51 respectively. Due to the limiting of active power, the PMSG based wind farm experiences a decrease in its output power to 0.80 p.u as illustrated in Figure 6.52 before returning to its rated output power. The rotor behaviour of the PMSG and the dc voltage of the converter is shown in Figures 6.53 and 6.54 respectively.

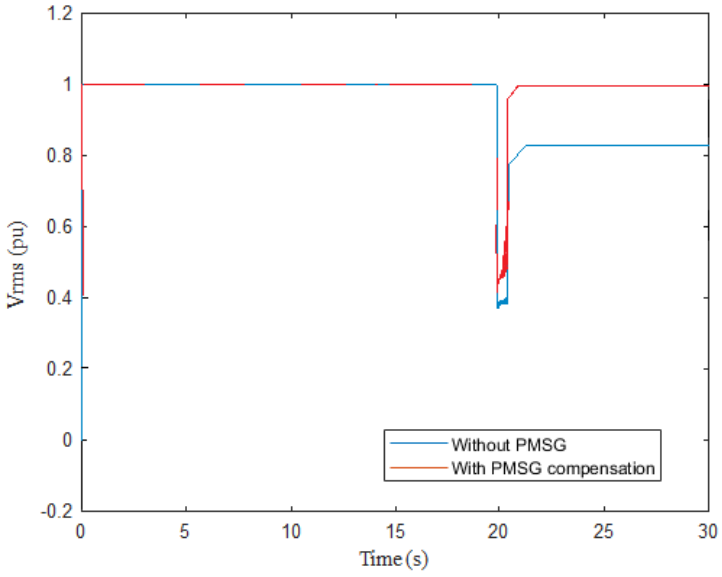


Fig 6.47. Grid  voltage of hybrid wind farm

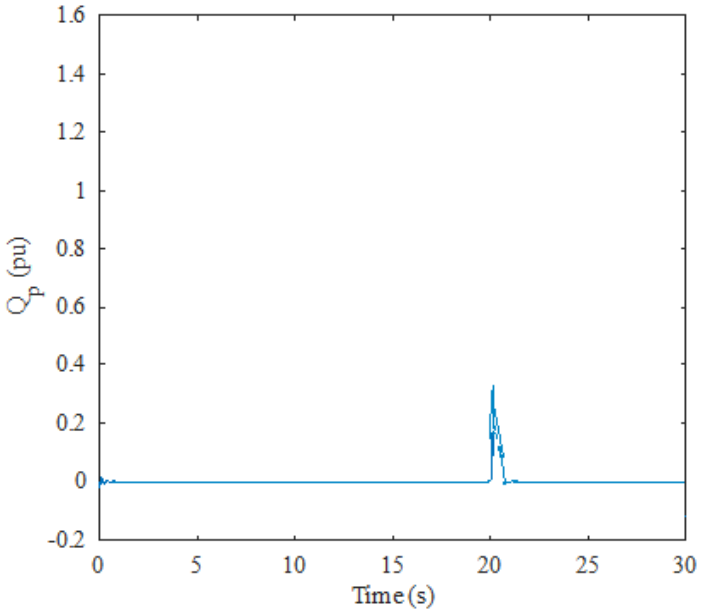


Figure 6.48 Reactive power output of PMSG wind farm.

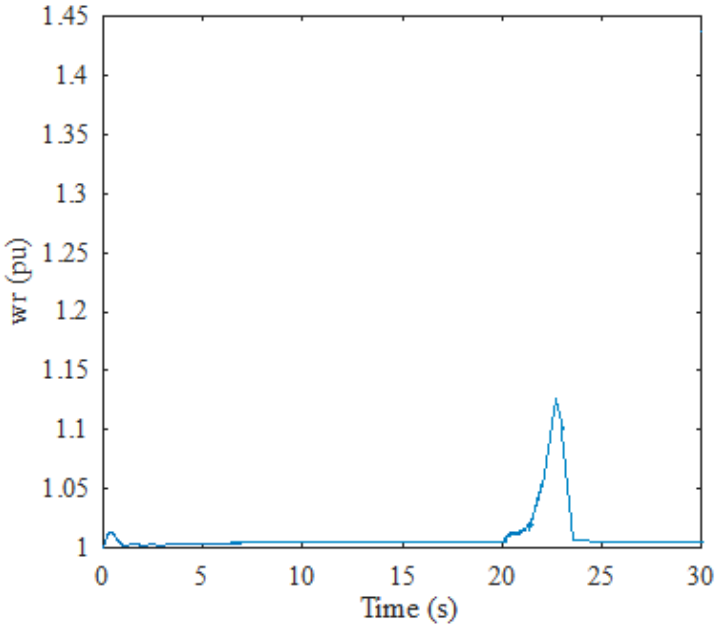


Figure 6.49. Rotor speed of FSIG

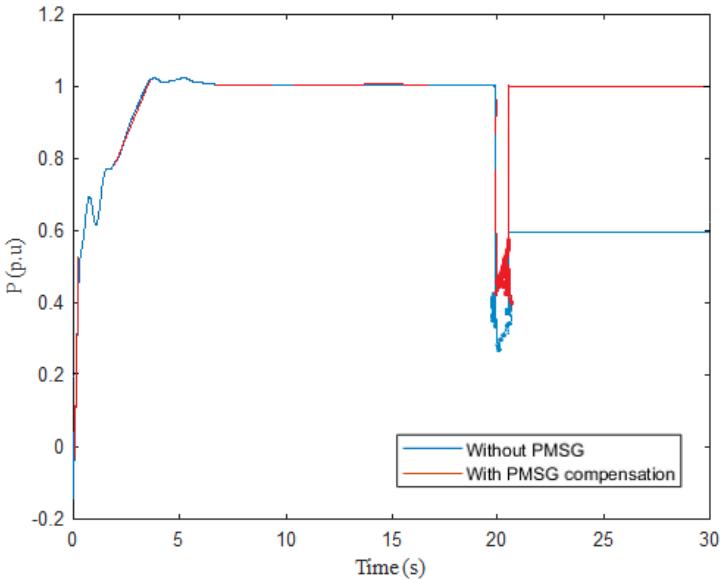


Figure 6.50 output of FSIG based wind farm

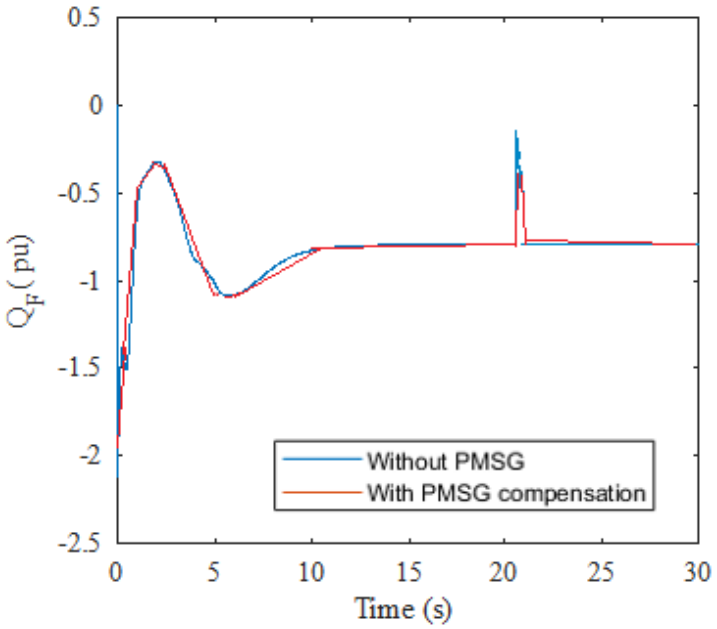


Figure 6.51. Reactive power output of FSIG wind farm.

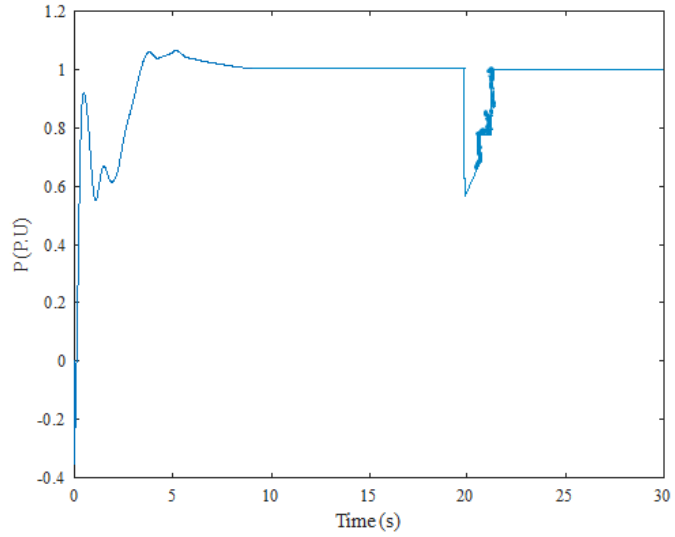


Figure 6.52 output of PMSG based wind farm

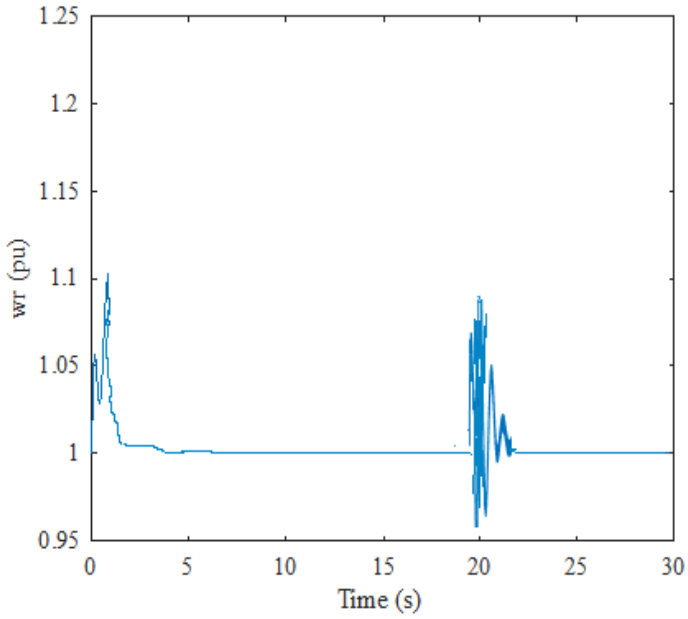


Figure 6.53 Rotor speed of PMSG

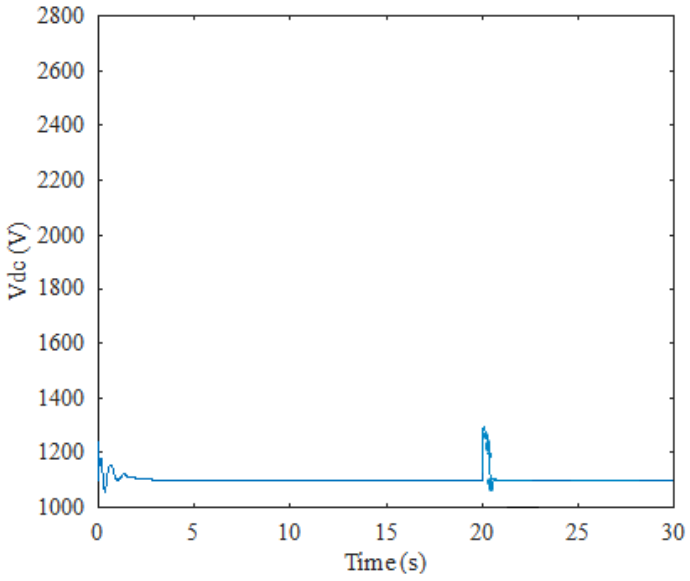


Figure 6.54. DC-link voltage

## 6.4.1. Balanced 3-Phase (LLL) Fault

The proposed control strategy is also tested on the balanced three-phase fault introduced into the hybrid wind system. From Figure 6.55, it can be seen that both grid voltage and sag level of the fault at the grid improved because the PMSG can generate 0.38 pu of reactive power, as shown in Figure 6.56. The rotor behaviour of the FSIG after the grid fault with the support of the PMSG is shown in Figure 6.57. It is observed that unlike the case of no reactive power support, the FSIG rotor regains synchronism and returns to its rated speed while the FSIG-based wind turbine returns to its rated operating point with an improved reactive power profile as shown in Figures 6.58 and 6.59 respectively. Due to the limiting of active power, the PMSG based wind farm experiences a decrease in its output power to 0.75 p.u as illustrated in Figure 6.60 before returning to its rated output power. The rotor behaviour of the PMSG and the dc voltage of the converter is shown in Figures 6.61 and 6.62 respectively.

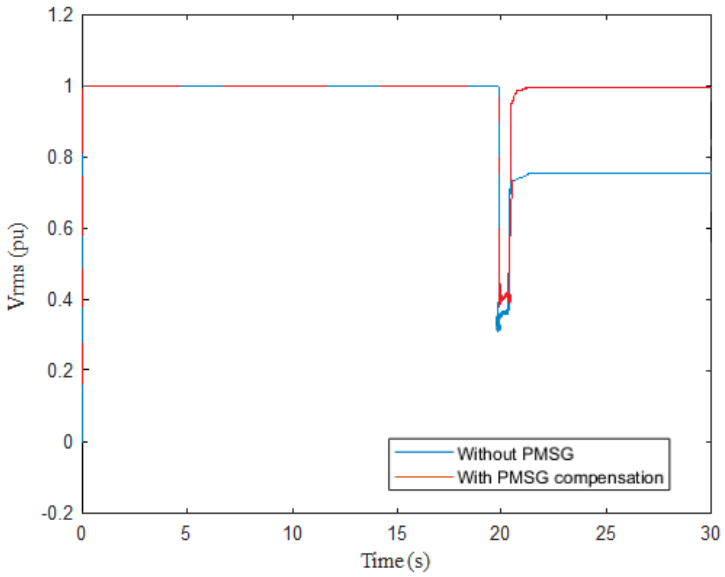


Figure 6.55. Grid  voltage of hybrid wind farm

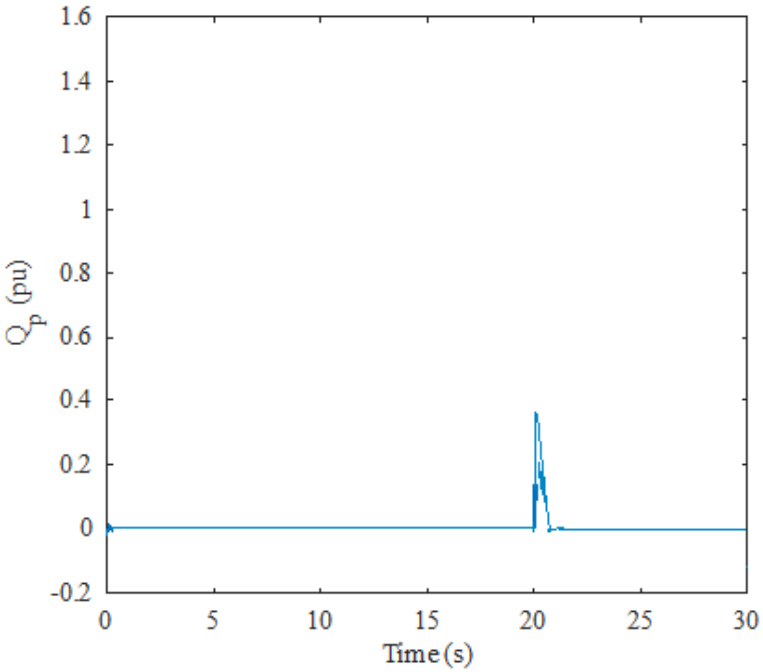


Figure 6.56. Reactive power output of PMSG wind farm.

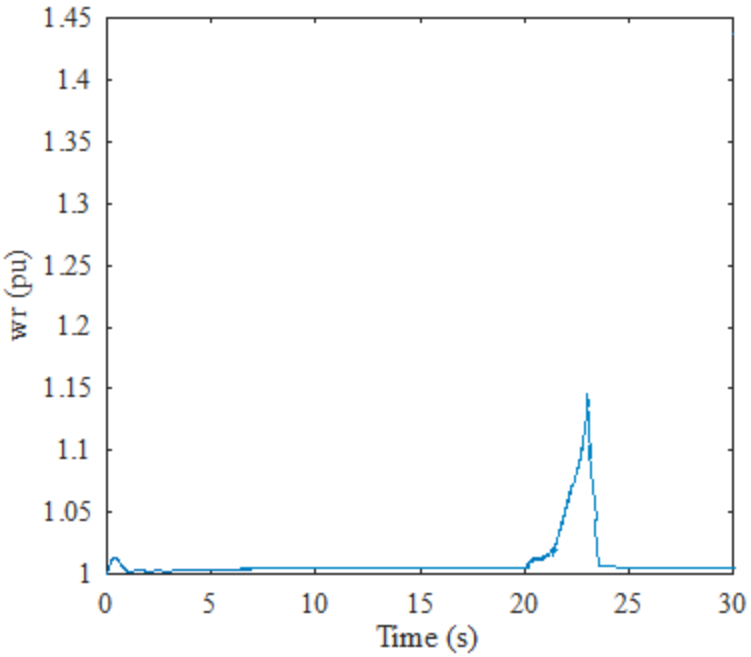


Figure 6.57. Rotor speed of FSIG

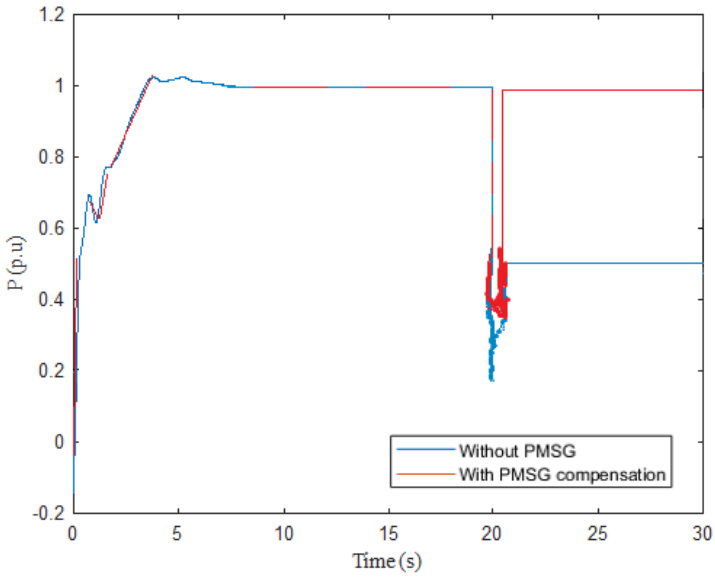


Figure 6.58. Active power output of FSIG based wind farm

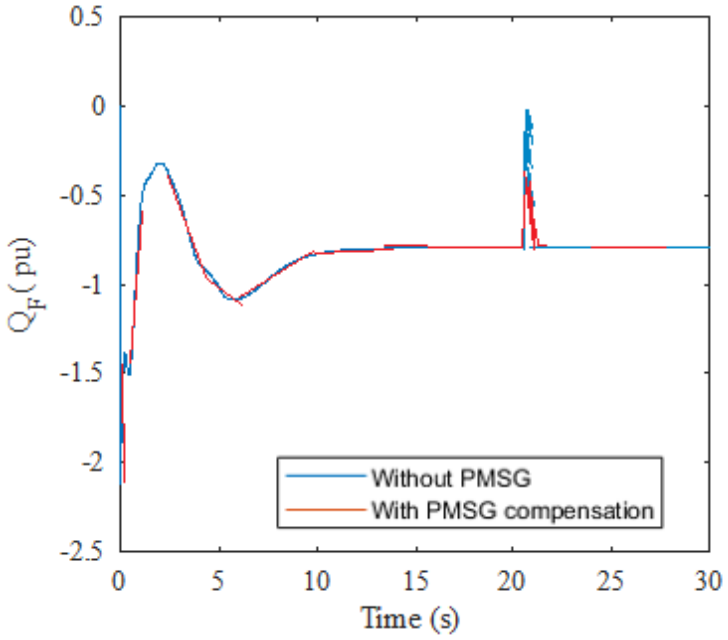


Figure 6.59. Reactive power output of FSIG wind farm.

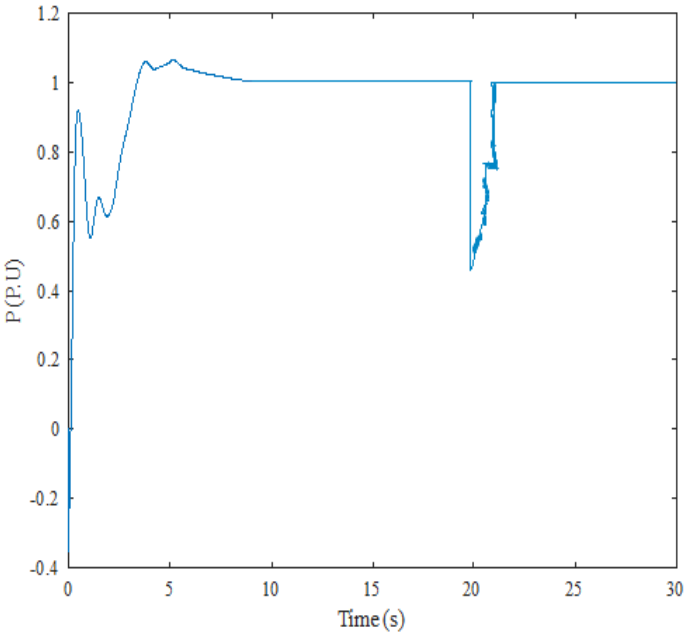


Figure 6.60. Output of PMSG based wind farm

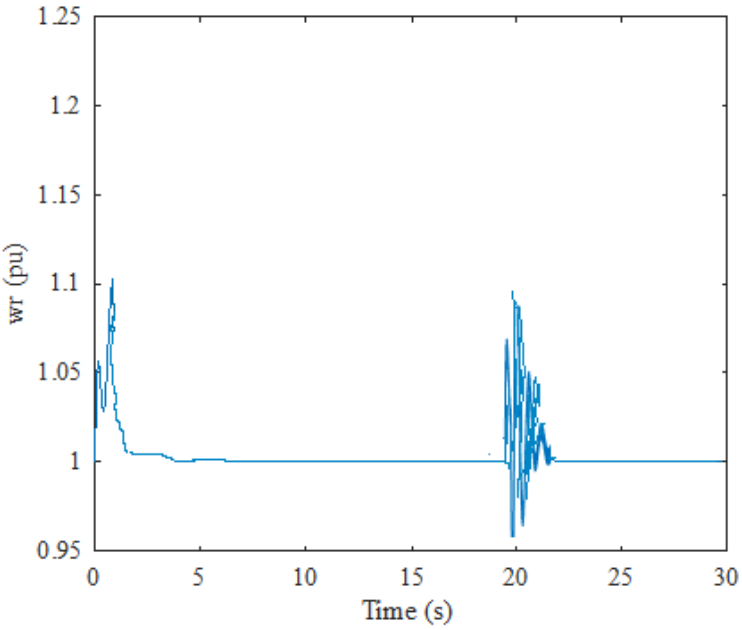


Figure 6.61. Rotor speed of PMSG

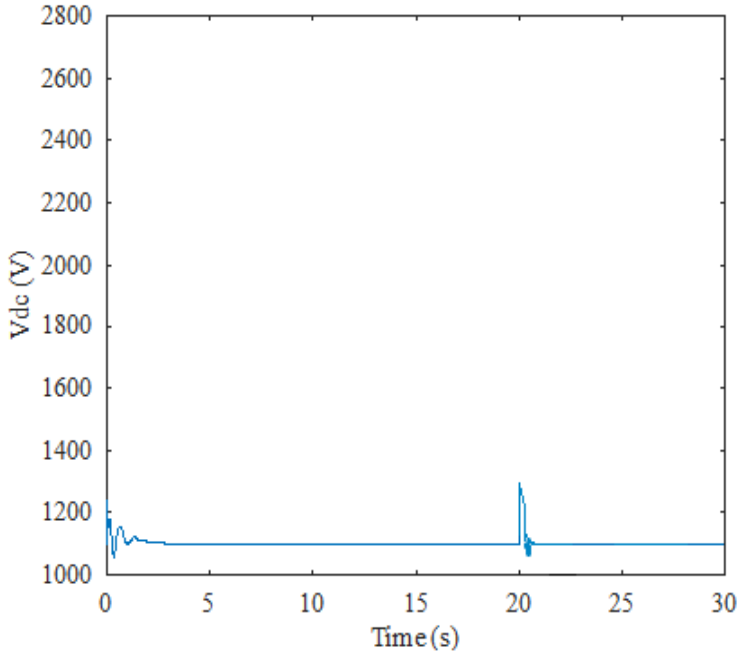


Figure 6.62. DC-link voltage

## 6.5. Comparison of the Proposed PMSG Control to Conventional STATCOM

For comparison of the proposed compensation strategy and the conventional STATCOM support of the FSIG based wind power system, the FSIG based wind farm is isolated from the hybrid wind farm and the same fault conditions discussed in Section 6.31 – 6.34 are introduced in the wind system containing only the FSIG based wind turbine. A 10 Mvar STATCOM is connected to the terminal of the FSIG wind power system to provide the required reactive power support during the fault duration. The STATCOM device is put into service at t=20 seconds when the different fault scenarios occur on the grid. The conventional STATCOM control strategy is presented in [127].

### 6.5.1. Single-Line-to-Ground (LG) Fault

A single-line-to-ground fault is introduced into the FSIG-based wind power system to study the behaviour of the system with STATCOM support. Figure 6.63 shows the reactive power profile of the WT with the grid fault condition. It is observed in Figure 6.64 that with reactive power support from the STATCOM, the active power profile of the wind turbine improves with the fault clearance. It is also observed that the fault level improves to 0.36 pu. However, with the coordinated control of the PMSG, the fault level in the FSIG wind turbine system improves to 0.40 pu under a single-line-to-ground fault. In Figure 6.65, it is seen that though the rotor speed of the FSIG is controlled to return to rated speed with the support of the STATCOM, the rotor speed of the FSIG returns to its rated speed quicker with the support provided from the coordinated control of the PMSG.

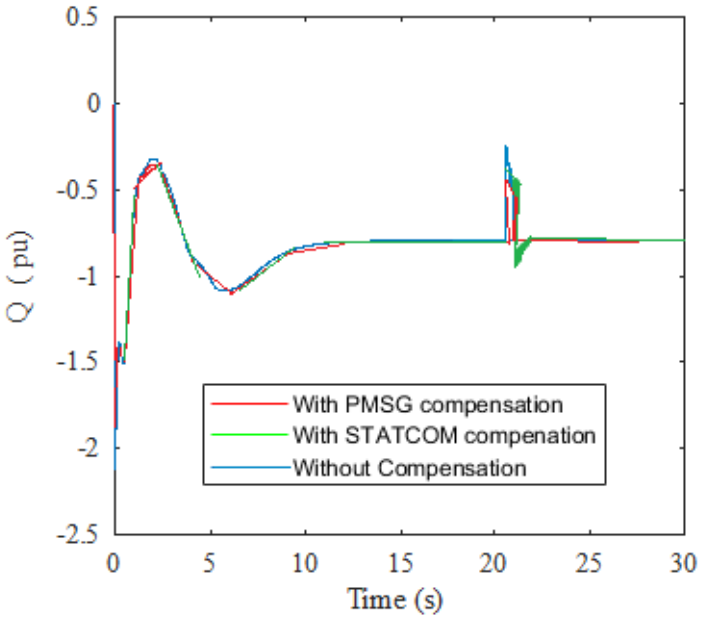


Figure 6.63. Reactive power output of FSIG based wind turbine

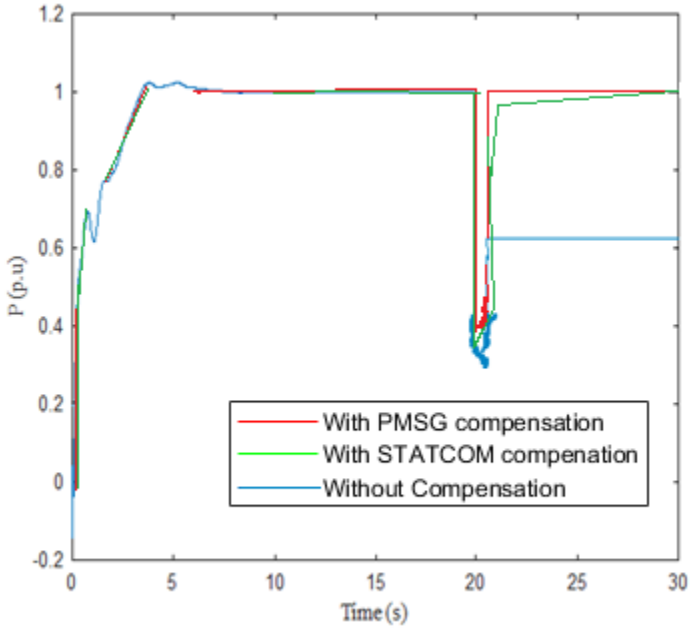


Figure. 6.64. Active power output of FSIG based wind turbine

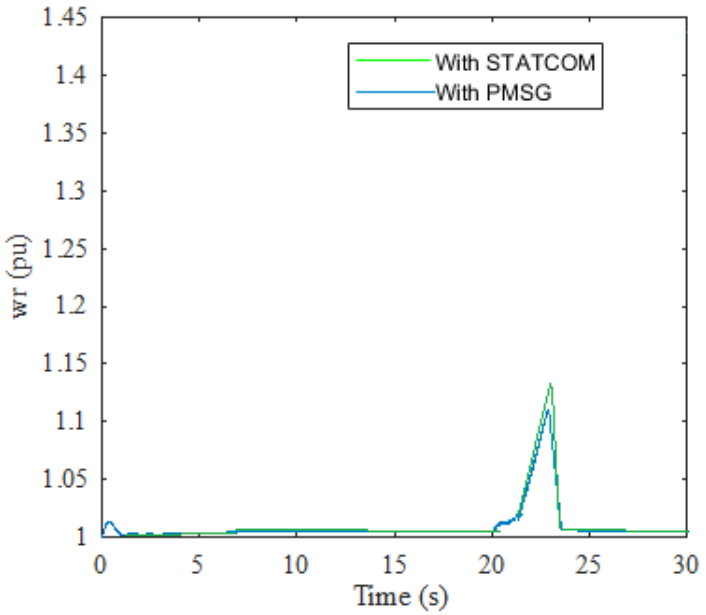


Figure. 6.65. Rotor speed of FSIG based wind turbine

## 6.5.2. Double-Line-to-Ground (LLG) Fault

A double-line-to-ground fault is introduced into the FSIG-based wind power system to study the behaviour of the system with STATCOM support. Figure 6.66 shows the reactive power profile of the WT with the grid fault condition. It is observed in Figure 6.67 that with reactive power support from the STATCOM, the active power profile of the wind turbine improves with the fault clearance. It is observed that the fault level improves to 0.30 pu. However, with the coordinated control of the PMSG, the fault level in the FSIG wind turbine system improves to 0.35 pu under a double-line-to-ground fault. Figure 6.68 shows the rotor behaviour of the FSIG with both the STATCOM and PMSG support.

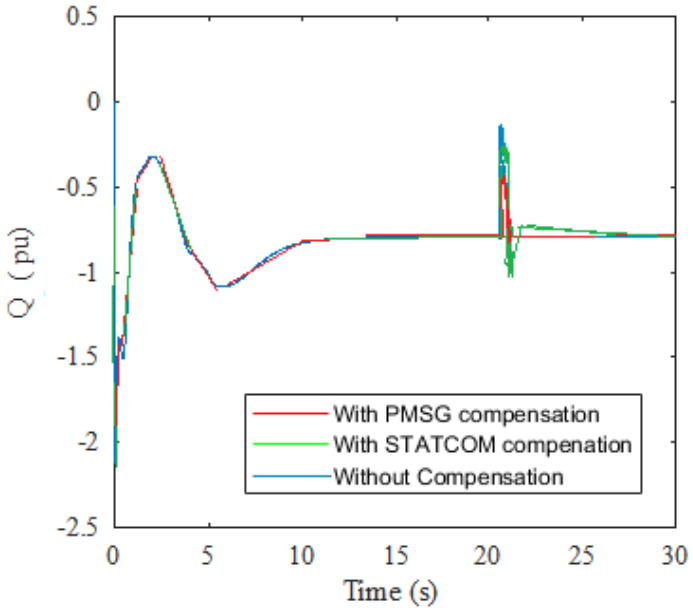


Figure 6.66. Reactive power output of FSIG based wind turbine

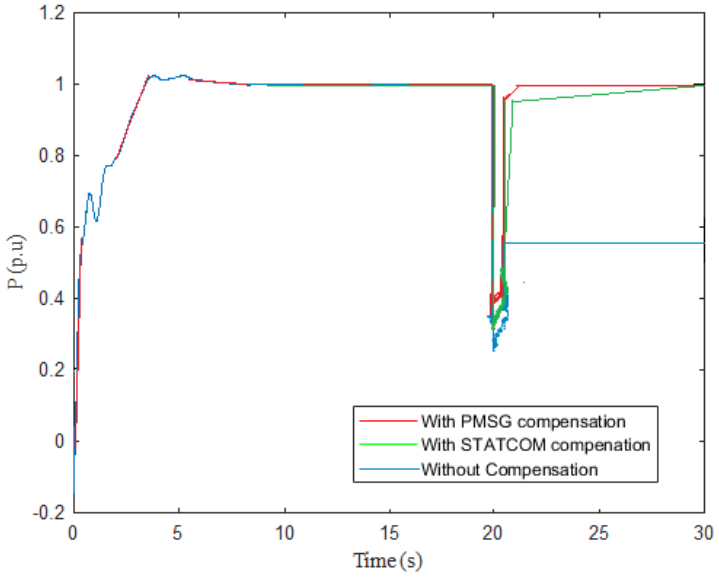


Figure. 6.67. Active power output of FSIG based wind turbine

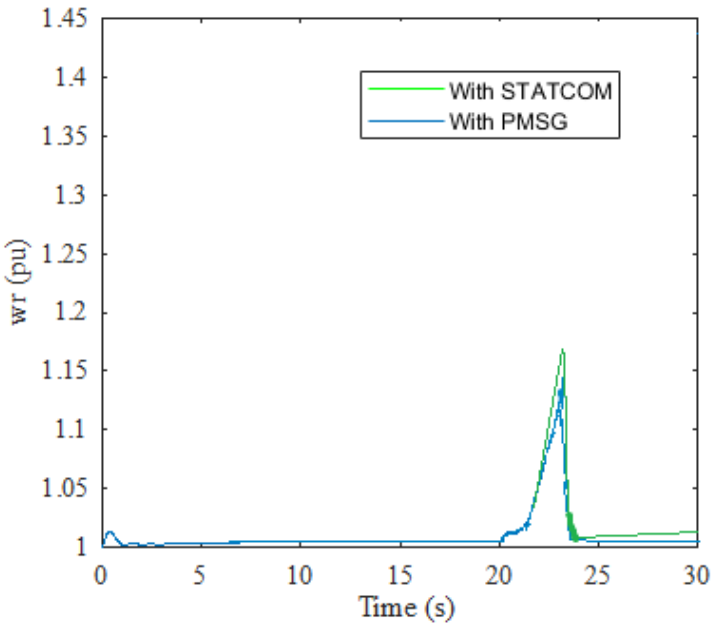


Figure. 6.68. Rotor speed of FSIG based wind turbine

## 6.5.3. Line-to-Line (LL) Fault

The reactive power profile of the FSIG based wind turbine under a line-to-line fault is shown in Figure 6.69. It is observed that under the fault condition, the FSIG based wind turbine with adequate reactive power support from the PMSG absorbs a lesser amount of reactive power from the grid when compared to the STATCOM support. It is observed in Figure 6.70 that with reactive power support from the STATCOM, the active power profile of the wind turbine improves with the fault clearance. It is also observed that the fault level improves to 0.32 pu with a line-to-line fault. However, with the coordinated control of the PMSG, the fault level in the FSIG wind turbine system improves to 0.38 pu under a line-to-line fault. Figure 6.71 shows the rotor behaviour of the FSIG with both the STATCOM and PMSG support.

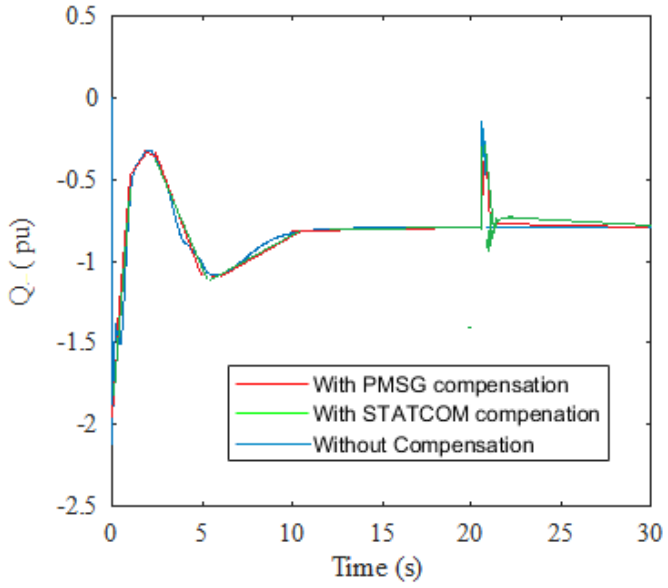


Figure 6.69. Reactive power output of FSIG based wind turbine

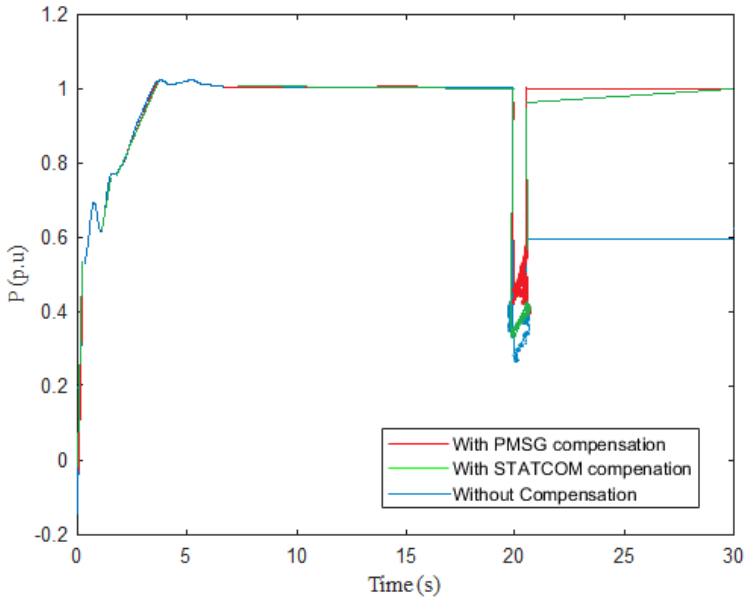


Figure. 6.70. Active power output of FSIG based wind turbine

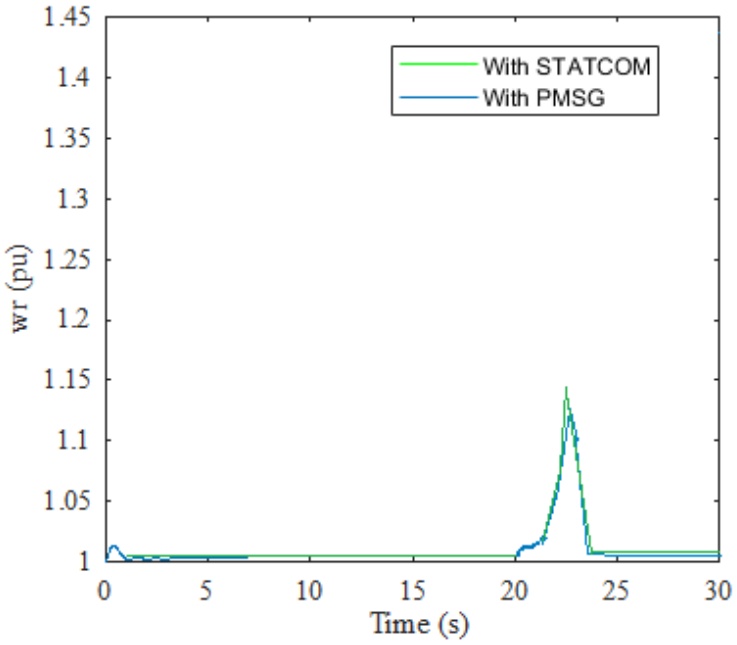


Figure. 6.71. Rotor speed of FSIG based wind turbine

## 6.5.4. Balanced 3-Phase (LLL) Fault

The reactive power profile of the FSIG based wind turbine under a balanced 3-phase fault is shown in Figure 6.72. It is observed that under the fault condition, the FSIG based wind turbine with adequate reactive power support from the PMSG absorbs a lesser amount of reactive power from the grid when compared to the STATCOM support. It is observed in Figure 6.73 that with reactive power support from the STATCOM, the active power profile of the wind turbine improves with the fault clearance. It can also be observed that the fault level improves to 0.28 pu. However, with the coordinated control of the PMSG, the fault level in the FSIG wind turbine system improves to 0.32 pu under a line-to-line fault. Figure 6.74 shows the rotor behaviour of the FSIG with both the STATCOM and PMSG support.

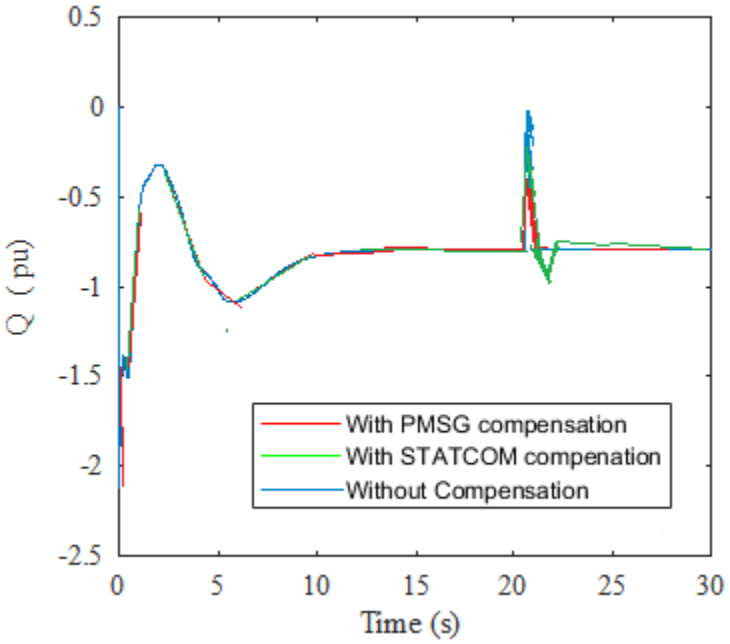


Figure 6.72. Reactive power output of FSIG based wind turbine

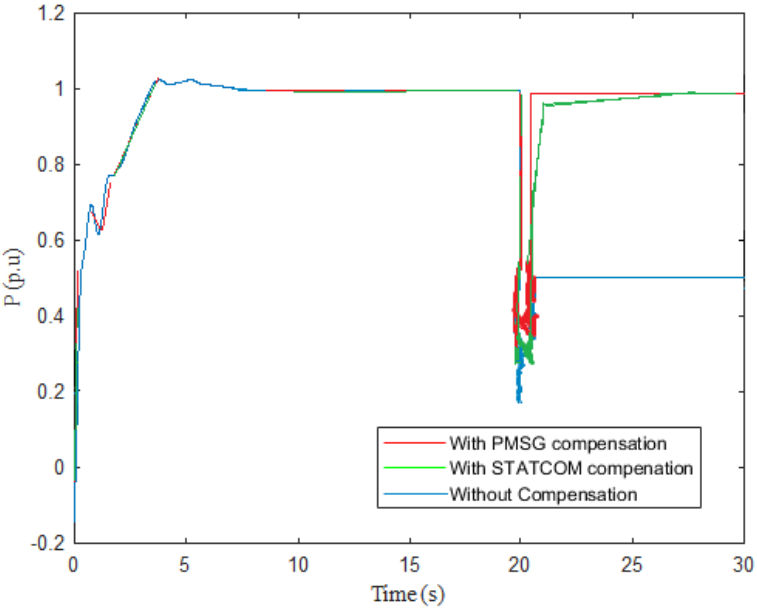


6.73. Active power output of FSIG based wind turbine

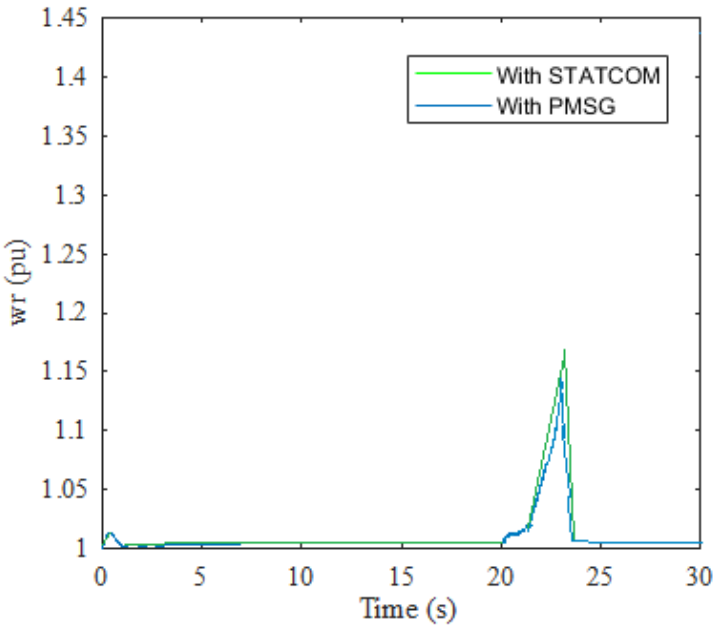


Figure. 6.74. Rotor speed of FSIG based wind turbine

## 6.5. Chapter Summary

This chapter examines the simulation results from the proposed coordinated control strategy of the hybrid wind farm. The wind farm is simulated and observed under four fault conditions namely: line-to-ground (LG), line-to-line (LL), double-line-to ground (LLG) and a balanced 3-phase (LLL) fault. Table 6.1 below presents a summary of the grid voltage of the hybrid wind farm under the different fault conditions. It can be seen that the grid voltage improves by 5%, 5.26%, 5.6% and 11% respectively when LG, LL, LLG and LLL faults respectively are introduced to the hybrid wind farm. The FSIG based wind turbine is disconnected from the hybrid wind system and simulated under the same fault conditions with reactive power support provided by a 10 Mvar STATCOM device. Table 6.2 presents a comparative summary of the

simulation results showing the improvements in the level of the fault depth on the FSIG wind turbine with the STATCOM and PMSG providing the necessary reactive power support.

**Table 6.1. Summary of the grid voltage of the hybrid wind farm**

| **Without compensation** | **LG** | **LL** | **LLG** | **LLL** |
|---|---|---|---|---|
| | 0.40 pu | 0.38 pu | 0.361 pu | 0.35 pu |
| **With compensation** | 0.42 pu | 0.40 pu | 0.38 pu | 0.39 pu |
| **% Improvement** | 5% | 5.26% | 5.6% | 11% |

**Table 6.2. Comparative summary of fault levels**

| | line-to-ground (LG) | double-line-to ground (LLG) | Line-to-line (LL) | balanced 3-phase fault (LLL). |
|---|---|---|---|---|
| Fault level | 0.28 pu | 0.23 pu | 0.25 pu | 0.20 pu |
| PMSG | 0.40 pu | 0.35 pu | 0.38 pu | 0.32 pu |
| STATCOM | 0.36 pu | 0.30 pu | 0.32 pu | 0.28 pu |

Though the capacity of the PMSG utilized in this thesis is 10 MW, the validity of the proposed hybrid control mechanism for providing support to the FSIG based wind turbine system was also tested using a 5 MW and 3 MW PMSG wind turbine system. Simulation results from the 3 MW PMSG wind system showed considerable similarity to the results of the 5 MW PMSG wind turbine. Figures 6.75 and 6.76 shows the output active power of the FSIG wind turbine system and the grid voltage of the hybrid wind farm when a single-line-to-ground fault which is less severe, is introduced into the hybrid wind system, with the rating of the PMSG wind system set at 5 MW and 10 MW. It is observed that with a 5 MW PMSG wind turbine supporting the FSIG based wind system, when the grid fault condition is introduced into the hybrid power system, the output active power of the FSIG is improved to 0.36 pu and the grid voltage is improved to 0.414 pu, representing a 3.5% improvement in grid voltage while the fault condition subsists. However when the capacity of the PMSG is increased to 10 MW, the ouput active power of the FSIG based wind system and the grid voltage of the hybrid wind farm improves to 0.40 pu and 0.428 pu respectively, representing a 5% improvement in grid voltage.

A balanced 3-phase fault is introduced into the hybrid wind power system in Figures 6.77 and 6.78. It is observed that with a 5 MW PMSG wind turbine supporting the FSIG based wind system, when the grid fault condition is introduced into the hybrid power system, the output active power of the FSIG is improved to 0.28 pu and the grid voltage is improved to 0.372 pu while the fault condition subsists, indicating a 6.2% improvement in grid voltage. However when the capacity of the PMSG is increased to 10 MW, the ouput active power of the FSIG based wind system and the grid voltage of the hybrid wind farm improves to 0.32 pu and 0.39 pu respectively, showing an improvement of 11% in the grid voltage

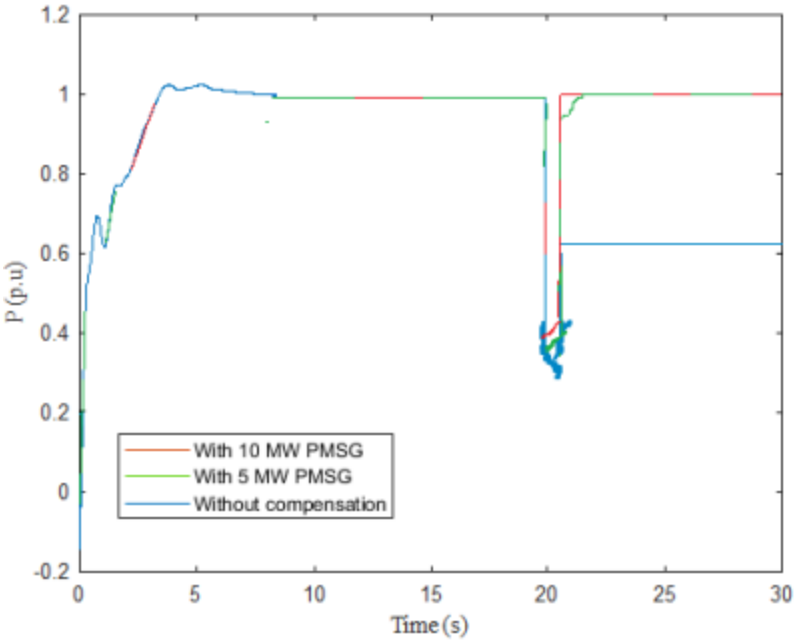


Figure 6.75. Active power output of FSIG based wind turbine

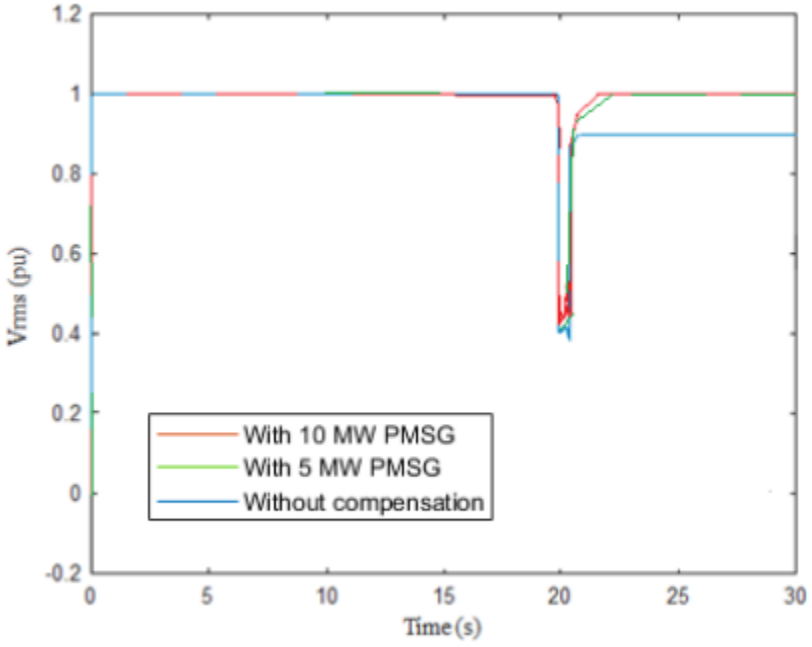


Figure 6.76. Grid voltage of the hybrid wind farm

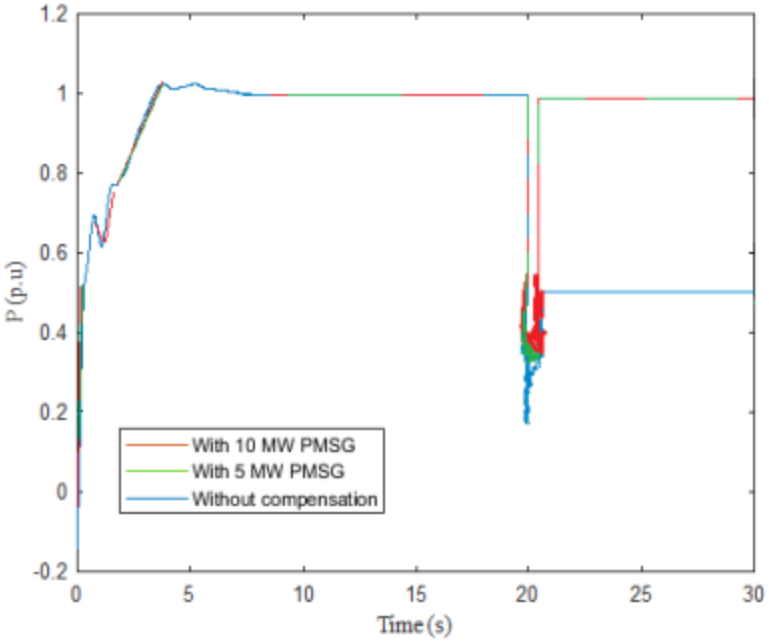


Figure 6.77. Active power output of FSIG based wind turbine

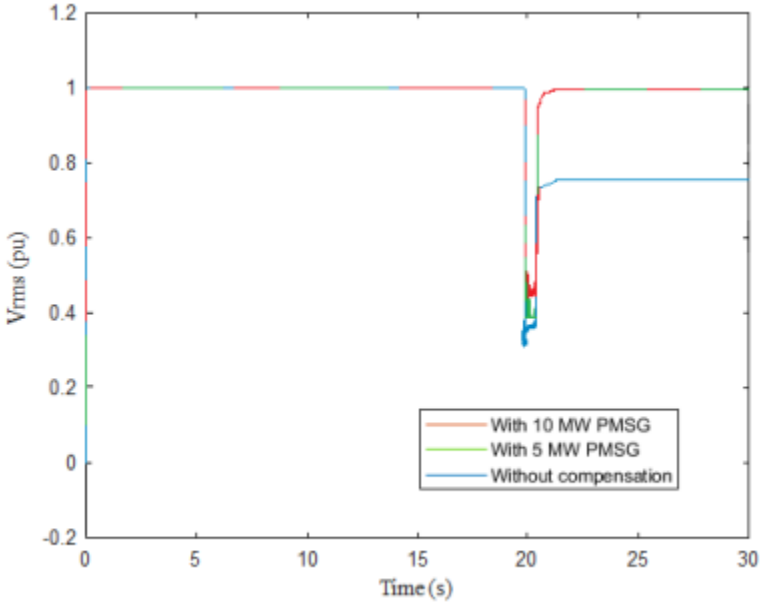


Figure 6.78. Grid voltage of the hybrid wind farm

The simulation results show that both the 5 MW and 10 MW PMSG wind turbine systems were able to provide adequate support to the FSIG wind turbine system. However, the 10 MW PMSG wind turbine system was able to better support the FSIG. It can therefore be concluded that the proposed hybrid solution is effective in providing support for the FSIG wind system during grid fault conditions. However, the design configuration of the PMSG wind system will determine the level of support provided to the nearby FSIG wind turbine system.

# Chapter 7

# Conclusions

## 7.1 Overview of the Thesis

There has been a large-scale grid integration of wind energy globally in the quest to reduce carbon emissions and embrace cleaner sources of energy. The fixed speed induction generator (FSIG) based wind turbine is a common sight in wind systems due to its lower costs, mechanical simplicity and robust construction. However, this class of wind turbine when connected directly to the grid does not have fault ride-through (FRT) capabilities during the occurrence of a grid fault and in steady-state cannot control the consumption of reactive power. This can cause the wind generator to experience large fluctuations resulting in the eventual tripping of the wind farm. To solve this problem, Flexible AC Transmission System (FACTS) devices such as the static synchronous compensator (STATCOM) are installed alongside FSIG based wind turbines to enhance voltage stability and reactive power control. This limitation of the FSIG based wind turbines has resulted in a technical migration to the variable speed wind turbines (VSWTs) powered by either the doubly-fed induction generator (DFIG) or the permanent magnet synchronous generator (PMSG). Irrespective of this technical migration from the FSWTs to the VSWTs, the FSWTs still represent a considerable percentage of globally installed wind turbines (WTs).

The PMSG-VSWT is becoming more attractive for wind energy systems. This class of WTs have fully-rated converters that make it possible to effectively control the active and reactive power coupled with a strong fault ride through (FRT) capability during grid disturbance. This makes it a very suitable choice for grid-connected operations. A unique characteristic of the PMSG-VSWT is the ability of its fully rated converters to support nearby DFIGs or FSIGs based wind turbines

making it a suitable choice for a hybrid wind farm system. Therefore, the combined installation of the PMSG wind system and the FSIG based wind system can effectively solve the problem of FRT and reactive power compensation associated with the FSIG based wind turbine by coordinated control of the power converters of the PMSG based wind turbine system. This helps in improving the FRT ability of the FSIG based wind system during a grid fault condition as well as generating electric power in a steady state.

## 7.2 Conclusions

In **chapter 2** the concept of wind turbine systems is introduced. For this thesis, the focus is on the FSIG and PMSG wind systems. Though there has been a technical shift from the FSWTs to the more efficient VSWTs, the FSWT still accounts for a non-negligible amount of WT systems. However, a major disadvantage of this class of wind turbine is its high mechanical stress during high wind speed conditions, low aerodynamic efficiency, difficulty in riding through a grid fault condition and the requirements of reactive power support. The PMSG on the other hand can readily ride through a grid fault condition without the need for external compensation devices, by totally decoupling the generator from the grid during a range of grid disturbances. A very important characteristic of the PMSG is its ability to enhance the voltage stability of nearby FSIG based wind farms. This characteristic of the PMSG is explored in this thesis. Chapter 2 also provides information on the modelling of the wind profile used in this thesis, therefore providing an answer to research question 7.

**Chapter 3** discusses the concept of voltage stability in the FSWT system. A review of the various technologies available for reactive power support and improving voltage stability of a grid-connected fixed speed wind farm is presented. The STATCOM was identified as the most commonly used device for reactive power support and voltage support in the FSWT system.

However, a major drawback of using the STATCOM is the arbitrary reactive current allocation during the compensation of reactive power, which can lead to over-compensation in the FSIG based wind system. This gap has been identified in this thesis and a suitable solution is proposed. Chapter three answers research question 2.

**Chapter 4** introduces the concept of hybrid wind power systems. In comparison to wind farms operating with a single type of WT, a hybrid wind farm operating with multiple types of WT generators can utilize the operational characteristics of the different WTs to improve system stability and performance, leading to a higher efficient operation of the wind farm. This thesis has identified three hybrid wind farm configurations, however, the PMSG-FSIG hybrid wind turbine system is chosen for this research. The proposed coordinated control strategy for the hybrid wind farm is presented and the hybrid wind farm is modelled in the simulation environment of Simulink. Chapter four answers research questions 3 and 4. Simulation results of the hybrid wind system in steady state have also been presented in Chapter 4 of the thesis.

**Chapter 5** focuses on the development of the proposed hybrid solution for reactive power compensation in the FSWT wind system. A reactive current allocation strategy is proposed and applied in designing a coordinated control strategy of the hybrid wind farm consisting of the PMSG and FSIG-based wind farms respectively. The reactive current component of the GSC of the PMSG is controlled based on the reactive current allocation strategy to provide reactive power support to the FSIG-based wind farm without the installation of additional auxiliary devices, and support grid voltage recovery of the hybrid wind farm. The active current component is also controlled to improve the output active power of the FSIG based wind system. Research question 5 is answered in Chapter 5. The proposed coordinated control mechanism of the GSC of the PMSG checks the network parameters of the FSIG based wind system during a

transient condition to see if there is provision to fulfil the requirements of the grid code and to determine the minimal reactive power need of the FSIG wind system. This way the PMSG can stabilize the FSIG based wind turbine, depending on the severity of the fault condition and design configuration of the hybrid wind farm.

**Chapter 6** presents the simulation results of the modelled hybrid wind farm consisting of the PMSG- and FSIG-based wind farms connected to the grid at PCC. The hybrid wind farm is simulated by observing the grid voltage and behaviour of the FSIG based wind farm with and without the proposed strategy. Different fault conditions have been introduced in simulation studies in Chapter 6 to test the proposed hybrid solution. The results show that the proposed coordinated control of the PMSG-FSIG hybrid system is valid for all fault conditions, therefore answering research question 7. The proposed coordinated control is compared to a conventional STATCOM device and the simulation results have shown that the PMSG when controlled to support the FSIG based wind system, is a better compensating device than the STATCOM.

Therefore, according to the research hypothesis of this thesis stated in Chapter 1 (repeated here for easy reading):

**The hybrid operation of a PMSG-based wind farm and a FSIG-based wind farm can compensate for the reactive power challenges associated with the FSIG-based wind farm, without any auxiliary devices, thereby improving the active power output and grid voltage of the hybrid wind system.**

This research has been able to validate the correctness of the hypothesis by the modelling, theoretical analysis and simulation results obtained in Chapters 4, 5 and 6. The results have shown that there is an improvement in the reactive power profile of the FSIG-based wind farm, the active

power output was also improved and there was a significant improvement in the grid voltage of the hybrid wind farm with a reduction in voltage sag levels.

This research has been able to contribute to the body of knowledge:

1. Modelling a hybrid wind system in the Simulink Matlab environment using an aggregate modelling approach. The transient behaviour of the FSWT is considered and the voltage equations of the individual WTs are considered in the modelling.
2. Unlike in the STATCOM where there is an arbitrary allocation of reactive current, a reactive current allocation method for the grid side converter of the PMSG is designed for reactive power compensation in the FSWT wind system.
3. The proposed current allocation method is implemented and a coordinated control strategy for the hybrid wind farm is developed to provide the required reactive power needed by the FSIG-wind system during a grid fault condition.

# References

[1] G. W. E. Council, "Global wind 2021 report Annual Market Update," Global Wind Energy Council (GWEC), Brussels, Belgium, 2021.

[2] K. Ohlenforst and G. W. E. Council, "Global Wind Report 2018," 2019.

[3] B. K. Sovacool, “Energy policymaking in Denmark: Implications for global energy security and sustainability”, Energy Policy, 61, pp. 829-839, 2013.

[4] Stats and Facts SAWEA, "South africa’s utility-scale wind & re industry," 2019.

[5] Department of Energy, Republic of South Africa, “Integrated Resource Plan (IRP2019”, 2019. Available: http://www.energy.gov.za/IRP/2019/IRP-2019.pdf

[6] Department of Mineral Resources and Energy, Republic of South Africa, “Wind atlas of South Africa”. Available: http://wasadata.csir.co.za/wasa1/WASAData

[7] H. Li and Z. Chen, "Overview of different wind generator systems and their comparisons," IET Renewable Power Generation, vol. 2, (2), pp. 123-138, 2008.

[8] J. Trapp et al, "Variable speed wind turbine using the squirrel cage induction generator with reduced converter power rating for stand-alone energy systems," in Industry Applications (INDUSCON), 2012 10th IEEE/IAS International Conference On, 2012, pp. 1-8.

[9] A. Awad et al, "Low voltage ride through capability enhancement of wind farms' generators: DVR versus STATCOM," in PES General Meeting| Conference & Exposition, 2014 IEEE, 2014, pp. 1-5.

[10] Apata, Oluwagbenga, and D. T. O. Oyedokun. "Wind turbine generators: Conventional and emerging technologies." 2017 IEEE PES Power Africa. IEEE, 2017.

[11] M. Laouer, A. Mekkaoui and M. Younes, "STATCOM and Capacitor Banks in a fixed-speed wind farm," Energy Procedia, vol. 50, pp. 882-892, 2014.

[12] Y. K. Gounder, D. Nanjundappan and V. Boominathan, "Enhancement of transient stability of distribution system with SCIG and DFIG based wind farms using STATCOM," IET Renewable Power Generation, vol. 10, (8), pp. 1171-1180, 2016.

[13] Market Watch, “Global Asynchronous Squirrel Cage Induction Generators Market Size 2020 Global Industry Share, Revenue, Business Growth Demand and Application Market Research Report to 2026.”

[14] Rubert, Tim, P. Niewczas, and D. McMillan. "Life extension for wind turbine structures and foundations." International Conference on Offshore Renewable Energy 2016. 2016.

[15] K. E. Okedu et al, "Wind farm stabilization by using DFIG with current controlled voltage source converters taking grid codes into consideration," IEEJ Transactions on Power and Energy, vol. 132, (3), pp. 251-259, 2012.

[16] K. Okedu et al, "Stabilization of wind farms by DFIG-based variable speed wind generators," in Electrical Machines and Systems (ICEMS), 2010 International Conference On, 2010, pp. 464-469.

[17] Beainy, Anissia, et al. "Comparison of different types of generator for wind energy conversion system topologies." 2016 3rd International Conference on Renewable Energies for Developing Countries (REDEC). IEEE, 2016.

[18] M. Rosyadi et al, "Stabilization of fixed speed wind generator by using variable speed PM wind generator in multi-machine power system," in Electrical Machines and Systems (ICEMS), 2012 15th International Conference On, 2012, pp. 1-6.

[19] S. Muyeen et al, "A variable speed wind turbine control strategy to meet wind farm grid code requirements," IEEE Trans. Power Syst., vol. 25, (1), pp. 331-340, 2010.

[20] Yao, Jun, et al. "Coordinated control of a hybrid wind farm with PMSG and FSIG during asymmetrical grid fault." International Journal of Electrical Power & Energy Systems 95 (2018): 287-300.

[21] M. P. Kazmierkowski et al, Control in Power Electronics: Selected Problems. Academic press, 2002.

[22] Masters, Gilbert M. Renewable and efficient electric power systems. John Wiley & Sons, 2013.

[23] Dubay, Kristen, et al. "Manufacturing Climate Solutions." (2009).

[24] Siemens AG. (2007). Nacelle of a Wind Turbine. Retrieved December 27, 2020, from http://www.powergeneration.siemens.com/press/press-pictures/windpower/nacelle-of-awind-turbine-2-3.htm.

[25] A. Betz, Introduction to the Theory of Flow Machines. Elsevier, 2014.

[26] A. Rolan et al, "Modeling of a variable speed wind turbine with a permanent magnet synchronous generator," in 2009 IEEE International Symposium on Industrial Electronics, 2009, pp. 734-739.

[27] M. Rahimi and M. Asadi, "Control and dynamic response analysis of full converter wind turbines with squirrel cage induction generators considering pitch control and drive train dynamics," International Journal of Electrical Power & Energy Systems, vol. 108, pp. 280-292, 2019.

[28] M. Yin et al, "Modeling of the wind turbine with a permanent magnet synchronous generator for integration," in 2007 IEEE Power Engineering Society General Meeting, 2007, pp. 1-6.

[29] I. Boldea, Synchronous Generators. CRC Press, 2015.

[30] Anderson, Paul M., Basant L. Agrawal, and James E. Van Ness. Subsynchronous resonance in power systems. Vol. 9. John Wiley & Sons, 1999.

[31] González-Longatt, F. M., Peter Wall, and Vladimir Terzija. "A simplified model for dynamic behavior of permanent magnet synchronous generator for direct drive wind turbines." *2011 IEEE Trondheim PowerTech*. IEEE, 2011.

[32] T. Ackermann, Wind Power in Power Systems. John Wiley & Sons, 2005.

[33] Apata, O., and D. T. O. Oyedokun. "An Overview of Control Techniques for Wind Turbine Systems." Scientific African (2020): e00566.

[34] D. Eltigani and S. Masri, "Challenges of integrating renewable energy sources to smart grids: A review," Renewable and Sustainable Energy Reviews, vol. 52, pp. 770-780, 2015.

[35] F. Blaabjerg and K. Ma, "Wind energy systems," Proc IEEE, vol. 105, (11), pp. 2116-2131, 2017.

[36] H. Wagner and J. Mathur, "Operation and control of wind energy converters," in Introduction to Wind Energy SystemsAnonymous Springer, 2018, pp. 63-74.

[37] Z. Jiang et al, "A review of individual pitch control for wind turbines," in 2016 IEEE 11th Conference on Industrial Electronics and Applications (ICIEA), 2016, pp. 399-404.

[38] R. B. Morim et al, "Analysis of wind turbine power generation with individual pitch control," in 2019 IEEE PES Innovative Smart Grid Technologies Conference-Latin America (ISGT Latin America), 2019, pp. 1-6.

[39] W. Tong, Wind Power Generation and Wind Turbine Design. WIT press, 2010.

[40] J. G. Njiri and D. Soeffker, "State-of-the-art in wind turbine control: Trends and challenges," Renewable and Sustainable Energy Reviews, vol. 60, pp. 377-393, 2016.

[41] M. Shan, J. Jacobsen and S. Adelt, "Field testing and practical aspects of load reducing pitch control systems for a 5 MW offshore wind turbine," in Annual Conference and Exhibition of European Wind Energy Association, 2013, pp. 101-105.

[42] Z. Chen and K. Stol, "An assessment of the effectiveness of individual pitch control on upscaled wind turbines," in Journal of Physics: Conference Series, 2014, pp. 012045.

[43] V. Petrović, M. Jelavić and M. Baotić, "Advanced control algorithms for reduction of wind turbine structural loads," Renewable Energy, vol. 76, pp. 418-431, 2015.

[44] E. Bossanyi, "Wind turbine control for load reduction," Wind Energy: An International Journal for Progress and Applications in Wind Power Conversion Technology, vol. 6, (3), pp. 229-244, 2003.

[45] M. Geyler and P. Caselitz, "Individual blade pitch control design for load reduction on large wind turbines," in European Wind Energy Conference (EWEC 2007), Milano, Italy, May, 2007, pp. 7-10.

[46] L. Fernandez, C. Garcia and F. Jurado, "Operating capability as a PQ/PV node of a direct-drive wind turbine based on a permanent magnet synchronous generator," Renewable Energy, vol. 35, (6), pp. 1308-1318, 2010.

[47] Haddad, Reemon Z., et al. "Performance analysis of radial and axial flux fractional horsepower motors." 2016 XXII International Conference on Electrical Machines (ICEM). IEEE, 2016.

[48] Pop, Adrian Augustin, et al. "Axial-flux vs. radial-flux permanent-magnet synchronous generators for micro-wind turbine application." 2013 15th European Conference on Power Electronics and Applications (EPE). IEEE, 2013.

[49] Faqih, Moh Rifqi, Sutedjo Sutedjo, and Endro Wahjono. "Design and Fabrication of a Radial Flux Permanent Magnet Synchronous Generator." 2019 International Electronics Symposium (IES). IEEE, 2019.

[50] Cheng, Ming, and Ying Zhu. "The state of the art of wind energy conversion systems and technologies: A review." Energy Conversion and Management 88 (2014): 332-347.

[51] P. K. Chaturvedi et al, "Switching losses and harmonic investigations in multilevel inverters," IETE Journal of Research, vol. 54, (4), pp. 297-307, 2008.

[52] F. Blaabjerg and K. Ma, "Wind energy systems," Proc IEEE, vol. 105, (11), pp. 2116-2131, 2017.

[53] Z. Zhang et al, "Robust Predictive Control of Three-Level NPC Back-to-Back Power Converter PMSG Wind Turbine Systems With Revised Predictions," IEEE Transactions on Power Electronics, vol. 33, (11), pp. 9588-9598, 2018.

[54] J. S. M. Ali and V. Krishnaswamy, "An assessment of recent multilevel inverter topologies with reduced power electronics components for renewable applications," Renewable and Sustainable Energy Reviews, vol. 82, pp. 3379-3399, 2018.

[55] Beainy, Anissia, et al. "Comparison of different types of generator for wind energy conversion system topologies." 2016 3rd International Conference on Renewable Energies for Developing Countries (REDEC). IEEE, 2016.

[56] Kadam, D. P., and B. E. Kushare. "Overview of different wind generator systems and their comparisons." International journal of engineering science & advanced technology 2.4 (2012): 1076-1081.

[57] H. Amaris, M. Alonso and C. A. Ortega, Reactive Power Management of Power Networks with Wind Generation. Springer Science & Business Media, 2012.

[58] L. G. Meegahapola, T. Littler and D. Flynn, "Decoupled-DFIG fault ride-through strategy for enhanced stability performance during grid faults," IEEE Transactions on Sustainable Energy, vol. 1, (3), pp. 152-162, 2010.

[59] A. Moghadasi, A. Sarwat and J. M. Guerrero, "A comprehensive review of low-voltage-ride-through methods for fixed-speed wind power generators," Renewable and Sustainable Energy Reviews, vol. 55, pp. 823-839, 2016.

[60] O. Apata and D. Oyedokun, "Novel reactive power compensation technique for fixed speed wind turbine generators," in 2018 IEEE PES/IAS PowerAfrica, 2018, pp. 628-633.

[61] M. Rastogi and A. H. Bhat, "Reactive power compensation using static synchronous compensator (STATCOM) with conventional control connected with 33kV grid," in Recent Advances in Engineering & Computational Sciences (RAECS), 2015 2nd International Conference On, 2015, pp. 1-5.

[62] Ramirez, Dionisio, et al. "Use of STATCOM in wind farms with fixed-speed generators for grid code compliance." Renewable Energy 37.1 (2012): 202-212.

[63] Hossain, Md Jahangir, H. R. Pota, and R. A. Ramos. "Robust STATCOM control for the stabilisation of fixed-speed wind turbines during low voltages." Renewable Energy 36.11 (2011): 2897-2905.

[64] Noroozian, M., et al. "Benefits of SVC and STATCOM for electric utility application." 2003 IEEE PES Transmission and Distribution Conference and Exposition (IEEE Cat. No. 03CH37495). Vol. 3. IEEE, 2003.

[65] Tamboli, Arif S., and H. T. Jadhav. "Hybrid STATCOM for Reactive Power Compensation." 2018 International Conference on Current Trends towards Converging Technologies (ICCTCT). IEEE, 2018.

[66] Ushkewar, Sandeep. "Mathematical Modelling of STATCOM for Reactive Power Compensation in Power System and Approach to the Renewable Energy." Emerging Trends in Electrical, Communications, and Information Technologies. Springer, Singapore, 2020. 167-174.

[67] Apata, O., and D. T. O. Oyedokun. "Impact Of Statcom On Voltage Stability Of Fixed Speed Wind Farms." 2020 IEEE PES/IAS PowerAfrica. IEEE, 2020.

[68] Tiwari, Vikas Kumar, and Atma Ram Gupta. "Application of SVC and STATCOM for Wind Integrated Power System." Recent Advances in Power Electronics and Drives. Springer, Singapore, 2021. 181-192.

[69] C. Wessels et al, "StatCom control at wind farms with fixed-speed induction generators under asymmetrical grid faults," IEEE Trans. Ind. Electron., vol. 60, (7), pp. 2864-2873, 2013.

[70] K. R. Reddy, N. R. Babu and P. Sanjeevikumar, "A review on grid codes and reactive power management in power grids with wecs," in Advances in Smart Grid and Renewable EnergyAnonymous Springer, 2018, pp. 525-539.

[71] Huang, Shun-Hsien, et al. "Voltage control challenges on weak grids with high penetration of wind generation: ERCOT experience." 2012 IEEE Power and Energy Society General Meeting. IEEE, 2012.

[72] Amini, Saeed, Md Tavakoli Bina, and Amin Hajizadeh. "Reactive power compensation in wind power plant using SVC and STATCOM." International Journal of Emerging Science and Engineering (IJESE) 2.5 (2014): 18-21.

[73] Demirovic, Nedzmija. "Impact of STATCOM and SVC to voltage control in systems with wind farms using induction generators (IG)." (2016): 80-6.

[74] Liu, Yu-Wei, et al. "Improvement of power quality by using advanced reactive power compensation." IEEE Transactions on Industry Applications 54.1 (2017): 18-24.

[75] F. O. Igbinovia et al, "Comparative review of reactive power compensation technologies," in Electric Power Engineering (EPE), 2015 16th International Scientific Conference On, 2015, pp. 2-7.

[76] Igbinovia, Famous O., et al. "Reputation of the Synchronous Condenser Technology in Modern Power Grid." 2018 International Conference on Power System Technology (POWERCON). IEEE, 2018.

[77] A. K. Sadigh and K. Smedley, "Review of voltage compensation methods in dynamic voltage restorer (DVR)," in Power and Energy Society General Meeting, 2012 IEEE, 2012, pp. 1-8.

[78] Meyer, Christoph, et al. "Optimized control strategy for a medium-voltage DVR—Theoretical investigations and experimental results." IEEE transactions on power electronics 23.6 (2008): 2746-2754.

[79] Kadia, J. V., and J. G. Jamnani. "Modelling and analysis of TCSC controller for enhancement of transmission network." International Journal of Emerging Technology and Advanced Engineering 2.3 (2012): 223.

[80] L. Wang, C. Lam and M. Wong, "Design of a thyristor controlled LC compensator for dynamic reactive power compensation in smart grid," IEEE Transactions on Smart Grid, vol. 8, (1), pp. 409-417, 2017.

[81] A. R. Fereidouni, B. Vahidi and T. H. Mehr, "The impact of solid state fault current limiter on power network with wind-turbine power generation," IEEE Transactions on Smart Grid, vol. 4, (2), pp. 1188-1196, 2013.

[82] H. Schmitt, "Fault current limiters report on the activities of CIGRE WG A3. 16," in Power Engineering Society General Meeting, 2006. IEEE, 2006, pp. 5 pp.

[83] Firouzi, M., and G. B. Gharehpetian. "Improving fault ride-through capability of fixed-speed wind turbine by using bridge-type fault current limiter." IEEE Transactions on Energy Conversion 28.2 (2013): 361-369.

[84] Jafari, M., et al. "Voltage sag compensation of point of common coupling (PCC) using fault current limiter." IEEE Transactions on Power Delivery 26.4 (2011): 2638-2646.

[85] Heydari, Hossein, and Amir Hassan Moghadasi. "Optimization scheme in combinatorial UPQC and SFCL using normalized simulated annealing." IEEE Transactions on Power Delivery 26.3 (2011): 1489-1498.

[86] Wiik, Jan A., et al. "Series connected power flow control using magnetic energy recovery switch (MERS)." 2007 Power Conversion Conference-Nagoya. IEEE, 2007.

[87] Wiik, Jan Arild, Olav Jakob Fonstelien, and Ryuichi Shimada. "A MERS type series FACTS controller for low voltage ride through of induction generators in wind farms." 2009 13th European Conference on Power Electronics and Applications. IEEE, 2009.

[88] Wiik, Jan Arild, Fransisco Danang Wijaya, and Ryuichi Shimada. "Characteristics of the magnetic energy recovery switch (MERS) as a series FACTS controller." IEEE transactions on power delivery 24.2 (2009): 828-836.

[89] Causebrook, Andrew, David J. Atkinson, and Alan G. Jack. "Fault ride-through of large wind farms using series dynamic braking resistors (March 2007)." IEEE Transactions on power systems 22.3 (2007): 966-975.

[90] Causebrook, Andrew, David J. Atkinson, and Alan G. Jack. "Low voltage ride-through: shifting the balance of power from blade pitch to electrical resistance." European Wind Energy Conference. 2006.

[91] Freitas, Walmir, Andre Morelato, and Wilsun Xu. "Improvement of induction generator stability using braking resistors." IEEE Transactions on power systems 19.2 (2004): 1247-1249.

[92] P. Huang et al, "Fault ride-through configuration and transient management scheme for self-excited induction generator-based wind turbine," IEEE Transactions on Sustainable Energy, vol. 5, (1), pp. 148-159, 2014.

[93] Moghadasi, Amir Hasan, Arif Islam, and Mohamadhadi Amini. "LVRT capability assessment of FSIG-based wind turbine utilizing UPQC and SFCL." 2014 IEEE PES General Meeting| Conference & Exposition. IEEE, 2014.

[94] A. Moghadasi and A. Islam, "Enhancing LVRT capability of FSIG wind turbine using current source UPQC based on resistive SFCL," in T&D Conference and Exposition, 2014 IEEE PES, 2014, pp. 1-5.

[95] Moghadasi, Amir, and Arif Islam. "Enhancing LVRT capability of FSIG wind turbine using current source UPQC based on resistive SFCL." 2014 IEEE PES T&D Conference and Exposition. IEEE, 2014.

[96] Huang, Po-Hsu, et al. "Fault ride-through configuration and transient management scheme for self-excited induction generator-based wind turbine." IEEE Transactions on Sustainable Energy 5.1 (2013): 148-159.

[97] Zhou, Hua, et al. "Improvement of transient voltage stability of the wind farm using SVC and TCSC." 2011 Asia-Pacific Power and Energy Engineering Conference. IEEE, 2011.

[98] Teleke, Sercan, et al. "Dynamic performance comparison of synchronous condenser and SVC." IEEE Transactions on Power Delivery 23.3 (2008): 1606-1612.

[99] J. Lu et al, "DG control strategies for grid voltage unbalance compensation," in Energy Conversion Congress and Exposition (ECCE), 2014 IEEE, 2014, pp. 2932-2939.

[100] F. Sulla, J. Svensson and O. Samuelsson, "Fault behavior of wind farms with fixed-speed and doubly-fed induction generators," in PowerTech, 2011 IEEE Trondheim, 2011, pp. 1-7.

[101] J. Yao et al, "Coordinated Control Strategy for Hybrid Wind Farms with DFIG-based and PMSG-based Wind Farms during Network Unbalance," Renewable Energy, 2017.

[102] M. Nehrir et al, "A review of hybrid renewable/alternative energy systems for electric power generation: Configurations, control, and applications," IEEE Transactions on Sustainable Energy, vol. 2, (4), pp. 392-403, 2011.

[103] K. S. Krishna and K. S. Kumar, "A review on hybrid renewable energy systems," Renewable and Sustainable Energy Reviews, vol. 52, pp. 907-916, 2015.

[104] Sawle, Yashwant, S. C. Gupta, and Aashish Kumar Bohre. "Review of hybrid renewable energy systems with comparative analysis of off-grid hybrid system." Renewable and Sustainable Energy Reviews 81 (2018): 2217-2235.

[105] Bajpai, Prabodh, and Vaishalee Dash. "Hybrid renewable energy systems for power generation in stand-alone applications: A review." Renewable and Sustainable Energy Reviews 16.5 (2012): 2926-2939.

[106] Leon, Andres E., et al. "An improved control strategy for hybrid wind farms." IEEE Transactions on Sustainable Energy 1.3 (2010): 131-141.

[107] Wang, Li, and Dinh-Nhon Truong. "Stability improvement of a hybrid DFIG-based and PMSG-based offshore wind farm fed to a SG-based power system using a STATCOM." Int. J. Smart Grid and Clean Energy 2.2 (2013): 230-236.

[108] Wang, Li, and Dinh-Nhon Truong. "Stability enhancement of a power system with a PMSG-based and a DFIG-based offshore wind farm using a SVC with an adaptive-network-based fuzzy inference system." IEEE transactions on industrial electronics 60.7 (2012): 2799-2807.

[109] Foster, Sarah, Lie Xu, and Brendan Fox. "Coordinated control and operation of DFIG and FSIG based Wind Farms." 2007 IEEE Lausanne Power Tech. IEEE, 2007.

[110] Foster, Sarah, Lie Xu, and Brendan Fox. "Coordinated reactive power control for facilitating fault ride through of doubly fed induction generator-and fixed speed induction generator-based wind farms." IET Renewable Power Generation 4.2 (2010): 128-138.

[111] Yao, Jun, et al. "Coordinated control strategy for hybrid wind farms with DFIG-based and PMSG-based wind farms during network unbalance." Renewable Energy 105 (2017): 748-763.

[112] Yao, Jun, et al. "Coordinated control of a hybrid wind farm with PMSG and FSIG during asymmetrical grid fault." International Journal of Electrical Power & Energy Systems 95 (2018): 287-300.

[113] Sulla, Francesco, Jörgen Svensson, and Olof Samuelsson. "Fault behavior of wind farms with fixed-speed and Doubly-Fed Induction Generators." 2011 IEEE Trondheim PowerTech. IEEE, 2011

[114] Muyeen, S. M., et al. "A variable speed wind turbine control strategy to meet wind farm grid code requirements." IEEE Transactions on power systems 25.1 (2009): 331-340.

[115] Liu, Ruikuo, et al. "Harmonic compensation capability-based coordinated control for hybrid wind farms under distorted grid voltage conditions." IET Renewable Power Generation 13.9 (2019): 1603-1614.

[116] Wang, Yi, and Lie Xu. "Coordinated control of DFIG and FSIG-based wind farms under unbalanced grid conditions." IEEE Transactions on Power Delivery 25.1 (2009): 367-377

[117] Geng, Hua, et al. "Unified power control for PMSG-based WECS operating under different grid conditions." IEEE Transactions on Energy Conversion 26.3 (2011): 822-830.

[118] Zeng, Hui, Yu Zhu, and Jinsong Liu. "Verification of DFIG and PMSG wind turbines' LVRT characteristics through field testing." 2012 IEEE International Conference on Power System Technology (POWERCON). IEEE, 2012.

[119] Herrera, Reyes S., and Patricio Salmerón. "Instantaneous reactive power theory: A reference in the nonlinear loads compensation." *IEEE Transactions on Industrial Electronics* 56.6 (2009): 2015-2022.

[120] A.R. Bergen, V. Vittal, Power System Analysis, 2nd ed., Prentice Hall, Upper Saddle River, NJ, 2000

[121] W. Qiao, L. Qu, R.G. Harley, Control of IPM synchronous generator for maximum wind power generation considering magnetic saturation, IEEE Transactions on Industry Applications 45 (June (3)) (2009) 1095–1105.

[122] J. Belhadj, X. Roboam, Investigation of different methods to control a small variable-speed wind turbine with PMSM drives, Journal of Energy Resources Technology, Transactions of the ASME 129 (September) (2007) 200–213.

[123] F. M. Gardner, Phaselock Techniques. New York: Wiley, 1979.

[124] H. Polinder, F. F. A. van der Pijl, G. . -J. de Vilder and P. J. Tavner, "Comparison of direct-drive and geared generator concepts for wind turbines," in IEEE Transactions on Energy Conversion, vol. 21, no. 3, pp. 725-733, Sept. 2006, doi: 10.1109/TEC.2006.875476.

[125] National Energy Regulator of South Africa (NERSA), "Grid connection code for Renewable Power Plants (RPPs) connected to the electricity Transmission System (TS) or the Distribution System (DS) in South Africa," July 2016.

[126] Rahimi, M.; Parniani, M. Coordinated control approaches for low-voltage ride-through enhancement in wind turbines with doubly fed induction generators. IEEE Trans. Energy Convers. 2010, 25, 873–883.

[127] Li, Shuhui, Ling Xu, and Timothy A. Haskew. "Control of VSC-based STATCOM using conventional and direct-current vector control strategies." *International Journal of Electrical Power & Energy Systems* 45.1 (2013): 175-186.

# APPENDIX A

Appendix A1: PMSG-WT model in Simulink

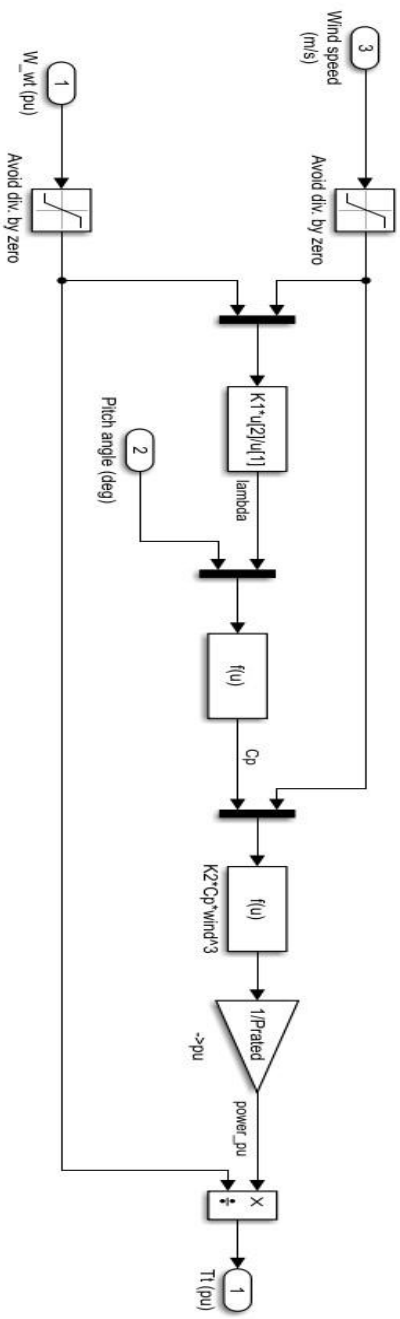

Appendix A2: PMSG Grid side converter model in Simulink

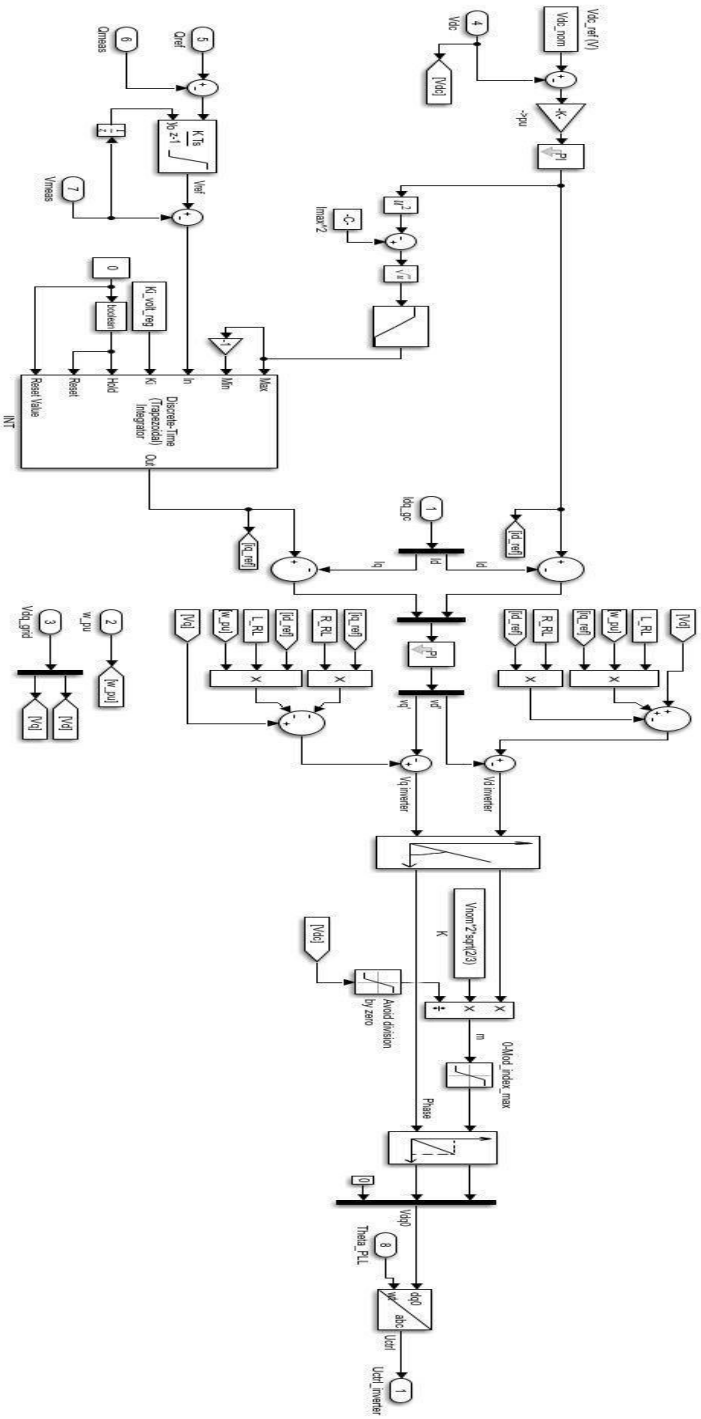

Appendix A3: FSWT model in Simulink

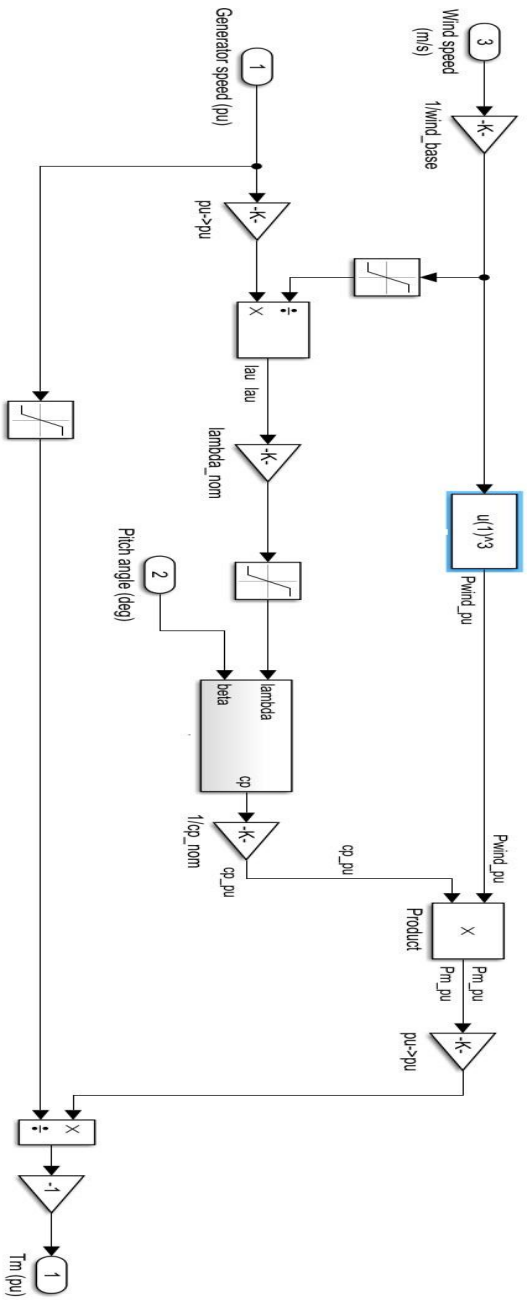

Appendix A4: PMSG speed control